Chem Soc Rev

REVIEW ARTICLE

View Article Online
View Journal | View Issue



Cite this: *Chem. Soc. Rev.*, 2019, **48**, 814

# Practical use of polymer brushes in sustainable energy applications: interfacial nanoarchitectonics for high-efficiency devices

Juan M. Giussi, M. Lorena Cortez, Waldemar A. Marmisollé and Omar Azzaroni *

The discovery and development of novel approaches, materials and manufacturing processes in the field of energy are compelling increasing recognition as a major challenge for contemporary societies. The performance and lifetime of energy devices are critically dependent on nanoscale interfacial phenomena. From the viewpoint of materials design, the improvement of current technologies inevitably relies on gaining control over the complex interface between dissimilar materials. In this sense, interfacial nanoarchitectonics with polymer brushes has seen growing interest due to its potential to overcome many of the limitations of energy storage and conversion devices. Polymer brushes offer a broad variety of resources to manipulate interfacial properties and gain molecular control over the synergistic combination of materials. Many recent examples show that the rational integration of polymer brushes in hybrid nanoarchitectures greatly improves the performance of energy devices in terms of power density, lifetime and stability. Seen in this light, polymer brushes provide a new perspective from which to consider the development of hybrid materials and devices with improved functionalities. The aim of this review is therefore to focus on what polymer brush-based solutions can offer and to show how the practical use of surface-grafted polymer layers can improve the performance and efficiency of fuel cells, lithium-ion batteries, organic radical batteries, supercapacitors, photoelectrochemical cells and photovoltaic devices.

Received 25th September 2018

DOI: 10.1039/c8cs00705e

rsc.li/chem-soc-rev

*Instituto de Investigaciones Fisicoquímicas Teóricas y Aplicadas (INIFTA), Departamento de Química, Facultad de Ciencias Exactas, Universidad Nacional de La Plata, CONICET, Diagonal 113 y 64 (1900), La Plata, Argentina. E-mail: azzaroni@inifta.unlp.edu.ar*

**Juan M. Giussi**

*Juan Martín Giussi studied chemistry at the Universidad Nacional de La Plata (UNLP) (Argentina), receiving his PhD in 2012. His postdoctoral studies were carried out at the Instituto de Investigaciones Fisicoquímicas y Aplicadas (INIFTA, La Plata, Argentina), Instituto de Ciencia y Tecnología de Polímeros (ICTP, Madrid, Spain) and CIC BiomaGUNE (San Sebastián, Spain). He is currently a fellow member of CONICET. He is also Senior Laboratory Instructor in Organic Chemistry at UNLP. His research interests include molecular design, synthesis and applications of hierarchical polymeric materials, polymer brushes and stimuli-responsive microgels.*

**M. Lorena Cortez**

*M. Lorena Cortez graduated with a degree in Biochemistry from University of Buenos Aires (FFyB – UBA) and obtained her PhD in Chemistry from the same university(FCEyN – INQUIMAE – UBA). Her doctoral work was centered on the development of bioelectrochemical sensors through the integration of nanocomposites on electrode surfaces. After two years of post-doctoral research on charge transport in supramolecular systems, she joined the Instituto de Investigaciones Fisicoquímicas Teóricas y Aplicadas (INIFTA) (UNLP-CONICET) as a staff member of CONICET. Her current research interests are centered around two main areas: design, synthesis and physicochemical characterization of soft functional interfaces, and development of new supramolecular materials and functionalization techniques for biosensing applications.*

## Introduction

Energy is the key element that allows our societies to grow and evolve in a sustainable manner. It is no exaggeration to say that this is one of the issues to which global institutions have paid the closest attention over the last decades.[1,2] Our use of energy is strongly correlated with many environmental problems, such as global warming, air pollution and climate change. This is the reason why clean, low-cost and high-efficient energy storage and conversion are essential for the sustainable development of our societies.

During the last decade, significant progress has been made in developing advanced technologies to face these challenges.[3,4] However, to enable cost-effective energy production, further improvement of performance and efficiency of current technologies is strongly needed.

In this respect, nano-architected hybrid materials are becoming increasingly important for developing energy conversion and storage devices with optimized properties.[5] Carefully designed nanostructured hybrid materials consisting of different, complementary building blocks can evolve into nanostructured materials with unique property combinations.[6] These materials may have specific interfaces or structures leading synergistically to explicit properties. Some may wonder why we are placing special emphasis on hybrid and nanostructured interfaces. The reason for this is that the performance of energy conversion and storage devices depends intimately on the interfacial characteristics of their constituting materials.[7] To express enhanced or concerted functions from different counterparts we need to integrate building blocks across complex interfaces.

It is also important to consider that creating such complex nanoarchitectures requires the tailored production and organization of nanoscale structural units into predefined configurations. Research efforts in this direction are often referred to as "*nanoarchitectonics*", a term popularized by Ariga and co-workers.[8] In that regard, the ample functional and structural versatility of polymer brushes make them "ideal" building blocks for "soft nanoarchitectonics".[9]

Polymer brushes refer to assemblies of macromolecules that are tethered by one end to a surface or interface.[10] There are two main strategies for generating polymer brushes: "grafting to" and "grafting from" (Fig. 1).[11] In the "grafting-to" technique, pre-synthesized polymers are anchored to a surface from solution.[12] In contrast, the "grafting-from" approach involves sequential growth of polymer chains from the surface.[13,14] It is useful to note that in many cases, for simplicity of expression, the term "polymer brush" is used as a synonym of the terms "tethered polymer chains" or "end-grafted polymers." However, strictly speaking, the term "polymer brush" should be associated with a layer of tethered polymer chains under specific conditions—when the behavior of the tethered layer is dictated by strong interactions between densely grafted polymer chains.[15]

From a historical perspective, the use of polymer brushes has been mostly circumscribed to the modification of surfaces for wetting,[16] adhesion,[17] lubrication,[18] detergency,[19] biocompatibility,[20] and colloidal stabilization applications.[21] Needless to say that these macromolecular interfacial architectures have also facilitated the construction of substrates displaying tailorable electrochemical,[22] nanomechanical,[23] photochemical,[24] and/or thermoresponsive[25] properties. The field of polymer brushes has evolved over the years and has now matured into an independent and identifiable subject that is increasingly

**Waldemar A. Marmisollé**

*Waldemar A. Marmisollé was born in Junín (Buenos Aires, Argentina) in 1984. He studied chemistry at the Universidad Nacional de La Plata (UNLP) receiving his degree in 2007 and his PhD in chemistry in 2011. He performed post-doctoral work at the Universidad de Buenos Aires (UBA) and he is now a fellow member of CONICET working at the Soft Matter Laboratory of the Instituto de Investigaciones Fisicoquímicas Teóricas y Aplicadas (INIFTA) (UNLP-CONICET). His research interests include conducting polymers and soft matter electrochemistry.*

**Omar Azzaroni**

*Omar Azzaroni studied chemistry at the Universidad Nacional de La Plata (UNLP) (Argentina), receiving his PhD in 2004. His postdoctoral studies were carried out at the University of Cambridge (UK) (2004–2006, Marie Curie Research Fellow) and the Max Planck Institute for Polymer Research (Germany) (2007, Alexander von Humboldt Research Fellow). He was then appointed as Max Planck Partner Group leader from 2009 until 2013. He has served as Vice-Director of the Instituto de Investigaciones Fisicoquímicas Teóricas y Aplicadas (INIFTA) (2012–2015). He is currently a fellow member of CONICET and head of the Soft Matter Laboratory of INIFTA. Since 2009, he is also Adjunct Professor of Physical Chemistry at UNLP. His research interests include nanostructured hybrid interfaces, supra- and macromolecular materials science and soft nanotechnology. More information can be found at: http://softmatter.quimica.unlp.edu.ar*

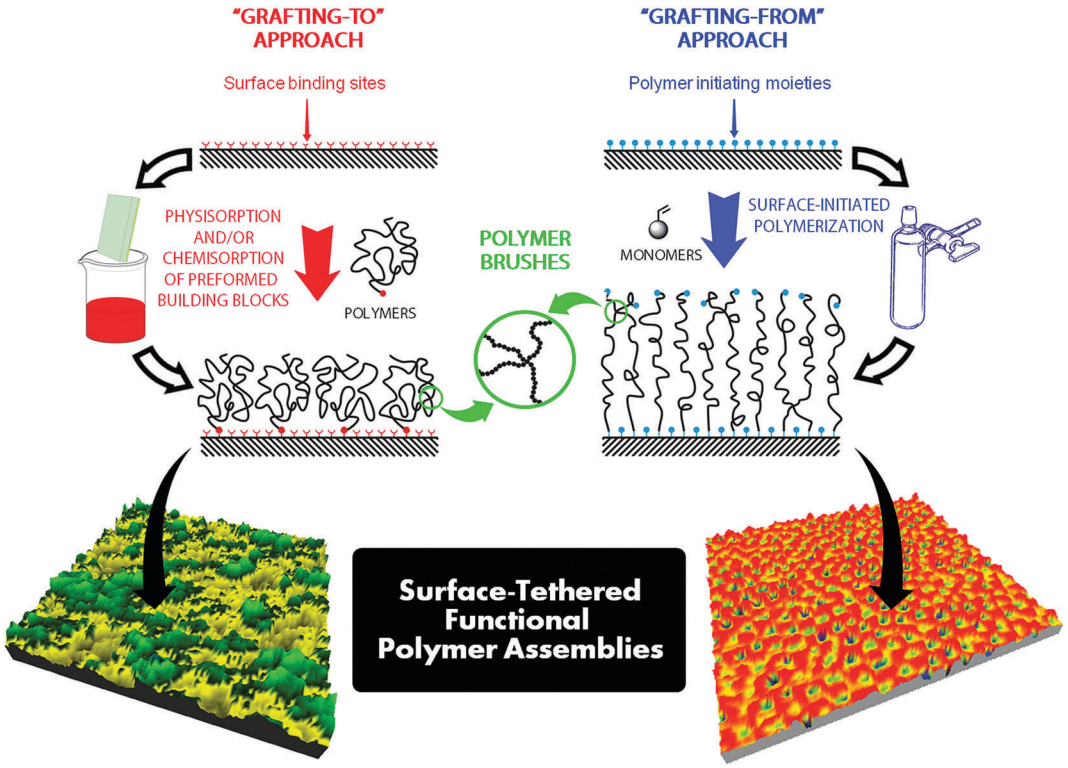


Fig. 1 Schematic illustration describing the main chemical strategies ("grafting-to" and "grafting-from" approaches) used to tether functional polymer brushes on different substrates.

shifting towards a new focus on energy-related applications. This trend has been accelerated by the fact that polymer brushes are fully compatible with a wide variety of technologically relevant surfaces and nanomaterials, including ITO,[26] halloysite[27] montmorillonite,[28] CdSe,[29] CdS,[30] GaAs,[31] gold colloids,[32] single-walled carbon nanotubes,[33] multi-walled carbon nanotubes,[34] and nanographene.[35]

The increasing interest in polymer brushes relies on their flexibility to create tailored films[36] displaying pseudo-3D spatial arrangements of functional units in which chemical composition, thickness, and grafting can be addressed with nanoscale precision.[37,38] This is particularly obvious when we think of polymer brushes as "soft" building blocks capable of conferring specific functions to a broad range of materials.[39–41] Exciting opportunities to create materials with a suite of designed properties are revealed when we think in this manner. Polymer brushes provide a complementary and new perspective from which to consider the synergy between macromolecular functional units and nanomaterials – or nano/microstructured substrates – and the subsequent integration of these hybrid assemblies into energy conversion and storage devices (Fig. 2).

Let us think for a moment about the multiple scenarios in which polymer brushes could enhance the functional performance of such devices. The last few years have seen dramatic advances in the use of low-dimensional materials for sustainable energy applications, such as graphene, semiconductor quantum dots and other inorganic nanostructures. Controlling their interfacial interactions and organization by tailoring their dimensions, composition and structure is the stepping stone to reach the objective of increasing the efficiency in energy conversion and storage. For example, nanoparticles themselves can be used as building blocks for two-dimensional arrays in solar cells and electrochemical devices. However, they can also generate highly interconnected three-dimensional hetero-supramolecular networks with superior performance if they are integrated into polymer brushes. Gaining nanoscale control over the structural arrangement of polymer brush-nanomaterial hybrids can lead to substantial improvement of electron and photoelectron transfer properties with immediate effects on the photovoltaic, photocatalytic and electrocatalytic outputs.

Polymer brushes represent a versatile chemical solution to confer specific functions to a molecular material through an appropriate chemical and/or macromolecular design.[42,43] They exhibit remarkable properties, including their ability to interact and preconcentrate ionic species, such as $Li^+$ ions. The high surface density of functional groups should provide a large number of interaction sites for surface or interface-related processes, this being an extraordinary property for energy storage applications. The flexibility of the grafted polymer chains shows promise in adapting to structural expansion and contraction during electrochemical processes. The formation of redox active polymer brushes on conductive substrates can improve the electron transfer characteristics of energy conversion devices. Functional polymer brushes can give rise to interfacial p/n junctions applicable to photoelectrochemical cells through the controlled integration of light absorbers, electron-transfer

 

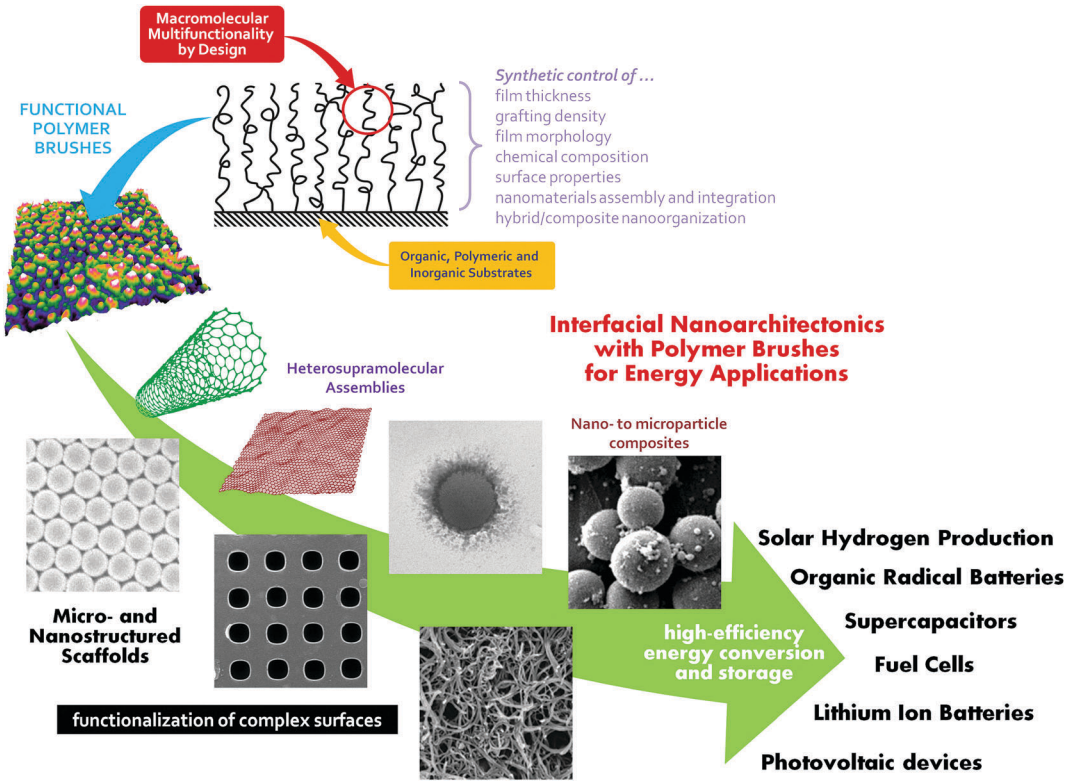


Fig. 2 Conceptual illustration describing the combination of polymer brushes with different nanomaterials and nanostructured platforms as strategy associated to the molecular/nanoarchitectonic design and construction of highly efficient energy conversion and storage devices.

mediators and catalysts. Additionally, the strong interfacial confinement derived from densely grafted polymer changes may facilitate the hopping of electrons or the transport of ions, which are advantageous for photovoltaic and electrochemical devices. We should bear in mind that in confined spaces the polymer segments are in close interaction with the surface, thereby leading to significant changes in their properties, including chemical reactivity, macromolecular organization and dynamics.

As follows from the above considerations, ample possibilities exist for the practical application of polymer brushes in the design of energy storage and conversion devices. In view of the recent progress in the practical use of polymer brushes as building blocks to increase the efficiency of energy conversion and storage devices, this review is specifically aimed at providing exposure of the emerging applications of these macromolecular systems as key structural and functional units in solar cells, solar fuel production, organic radical batteries, photoelectrochemical cells, lithium-ion batteries, supercapacitors and fuel cells.

## Proton exchange membranes

Proton exchange membrane fuel cells (PEMFCs) continue to be at the forefront of alternative energy technologies.[44] These electrochemical systems, that consume hydrogen or methanol to generate electricity, are clean energy sources capable of reaching high-power density and efficiency with low emission levels. For these reasons, PEMFCs are excellent candidates for various purposes, including electric vehicles, portable devices or even power stations for home use. Although fuel cell technologies have been known to industry from a long time, technological progress and sustained investment in this research field over the last decade made possible the fabrication and commercialization of low-cost fuel cell devices.[45] In addition, important technical advances in materials science facilitated the construction of PEMFCs with lowered amounts of precious metals, thus making fuel cells a dynamic and vibrant area also in the energy marketplace.

Historically, perfluorinated polyelectrolytes, such as Nafion, have been the "golden standard" for preparing proton exchange membranes.[46] In the case of Nafion, phase segregation between hydrophobic and hydrophilic domains is responsible for generating hydrophilic, proton-conducting ionic nanochannels decorated with sulfonic groups.[47] However, these perfluorinated polymers are costly to produce, lack mechanical strength and, more importantly, their proton-conducting characteristics are highly dependent on the humidity. For instance, dehydration of Nafion in low humidity conditions triggers the collapse of the physical architecture of the membrane, affecting the dimensional stability of the proton conducting channels and leading to a significant loss of conductivity.

In this context, different research groups resorted to polymer brushes as key elements to find new technologies enabling the facile and low-cost production of efficient proton conducting platforms.

On that premise, Azzaroni and his collaborators[48] proposed an approach to prepare robust proton conducting membranes based on the use of ordered two-dimensional macroporous silicon membranes functionalized with poly(sulfopropyl methacrylate) brushes (Fig. 3A). The silicon hybrid membranes were fabricated through pore-confined surface-initiated atom transfer radical polymerization and led to proton exchange membranes displaying proton conductivities in the range of $10^{-2}$ S $cm^{-1}$. This strategy relies on the formation of a well-defined polyelectrolyte environment inside a robust rigid scaffold in order to avoid structural transformations of the conducting channels under varying humidity conditions (Fig. 3B).[49] In principle, polyelectrolyte domains decorated with sulfonate groups are ideal to create hydrophilic channels in PEMs; however, dehydration at low relative humidity (RH) is still a major problem promoting a marked decrease in the proton conductivity. These authors demonstrated that this problem can be easily circumvented by means of adding PEGylated monomers (monomers with polyethylene glycol side chains) to the poly(sulfopropyl methacrylate) brushes.[50] By simply copolymerizing sulfopropyl methacrylate (SPM) and monomethoxy oligo-(ethylene glycol)-methacrylate (MeOEGMA) in a 10 : 1 monomer ratio, proton-conducting membranes with outstanding properties were prepared (Fig. 3C and D). In these systems, PEGylated co-monomers exhibiting excellent hydroscopic properties are responsible for retaining water molecules in the macromolecular environment through hydrogen bonds with the ethylene oxide units of the polymer brushes.

The construction of proton conducting membranes using a rigid scaffold presenting aligned nanochannels has been also explored by Fang *et al.*[51] through the integration of poly (sodium 2-acrylamino-2-methylpropane sulfonate) (PAMPS) brushes into $TiO_2$ nanotube array membranes *via* surface-initiated free radical polymerization. The implementation of this "grafting from" approach facilitated the control over the degree of polymer filling of the nanoporous membrane. These authors observed that, for temperatures below 120 °C, proton conductivities for both partially and fully filled $TiO_2$ membranes are almost the same. Control experiments confirmed that proton conductivity of PAMPS-modified membranes is significantly higher than that of the unmodified $TiO_2$ aligned nanoscaffold. These experimental observations might suggest that the proton conductivity within this temperature range is largely dominated by the ionic segments close to thepolymer–$TiO_2$ interface. Then, impedance studies indicated that parity between conductivity values of both partially and fully filled nanomembranes no longer applied once the temperature increases to 140 °C. At this temperature, the proton conductivity of fully

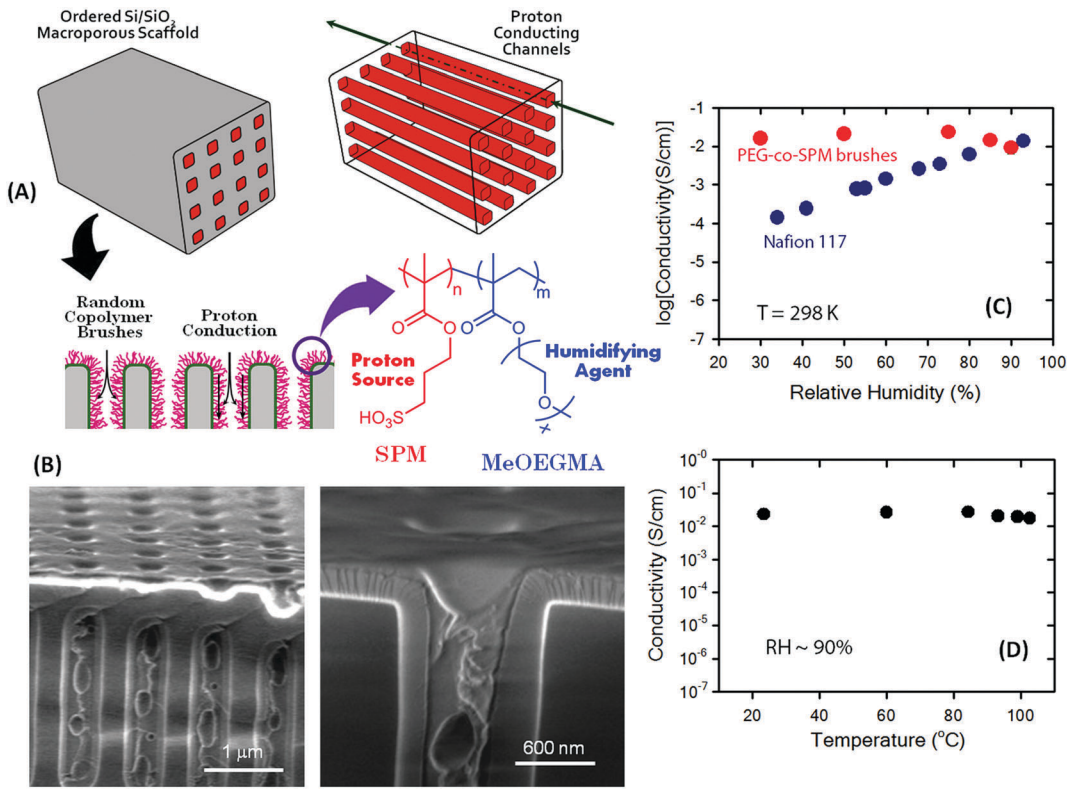


Fig. 3 (A) Illustration of the ordered two-dimensional macroporous silicon membrane modified with the polymer brushes. The cartoon also depicts chemical structure of the random copolymer polySPM-*co*-MeOEGMA brushes grown inside the membrane pores. (B) Scanning electron micrographs corresponding to the silicon membrane modified with polySPM-*co*-MeOEGMA brushes. (C) Proton conductivity as a function of relative humidity for the silicon membrane modified with polySPM-*co*-MeOEGMA brushes and a Nafion 117 membrane. (D) Proton conductivity as a function of temperature for a silicon membrane modified with polySPM-*co*-MeOEGMA brushes. Reproduced with permission from Yameen *et al.*, *Angew. Chem., Int. Ed.*, 2009, **48**, 3124. Copyright 2009 Wiley-VCH Verlag GmbH & Co. KGaA.

 

filled PAMPS-modified membranes ($1.25 \times 10^{-1}$ S cm$^{-1}$) is almost 30% higher than that of partially filled $TiO_2$ scaffolds.

In the same spirit, Zharov and co-workers[52] prepared proton-conducting membranes through the modification of mesoporous silica colloidal membranes with polymer brushes[53,54] exhibiting different degrees of sulfonation thus providing proton conductivity. In this interesting approach, the assembled colloidal scaffold not only provides mechanical and structural stability but also defines the network of interconnected mesopores.

Colloidal membranes modified with copolymer brushes of 3-sulfopropylmethacrylate (SPM) and 2-ethoxy-ethylmethacrylate (EEMA) exhibited a sigmoidal dependence of the proton conductivity on the content of sulfonic acid groups. In particular, proton conductivity of the polymer brush-modified membrane does not increase significantly after reaching *ca.* 75% sulfonic acid group content. This behavior has been interpreted considering that the ion-rich clusters become interconnected when sulfonic acid groups constitute 50–60% of the monomer units, leading to a sharp increase in proton conductivity. Proton conductivity measured for colloidal membranes modified with pure SPM brushes was 10.7 mS cm$^{-1}$, this being a value comparable to that of Nafion. Noteworthy, fuel cell performance decreased after increasing the content of sulfonic acid groups in the copolymer brushes beyond 65–70%. This observation has been ascribed to the influence of the sulfonic acid group content on the methanol permeability of the membranes which in turn affects the performance of the direct methanol fuel cell.

On the other hand, the formation of composites integrating halloysite nanotubes (HNTs) modified with poly(sodium styrenesulfonate) brushes (SHNTs) into chitosan (CS) matrices has been proposed as a plausible strategy to fabricate hybrid membranes exhibiting enhanced proton conduction properties (Fig. 4A).[55] In these systems, the strong electrostatic interactions between the anionic nanotubes and the cationic polymer matrix enhances the thermal and mechanical stability of membranes while, at the same time, the high aspect ratio of the nanotubes decorated with polyanionic brushes facilitates the formation of continuous pathways for proton hoping, thus conferring enhanced proton transfer properties to the nanocomposite. Fig. 4B shows the differences between chitosan

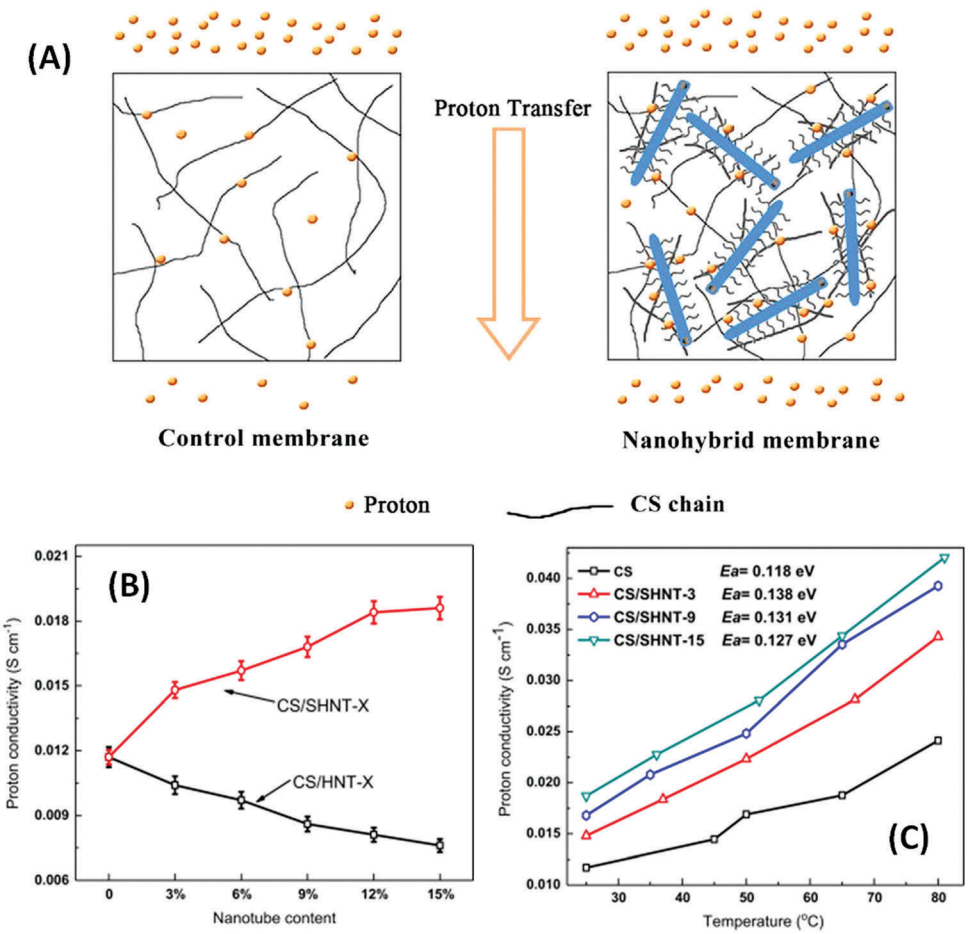


Fig. 4 (A) Schematic depiction of the nano/microstructure of CS/SHNT-*X* nanohybrid membranes. (B) Proton conductivity as a function of the nanofiller content (HNT-*X* and SHNT-*X*) measured at 25 °C and 100% RH. (C) Temperature-dependent conductivity of CS control and nanohybrid membranes at 100% RH. The nanomembranes are designated as CS/HNT-*X* or CS/SHNT-*X* representing HNTs or SHNTs as the nanofillers, where *X* (*X* = 3, 6, 9, 12, or 15) represents the weight percentage of nanotubes to CS. Reproduced with permission from Bai *et al.*, *J. Membr. Sci.*, 2014, **454**, 220. Copyright 2014 Elsevier B.V.

membranes loaded with unmodified HNTs and SHNTs. Increasing the HNT content from 3% to 15% leads to decrease in proton conductivity from 0.0104 to 0.0076 S $cm^{-1}$. This observation has been ascribed to a decrease in water uptake (decrease in proton carriers and H-networks) and a decrease in the ion exchange capacity (reduction of proton-hopping sites). On the contrary, the incorporation of SHNTs results in a significant increase in proton conductivity; *e.g.*: 26.5% proton conductivity enhancement is achieved when loading 3% SHNTs into the CS membrane. These unique proton transport properties stemming from the integration of polymer brushes on the HNTs have been attributed a combination of factors. These include: (a) the formation of sulfonic acid-amide acid–base pairs that create low-barrier proton-hopping sites, (b) the high aspect ratio of nanotubes that creates long-range uninterrupted pathways for proton transport, and (c) the insertion of long polyelectrolyte brushes into the CS matrix to increase the population of proton exchange sites. Fig. 4C shows the temperature-dependent conductivity curves of nanohybrid membranes under 100% RH. It is observed that CS/SHNT-*X* nanomembranes display much higher activation energy ($E_a$) values (ranging 0.127–0.138 eV) as compared to CS control membranes. The enhancement in proton conductivity accompanied with an increase in $E_a$ strongly suggests that the proton transfer mechanism in the CS matrix is altered upon incorporation of the nanotubes modified with the sulfonated polymer brushes.

An analogue strategy based on brush/titanate nanotube composites was adopted for constructing proton conducting platforms with good proton conductivity properties even under low humidity conditions.[56] Electrochemical impedance spectroscopy measurements performed at 60 °C of composite membranes constituted of titanate nanotubes functionalized with PAMPS brushes revealed that proton conductivity responds markedly to changes in relative humidity from 0 to 30%. Proton conductivity increased from $1.28 \times 10^{-3}$ to $5.21 \times 10^{-3}$ S $cm^{-1}$ with increasing relative humidity from 0 to 30% and remained constant under higher humidity levels. It is interesting to note that a comparison of proton conductivities under the same conditions for PAMPS brushes–titanate nanotubes composites, pristine PAMPS polymer samples and a physical mixture of PAMPS polymer and titanate nanotubes clearly indicates that the higher conductivity values are obtained when PAMPS chains are covalently grafted on the nanomaterial. Hence, as already discussed above, these results might reinforce the idea that proton conductivity is strongly influenced by the characteristics of the polymer–$TiO_2$ interface. In this sense, the covalent formation of PAMPS brushes on the titanate nanotubes promotes the intimate contact between the polymeric and inorganic counterparts with the concomitant favorable effect on the proton conductivity. At the same time, the strong confinement of the densely grafted hydrophilic PAMPS chains favors the retention of water, decreases the stringent humidity requirements and shifts to less demanding conditions for proton transport. As expected, the grafting density and the molecular weight of grafted PAMPS brushes have strong effects on the proton conductivity of the nanoarchitectured composite. An increase in grafting density promotes an increase in proton conductivity due to a decrease in the proton hopping distance between sulfonic acid groups in neighboring polyelectrolyte chains. However, further increase in the grafting density promotes conformational constraints in the polyelectrolyte chains; and the decreased flexibility of the macromolecular environment increases the resistance to proton transport. Similarly, the effect of the molecular weight of the grafted PAMPS chains on the proton conductivity also exhibits a non-monotonic behavior. Proton conductivity initially increases and then decreases upon increasing the molecular weight of the grafted polyelectrolyte chains due to conformational constraints imposed by the increasing chain length that ultimately hamper the proton hopping within the polymer brush.[57]

Under a different design approach, Yameen and co-workers[58] put forward the use of $SiO_2$ nanoparticles functionalized with poly(monomethoxy oligoethylene glycol methacrylate) (PMeOEGMA) brushes as humidifying nano-additives for the construction of nanocomposite Nafion membranes (Fig. 5A). In this strategy, $SiO_2$ nanoparticles are first modified with (PMeOEGMA) brushes through surface initiated atom transfer radical polymerization (SI-ATRP) and then dispersed in a Nafion solution prior to forming the nanocomposite membrane *via* solution casting. Electrochemical impedance characterization revealed that simple addition of 1 wt% PMeOEGMA brushes–$SiO_2$ NP nanocomposites to Nafion membranes is enough to promote significant performance improvement. For instance, the nanocomposite Nafion membrane with 1 wt% of PMeOEGMA brushes–$SiO_2$ NP nano-additive underwent an increase in proton conductivity by one order of magnitude at 20% RH and 25 °C. These authors showed that even under increasing temperature conditions the proton conductivity of membranes containing the nano-additives was higher than that of Nafion. By way of example, at a working temperature of 55 °C, the proton conductivity of nano-additive-Nafion composite membranes under 20% RH was ~5.7 times higher than that of Nafion (Fig. 5B).

Concurrently, inspired by the water storage mechanisms in plant cells, Zhang *et al.*[59] proposed the use of hollow polymer microspheres bearing sulfonated polymer brushes as nano-additives to improve the performance of sulfonated poly(ether ether ketone) (SPEEK) proton conducting membranes. The colloidal building blocks were synthesized through SI-ATRP of styrene from $SiO_2$@poly(methacrylic acid-*co*-divinylbenzene-*co*-chloromethyl styrene) core–shell microspheres. The hollow microspheres grafted with sulfonated polystyrene brushes were obtained by sulfonation of the polystyrene brushes, and subsequent removal of the silica core using HF. The hybrid membranes were fabricated by solution casting of a dispersion containing SPEEK and the hollow microspheres in dimethylformamide (DMF). Physical and electrochemical characterizations of pristine and hybrid membranes indicated that water retention, methanol resistance and proton conductivity were increased by incorporation of the polymer microspheres in the SPEEK membrane in the loading range from 2.5 to 15 wt%. For example, the integration of the microspheres (15 wt%) into the

 

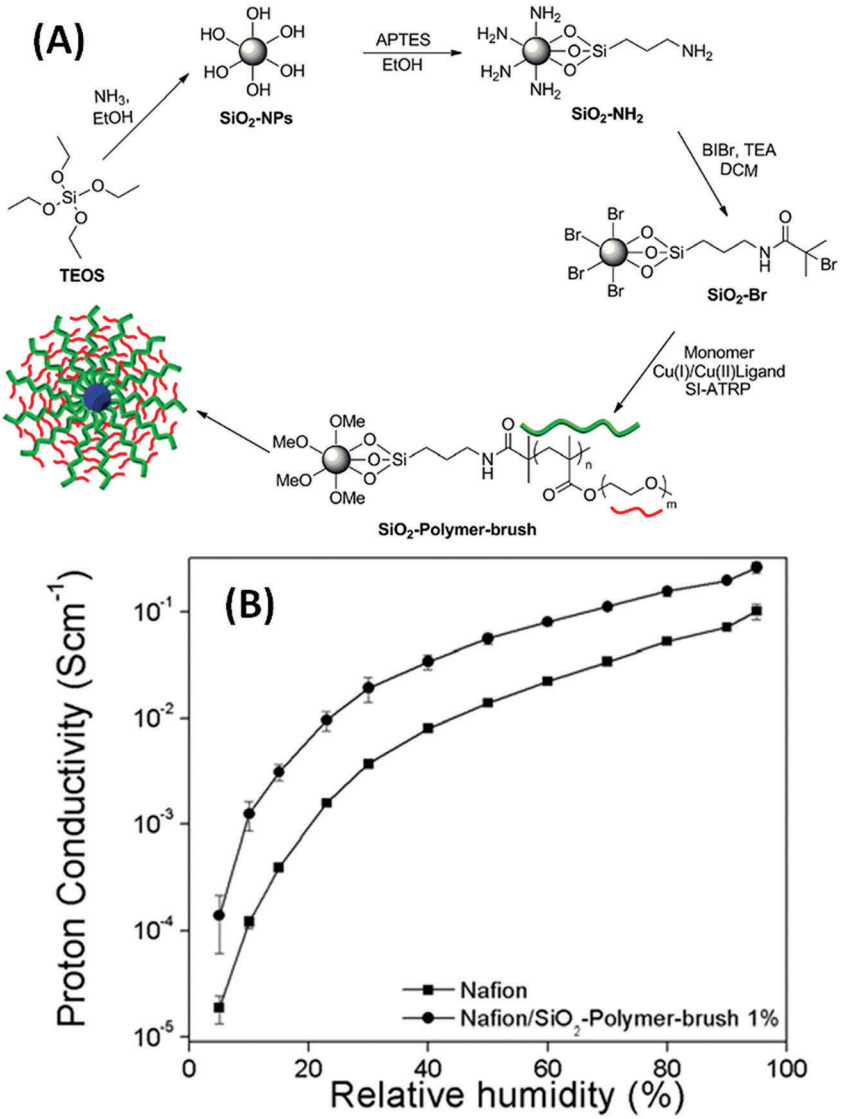


Fig. 5 (A) Schematic illustration describing the polymer brush functionalization of the silica NPs. (B) Proton conductivity as a function of relative humidity for Nafion and Nafion/$SiO_2$–polymer-brush nanocomposite proton exchange membranes at 55 °C. Reproduced with permission Farrukh *et al.*, *Polym. Chem.*, 2015, **6**, 5782–5789. Copyright 2011 Royal Society of Chemistry.

SPEEK membrane resulted in an increase in proton conductivity from 0.18 S $cm^{-1}$ to 0.33 S $cm^{-1}$ when measured at 75 °C and 100% RH. The marked improvement in the performance of the hybrid SPEEK membranes can be interpreted in terms of the functional capability of the hydrophilic microspheres to act not only as water reservoirs located within the membrane environment but also as a highly accessible source of sulfonate groups, thus providing additional proton hopping sites for efficient proton conduction.

As an alternative, the materials science community began to explore the use of carbonaceous nanomaterials functionalized with polymer brushes as building blocks for the fabrication of proton conducting membranes. In this context, several authors showed that the incorporation of carbon nanomaterials, such as carbon nanotubes or graphene, in the polymer matrix can prompt notable and positive effects on the ion conductivity, mechanical strength, and dimensional stability of proton conducting membranes.

Seminal work by Jiang and co-workers[60] demonstrated that the construction of tunable ion-conducting nanochannels *via* direct assembly of graphene oxide (GO) sheets functionalized with cross-linked polyelectrolyte brushes is feasible. Their investigations involved the use GO/poly(vinylphosphonic acid-*co*-ethyleneglycol dimethacrylate) (GO–poly(VPA-*co*-EGDMA)) core–shell nanosheets prepared by surface-initiated precipitation polymerization.

This approach enabled the formation of organized nanochannels with interconnected hydrogen-bonded networks resulting in proton conductivities up to 32 mS $cm^{-1}$ at 51% RH. It is hypothesized that this high proton conductivity is mainly due to the efficient organization of proton carriers across the membrane leading to long-range ionic nanochannels (Fig. 6A).

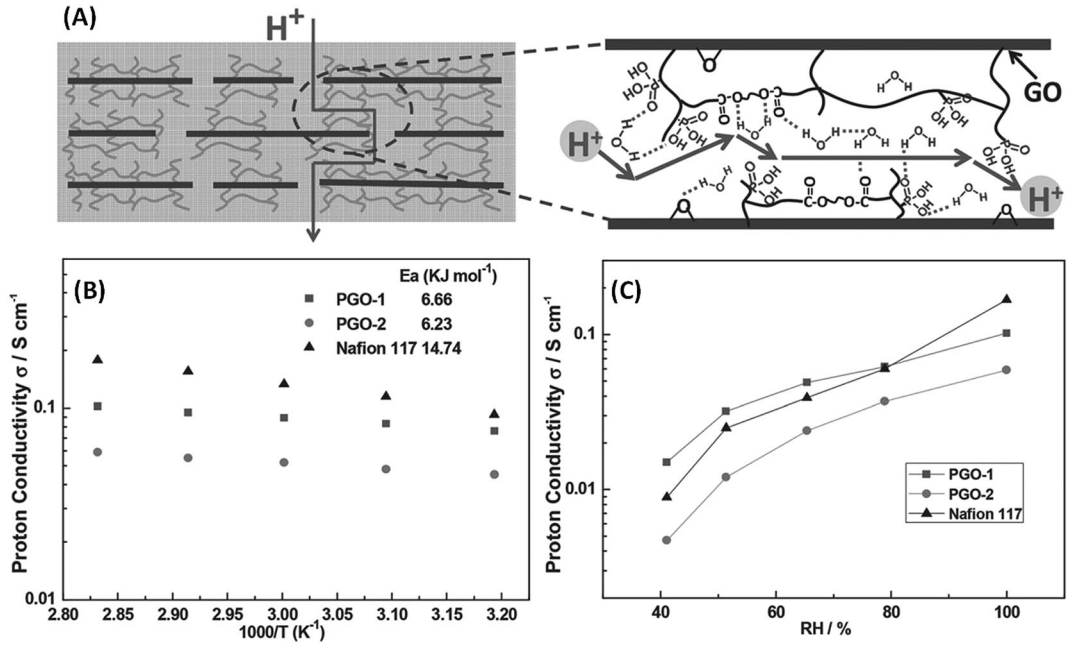


Fig. 6 (A) Cartoon describing the proton transport along the hydrogen-bonded network within the polymer-filled nanochannels. Proton conductivity of GO–poly(VPA-*co*-EGDMA) (PGO) nanosheets and Nafion 117 membranes as a function of temperature at 100% RH (B) and as a function of relative humidity (RH) at 80 °C (C). Note that PGO-2 samples were synthesized by the same procedure and formula as PGO-1 but with shorter polymerization time. Hence, the polymer content is higher in PGO-1 samples. Reproduced with permission from He *et al.*, *Adv. Funct. Mater.*, 2015, **25**, 7502. Copyright 2015 Wiley-VCH Verlag GmbH & Co. KGaA.

The performance of these membranes is comparable to Nafion not only in terms of proton conductivity (Fig. 6B and C), but also in terms of methanol permeability. The in-plane orientation of GO nanosheets, which are impermeable to methanol, together with the surface-grafted polymer networks configure a local environment that is unfavorable for methanol diffusion. Permeability measurements using 2 M methanol indicated that methanol permeability values for GO/poly(phosphonic acid) nanomembranes and Nafion 117 were $4.3 \times 10^{-7}$ and $1.6 \times 10^{-6}$ cm$^2$ s$^{-1}$, respectively.

This concept was further extended by Ahmadian-Alam *et al.*[61] to the preparation of super-acidic polymer/GO hybrid nanosheets through the formation of sulfonated poly(urea-*co*-urethane) brushes on the GO surface. Electrochemical impedance spectroscopy measurements performed at room temperature indicated that anhydrous proton conductivity in these hybrid nanomembranes may be as high as 3.7 mS cm$^{-1}$.

Zhao *et al.*[62] proposed the use graphene oxide functionalized with sulfonic acid-containing polymer brushes (SP-GO) as nanofillers incorporated into sulfonated poly(ether ether ketone) (SPEEK) matrices with the aim of fabricating composite membranes with enhanced proton conducting properties (Fig. 7). The sulfonic brush functionalization of the GO sheets promotes the dispersion of the nanomaterials into the SPEEK polymeric matrix and facilitates the generation of inter-connected ionic pathways through the exposed sulfonic acid groups on the GO surface. The proton transfer channels mainly operate along the SPEEK/SP-GO interface, thereby lowering the proton transfer activation energy and enhancing the proton conductivities of the nanocomposite membranes. Pristine SPEEK membranes exhibit conductivity values close to 0.015 S cm$^{-1}$ at 25 °C and 100% RH, whereas the addition of 2.5 wt% SP-GO to the SPEEK matrix leads to a proton conductivity of 0.0215 S cm$^{-1}$. Proton conductivities can be further enhanced by increasing the length of the grafted chains on the GO surface. As a matter of fact, the use of sulfonated brushes with longer polymer chains led to a 178% increase in anhydrous proton conductivity compared with pristine SPEEK membranes. The reason of this marked conductivity improvement has been ascribed to a combination of factors that include the high aspect ratio of the GO sheets that facilitates the interconnection between ionic clusters, the increased water uptake providing additional proton carriers, and the sulfonated brushes that provide additional pathways for proton conduction.

Recently, this approach was also extended to the use sulfonated poly(arylene ether sulfone) and perfluorosulfonic acid composite membranes containing perfluoropolyether-functionalized GO sheets resulting in proton exchange membranes with improved properties.[63] Wang *et al.*[64] demonstrated that use of acid–base block copolymer brushes constituted of dimethyl vinylphosphonate (DMVP) and vinyl imidazole (VI) blocks grafted on graphene oxide can enhance the proton conduction of SPEEK and chitosan matrices. It was found that the strong electrostatic interactions among the building blocks and the matrix yields long-range interfacial networks that, in turn, lead to a marked enhancement in proton conduction.

The incorporation of graphene oxide modified with polymer brushes constituted of sulfopropyl methacrylate and

 

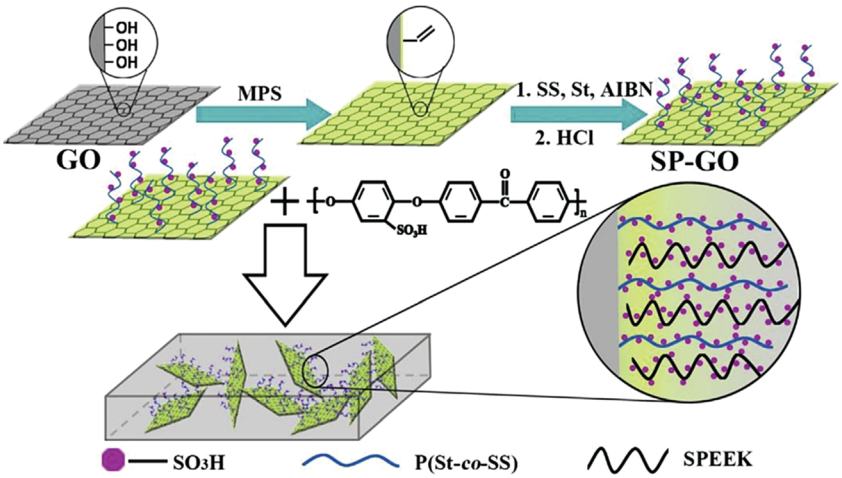


Fig. 7 Schematic illustration describing the preparation of sulfonated poly(ether ether ketone) (SPEEK) matrices incorporating graphene oxide functionalized with sulfonic acid-containing polymer brushes (SP-GO) as nanofillers. MPS: 3-(methacryloxy)propyltrimethoxysilane. St: styrene. AIBN: 2-azobisisobutyronitrile. SS: sodium-*p*-styrenesulfonate. Reproduced with permission from Zhao *et al.*, *J. Power Sources*, 2015, **286**, 445–457. Copyright 2015 Elsevier B.V.

poly(ethylene glycol) methyl ether methacrylate (GO–poly(SPM-*co*-PEGMEMA)) in a Nafion matrix also resulted in an enhancement of the proton conductivity (Fig. 8A).[65] In these composites the sulfonic moieties in the polymer brushes promote the generation of efficient pathways for proton conduction at the Nafion–GO interface and provide additional proton binding sites to facilitate the proton hopping through the matrix (Fig. 8B). At the same time, the hygroscopic PEGylated segments increase the water retention properties of the membrane, thereby improving the proton conduction properties at low humidity. With 1 wt% GO–poly(SPM-*co*-PEGMEMA) loading, the composite Nafion membrane exhibited an increase in proton conductivity by one order of magnitude compared to pristine Nafion, whereas the peak power density increased by 135.5% (Fig. 8C). These results illustrate the great potential of these systems for fuel cell applications.

More recently, Rao and co-workers[66] explored the application of polymer brushes in the synthesis of proton conducting hybrids with strong bonds generated through covalent cross-linking. The authors showed that with the aid of functional polysiloxane brushes grafted on GO sheets, the cross-linking density of the nanocomposite sulfonated polysulfone (SPSU) membrane can be manipulated by simply controlling the amount of polymer brush–GO hybrids incorporated into the membrane. The presence of the polysiloxane brushes reduces the aggregation of the inorganic filler into the polymer matrix and improves the interfacial interactions between polymer and inorganic counterparts with the concomitant positive effects on methanol permeability and proton conductivity. These cross-linked hybrid membranes display conductivity values up to 0.462 S $cm^{-1}$ at 90 °C under hydrated conditions together with low methanol permeability characteristics ($1.71 \times 10^{-6}$ $cm^2$ $s^{-1}$ at 30 °C). The use of carbonaceous nanomaterials modified with functional polymer brushes as nanofillers in proton conducting membranes has not been exclusively circumscribed to the use of graphene. Similar conceptual approaches have been explored using polymer brush–carbon nanotube hybrids as building blocks in composite membranes resulting in nano-architectured systems displaying excellent water-retention properties and enhanced proton conductivities.[67]

## Composite polymer electrolytes for lithium batteries

Polymer electrolytes (PEs) are playing an increasingly important role in most energy storage/conversion devices, and particularly in lithium-ion batteries.[68] The electrolyte is a key component of the battery with a strong influence on the cell capacity, the operation conditions and the cyclability.[69] Even though liquid electrolytes exhibit high ionic conductivities, serious safety issues associated with the leakage of electrolytes and the exposure to lithium metal electrodes have hampered the widespread use of lithium-ion batteries based on liquid electrolytes. Within this framework, polymer electrolytes[70] emerged as a plausible alternative to liquid electrolytes due to some interesting advantages that include good resistance to volume changes during the charge/discharge process, design flexibility, better processability and, which is more important, improved safety characteristics. In a seminal work, Sato and his collaborators[71] introduced an innovative idea for fabricating leak- and vapor-free, solid electrolytes displaying highly ion-conductive network channels. Their strategy was based on the three-dimensional assembly of silica particles modified with ionic liquid-type polymer brushes (Fig. 9A–C).

In these 3D nanoarchitectures, polymer brushes give rise to domains that are continuously connected forming network channels responsible for the ionic conduction. Integration of this polymer electrolyte hybrid nanoarchitecture into a bipolar lithium-ion rechargeable battery (Fig. 9D) led to a unit cell

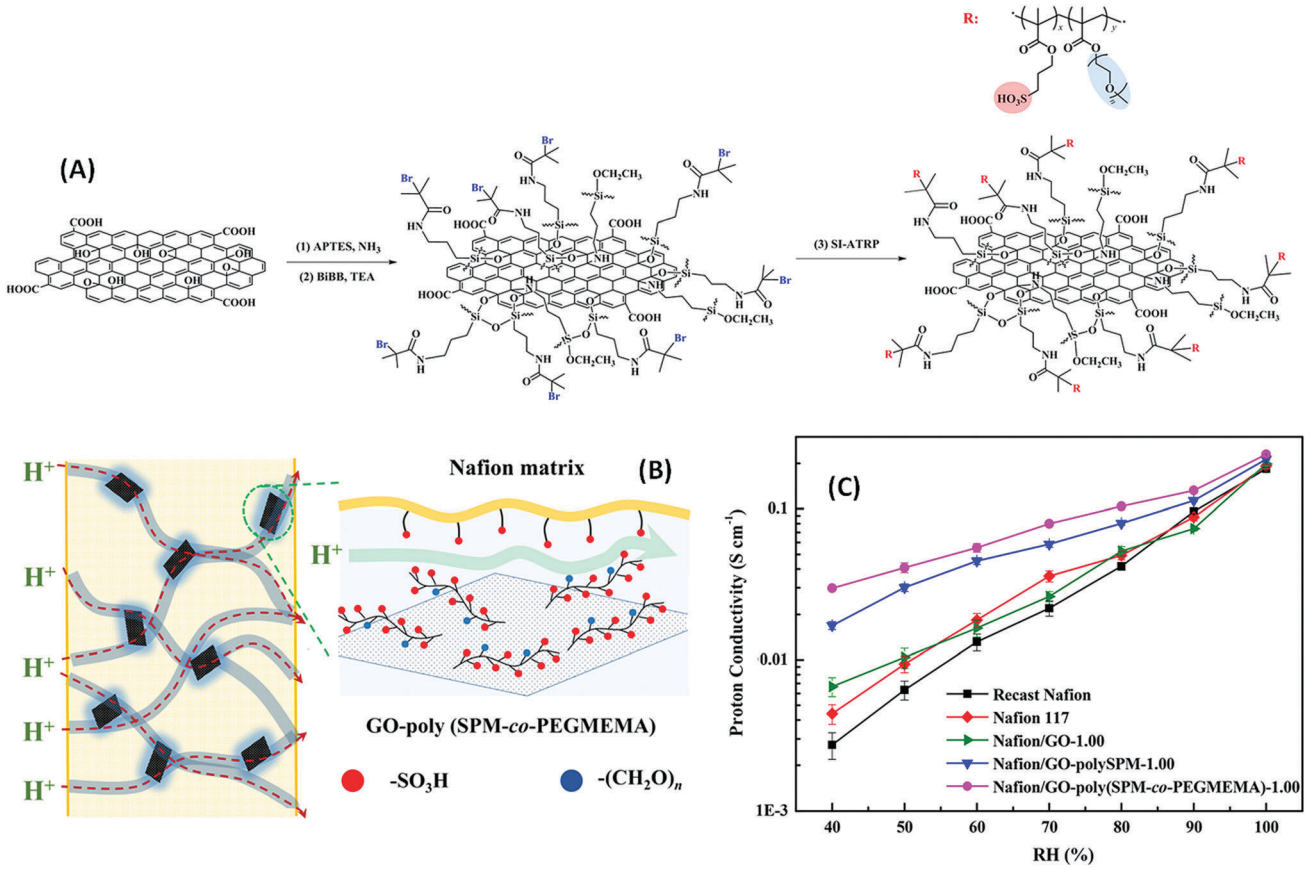


Fig. 8 (A) Modification of GO nanosheets with copolymer brushes. (B) Schematic depiction of the Nafion/GO–poly(SPM-*co*-PEGMEMA) membrane and the hydrophilic proton conducting pathways inside the composite system. (C) Proton conductivity as a function of relative humidity corresponding to Nafion-based GO–brush composite membranes, recast Nafion and Nafion 117 at 80 °C. Reproduced with permission from He *et al.*, *ACS Appl. Mater. Interfaces*, 2017, **9**, 27676. Copyright 2017 American Chemical Society.

exhibiting a discharge specific capacity and Coulombic efficiency of 2.3 mA h and 95%, respectively, at the fifth charge and discharge operation cycle. The Coulombic efficiency after 50 cycles was 98% (Fig. 9E). The same group further extended this concept to the modification of silica particles with other ionic liquid-like polymer brush, *N*,*N*-diethyl-*N*-(2-methacryloylethyl)-*N*-methylammonium bis(trifluoromethylsulfonyl)imide (DEMM-TFSI).[72] Interestingly, these authors observed a correlation between the chain length, *i.e.*: molecular weight, of the grafted polymer brush and the ionic conductivity. Composite films made from crystal-like hybrid polymer brush/silica particles having long polymer brushes do not exhibit high ionic conductivity properties due to the entanglement of the polymer chains, thus precluding the formation of effective ion-conducting paths in the matrix. However, on the other hand, 3D hybrids decorated with relatively short polymer brushes displayed high ionic conductivity values resulting from the formation of an optimum 3D conductive path in the hybrid polymer–silica matrix.

Applying a similar approach, Wang *et al.*[73] modified $SiO_2$ particles with poly(*p*-vinylbenzyl) trimethylammonium tetrafluoroborate (P[VBTMA][BF4]) brushes with the aim of creating core–shell structured nanocomposite solid-state polyelectrolytes using nanosilica as rigid scaffolds. Systematic studies were undertaken in order to establish the optimum composition of the solid-state nanocomposite. In this way, electrochemical impedance measurements confirmed that $SiO_2$–(P[VBTMA][BF4]) nanocomposites with a polymer brush content of 47% exhibited the highest ionic conductivity values at room temperature, 104 mS $cm^{-1}$.

It is noteworthy that $SiO_2$–P[VBTMA][BF4] nanocomposites with different contents of P[VBTMA][BF4] brushes display higher ionic conductivity than the pure polymer (P[VBTMA][BF4], 18.6 μS $cm^{-1}$), even though the conductivity decreases upon increasing the polymer brush content above 47%. These results have been interpreted in terms of the highly conductive layer formed at the polymer–silica interface. As the P[VBTMA][BF4] brush grows up on the silica surface, the population of ionic carriers increases, the ionic channels become wider and the ionic conductivity increases. However, after certain polymerization time, further polymer brush growth leads to a decrease in the fraction of the highly conductive layer with the concomitant decrease in the ionic conductivity of the $SiO_2$–P[VBTMA][BF4] nanocomposite.

In a similar vein, Liu and coworkers proposed the construction of composite polymer electrolytes for lithium batteries through the modification of silica particles with copolymer

 

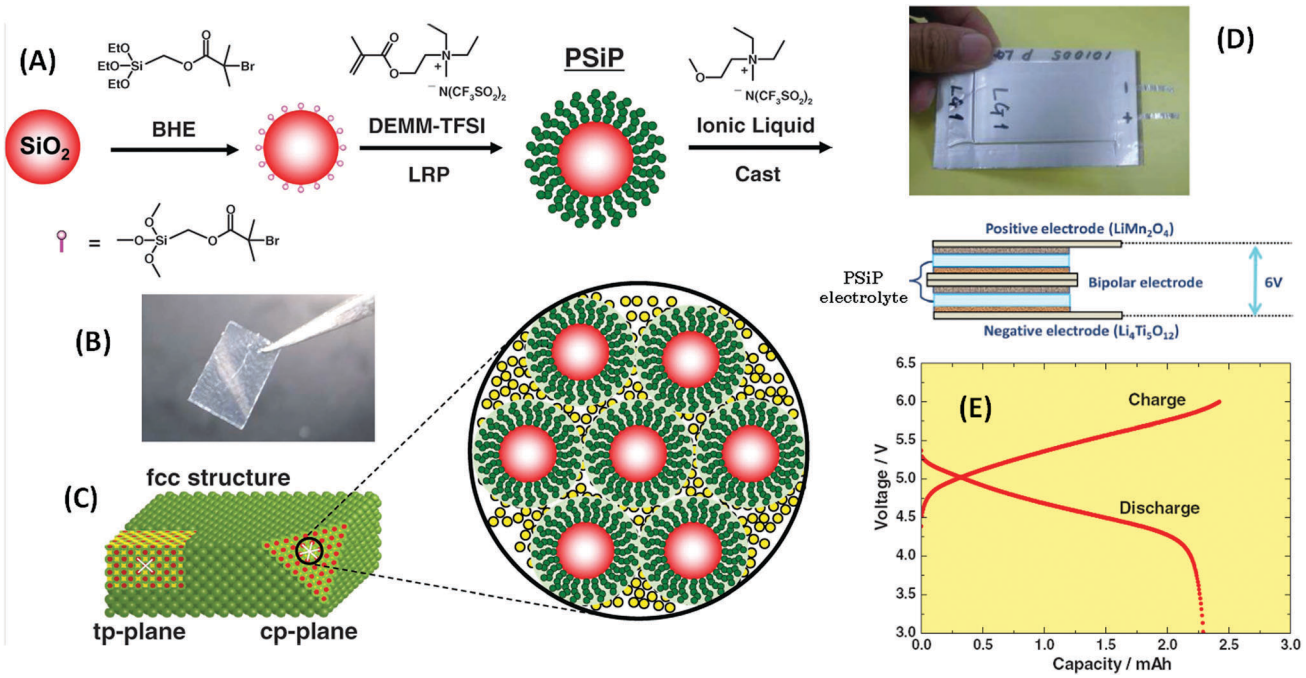


Fig. 9 (A) Scheme illustrating the preparation of the nanostructured hybrid solid-state electrolyte through the three-dimensional assembly of silica particles modified with ionic-liquid polymer brushes (PSiPs). (B) Photograph and (C) structure of PSiP arrays in the solid state. (D) Photograph and illustration of bipolar-cell structure. (E) Charge/discharge curve of a lithium-ion battery using PSiP/IL solid electrolyte. Reproduced with permission from Sato *et al.*, *Adv. Mater.*, 2011, **23**, 4868. Copyright 2011 Wiley-VCH Verlag GmbH & Co. KGaA.

brushes (Fig. 10A).[74] In principle, the integration of anionic groups into the polymer brush backbone would help limit the anion mobility, thus prompting an increase in the lithium transference number. However, composite nanoparticles grafted by poly(lithium 4-styrenesulfonate) brushes only exhibited moderate conductivity values. This observation was ascribed to the entrapment of the lithium ions inside the dense polyelectrolyte brushes that, in turn, limits the overall ionic conductivity. On the other hand, composite polymer electrolyte constituted of poly(ethylene oxide)methacrylate-*co*-poly(styrene sulfonate) copolymer brushes equipped with long poly(ethylene oxide) (PEO) side chains led to a marked increase in conductivity ($\sim 10^{-6}$ S cm$^{-1}$) (Fig. 10B). According to Schaefer *et al.*[75] tethered PEG chains can facilitate the dissociation between lithium cations and sulfonate groups, thus explaining the improvement in conductivity when PEO chains are incorporated in the anionic polymer brushes.

Within this framework, the assembly of PEG brushes on mesoporous silica particles has been devised as a plausible route for developing nanohybrid solid polymer electrolytes.[76] The proposed route relied on the dual functionalization of the mesoporous framework with (2-[(trifluoromethanesulfonyl-imido)-*N*-4-sulfonylphenyl]ethyl)trimethoxysilane (TMS-TFSISPE) and [methoxy(polyethyleneoxy)propyl] trimethoxysilane (TMS-PEO). This functionalization promotes the weak coordination and the solvation of $Li^+$ ions by the anionic sulfo-imide groups and the PEG chains, respectively. The presence of PEO brushes on the silica surface facilitates the dispersion of the mesoporous silica nanoparticles into the polymer PEO matrix. The flexibility of the PEO chains plays a determinant role in the ion conduction properties of the polymer matrix provided that the inherent crystallinity of PEO segments has a deleterious effect on long-range ion transport. For this reason, the inclusion of the mesoporous silica nanoparticles co-grafted with PEG brushes into the PEO polymer matrix has been employed as a strategy for preventing PEO chains from crystallization, thereby promoting an enhancement of the ionic conductivity. In fact, the formation of crystalline domains is fully suppressed by simply adding 1 wt% PEG-modified silica particles to the PEO matrix. The incorporation of the hybrid silica particles into the PEO matrix not only confers exceptional ionic conductivity properties but also improves the mechanical properties of the solid polymer electrolyte. The ionic conductivity of nanohybrid electrolytes containing 30 wt% brush-coated particles was $10^{-3}$ S cm$^{-1}$ at 25 °C, whereas under similar conditions, the ionic conductivity of the same PEO matrix in the absence of nanoparticle additives was $\sim 2 \times 10^{-5}$ S cm$^{-1}$. This strong conductivity enhancement (two orders of magnitude) has been attributed to the large amount of lithium charge carriers provided by the TFSISPE groups hosted in the inner mesoporous environment of the silica particles and the presence of PEG brushes that favor the solvation and displacement of $Li^+$ ions across multiple sites in the hybrid matrix.

Another interesting strategy to create composite polymer electrolytes for lithium batteries relies on the use of graphene sheets modified with polymer brushes. Shim *et al.*[77] demonstrated that a series of conducting nanocomposites can be readily prepared by combining an organic/inorganic hybrid

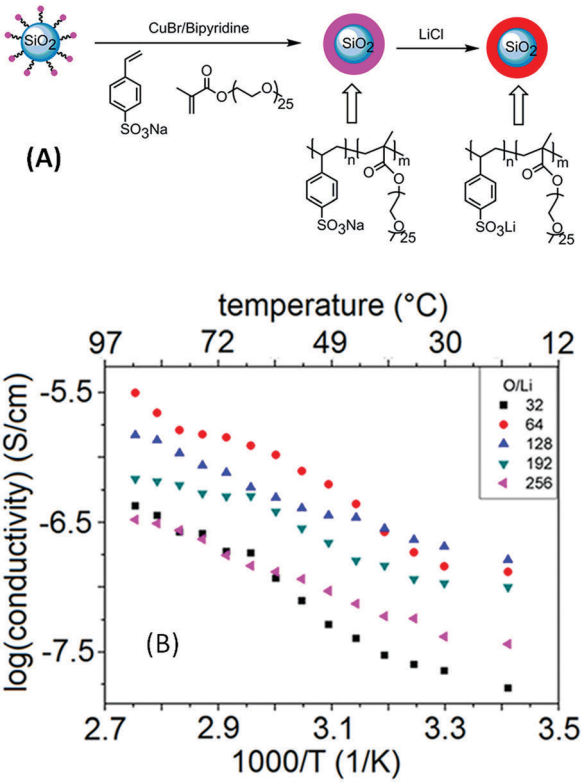


Fig. 10 (A) Scheme describing the synthesis of poly(sodium 4-styrenesulfonate) brushes on silica particles (Si-PSSNa) and the corresponding lithiation process yielding Si-PSSLi. (B) Temperature dependence of ion conductivity for Si-PSSLi–PEGMA/PEGDME electrolytes at different O/Li ratios. Reproduced with permission from Zhao *et al.*, *ACS Appl. Mater. Interfaces*, 2015, **7**, 19335–19341. Copyright 2015 American Chemical Society.

branched-graft copolymer (BCP) and graphene oxide modified with poly(ethylene glycol) brushes (PGO) as the polymer matrix and the filler material, respectively. In this case, the hybrid branched-graft copolymer was constituted of poly(ethylene glycol) methyl ether methacrylate (PEGMA) and 3-(3,5,7,9,11,13,15-heptaisobutylpentacyclo-[9.5.1.13,9.15,15.17,13]octasiloxane-1-yl)-propyl methacrylate (MA-POSS). Electrochemical characterization performed at 30 °C revealed that the ionic conductivity of the composite polymer electrolyte containing 0.2 wt% of PGO was one order of magnitude higher than that of BCP ($2.1 \times 10^{-4}$ and $1.1 \times 10^{-5}$ S cm$^{-1}$, respectively). The improvement in the ionic conductivity has been ascribed to the Lewis acid–base interaction between the PGO and the lithium salt, resulting in a larger amount of lithium salt that can be dissociated in the composite polymer matrix. Noteworthy, the incorporation of graphene oxide modified with poly(ethylene glycol) brushes not only increases the ionic conductivity but also improves the thermal and mechanical stability of the composite polymer electrolytes. Performance evaluation of lithium-ion batteries showed that the electrochemical systems equipped with composite polymer electrolytes containing 0.2 wt% of PGO resulted in better cycling performance as compared with pristine BCP polymer matrix, owing to the lithium-conducting pathways provided by the PGO building blocks.

Along similar lines, Ye *et al.*[78] demonstrated that the lithium salt dissociation, the content of amorphous phase and the segmental mobility in solid state polymer electrolytes can be significantly improved by employing graphene functionalized with ionic liquid-like polymer brushes (PIL(TFSI)-FG) as nanofillers incorporated in PEO/Li$^+$ polymer electrolytes. These authors showed that the addition of PIL(TFSI)-FG in PEO/Li$^+$ matrices favors the dissociation of the lithium salt and suppress the formation of crystallized PEO domains. Indeed, the incorporation of graphene functionalized with polymer brushes results in a significant increase in Li ion conductivity of PEO/Li$^+$ systems by $>2$ orders of magnitude and $\sim$20-fold at 30 °C and 60 °C, respectively. In this regard, differential scanning calorimetry characterization confirmed that PEO/Li$^+$/PIL(TFSI)-FG-brush composites exhibited higher segmental mobility suggesting that the addition polymer brush-functionalized graphene plays a key role in facilitating the movement of chains and creating a dynamic, disordered polymeric environment that ultimately leads to an increase in conductivity. It is evident that this improvement in ionic conductivity has concomitant effects on the battery performance. As a matter of fact, the discharge capacity of a Li/PEO–Li$^+$/LiFePO$_4$ cell measured at 0.1C and 60 °C during cycling shows a significant improvement from 120 to 156 mA h g$^{-1}$ after adding 0.6 wt% of polymer brush-FG to the PEO–Li$^+$ polymer electrolyte.

The experimental results discussed in this section suggest that polymer brushes can play a decisive role in defining the structural, morphological and functional properties of composite polymer electrolytes and, concomitantly, lead to new ways of improving the electrochemical performance of lithium-ion batteries.

## High-capacity anodes for lithium-ion batteries

One of the most urgent challenges in materials science is the development of new lithium-ion batteries exhibiting enhanced capacity and cycling stability.[79] The main strategy to reach that goal is to design hybrid anode materials equipped with dual capabilities: (i) ample availability of active sites, and (ii) structural adaptability to volume changes during the charging/discharging process.[80] In this context, graphene sheets with high conductivity, excellent mechanical flexibility and ultra-high specific surface area is generally considered as an excellent candidate for enduring the strain caused by volume changes.[81] At the same time, the assembly of graphene sheets also provides conducting networks that help in boosting the electrochemical performance of the electrode.[82] In particular, the use of graphene paper[83] prepared by vacuum filtration-induced directional flow assembly is gaining acceptance as a promising substitute for the traditional graphite anode of lithium-ion battery. However, one of the limitations of graphene paper is the low discharge capacity arising from the compact layered structure of the nanostructured system that introduces a kinetic barrier to diffusion of Li ions in and out the anode during the charge–discharge process.

In this regard, it has been shown that polycaprolactone (PCL) brushes grafted onto graphene sheets confer strength and flexibility to the graphene paper.[84] Physical characterization revealed that graphene paper made of PCL–graphene hybrids is 5-fold stronger than paper made of unmodified graphene. In addition, the stabilized discharge capacity of PCL-modified graphene paper is 2.7 times higher than that of an anode made of unmodified graphene paper. These results can be understood if we consider that PCL brushes not only increase the interlayer spacing of the graphene papers but also introduce additional oxygen atoms along the grafted polymer chains, which can interact with incoming Li ions. Or, in other words, PCL brushes provide more active site for Li ions to be hosted in the graphene anode with the concomitant improvement in the anode performance.

## Organic radical batteries

There is currently great interest in broadening the horizons of organic radical batteries (ORBs).[85] Contrary to other electrochemical energy-storage devices, ORBs do not rely on the use of metals, thus lessening the environmental impact of their production. Their operation is based on stable organic radicals displaying an unpaired electron in the ground state. One of the attractive features of these systems is the fact that organic radicals undergo simple redox reactions by only requiring the transfer of a single electron per active site without involving intercalation processes or significant structural changes, as is the case of Li-ion batteries.[86] As a result, ORBs exhibit superior redox kinetics with high electron-transfer rates that, in turn, translates into high charging and discharging currents and, hence, high power densities.[87]

One of the first attempts to optimize the operation of ORBs through the integration of polymer brushes was reported by Lin *et al.*[88] These authors developed nitroxide polymer brushes grafted on silica nanoparticles as binder-free cathodes for ORBs (Fig. 11A). These polymer brushes (PTMA) were constituted of a methacrylate backbone bearing 2,2,6,6-tetramethylpiperidin-1-oxyl-4-yl (TEMPO) groups. TEMPO is a very stable radical that is oxidized to an oxoammonium cation when charging, and the oxoammonium cation is then reduced to a nitroxide radical upon discharging (Fig. 11B).[89] One of the appealing aspects of using polymers brushes grafted on silica particles is that this strategy prevents the electroactive polymer from dissolving into the electrolyte (Fig. 11A), which significantly improves the cycle-life performance of the batteries. In this sense, electrochemical characterization (Fig. 11C) showed that the discharge capacity of the polymer brushes was 84.9–111.1 mA h $g^{-1}$ and the electrodes modified with PTMA brushes had a very good cycle-life performance of 96.3% retention after 300 cycles.

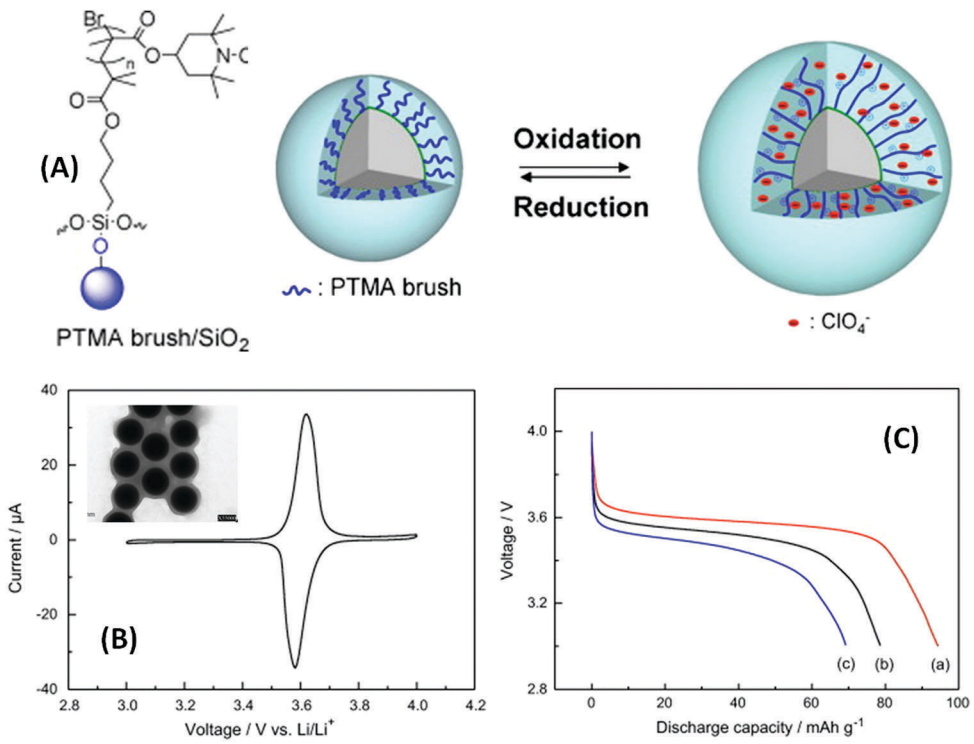


Fig. 11 (A) Nitroxide polymer brushes grafted onto silica nanoparticles as cathodes for organic radical batteries (B) cyclic voltammogram for the PTMA brush/silica nanoparticles (40 nm) composite electrodes in 1.0 M $LiClO_4$ in ethylene carbonate (EC)/diethyl carbonate (DEC) (= 1 : 1, v/v) at a scan rate of 0.1 mV $s^{-1}$ at 25 °C. The inset shows a TEM micrograph for the PTMA brush/silica nanoparticles with a particle size of 400 nm (scale bar = 200 nm). (C) Discharge curves of the PTMA brush/silica nanoparticles (40 nm) composite cathodes in 1.0 M $LiClO_4$ in ethylene carbonate (EC)/diethyl carbonate (DEC) (= 1, v/v) at (a) 10, (b) 30, and (c) 50 C at 25 °C. Reproduced with permission from Lin *et al.*, *J. Power Sources*, 2011, **196**, 8098. Copyright 2011 Elsevier B.V.

Some studies have shown that the thickness of the nitroxide polymer brush has a major influence on the electrochemical properties of the macromolecular assembly.[90] In the case of the oxidation of poly(2,2,6,6-tetramethylpiperidin-4-yl methacrylate) (PTMPM) to PTMA brushes, cyclic voltammetry and impedance spectroscopy indicate that thick brushes ($h > 55$ nm) are not sufficiently oxidized even after 10 min oxidation time. Furthermore, cyclic voltammetry reveals that when the brushes are thicker than 55 nm, the separation of peak potentials ($\Delta E_p$) increases, and the current density is no longer directly proportional to the brush thickness. In a similar vein, electrochemical and X-ray photoelectron spectroscopy also confirmed that prolonged oxidation times promote the over-oxidation of the polymer brush with a concomitant decrease in the energy capacity.

Lee and co-workers proposed the fabrication of electrodes for organic radical batteries using three-dimensionally ordered macroporous polypyrrole architectures modified with polymer brushes (Fig. 12A).[91] The electrodes were ingeniously fabricated

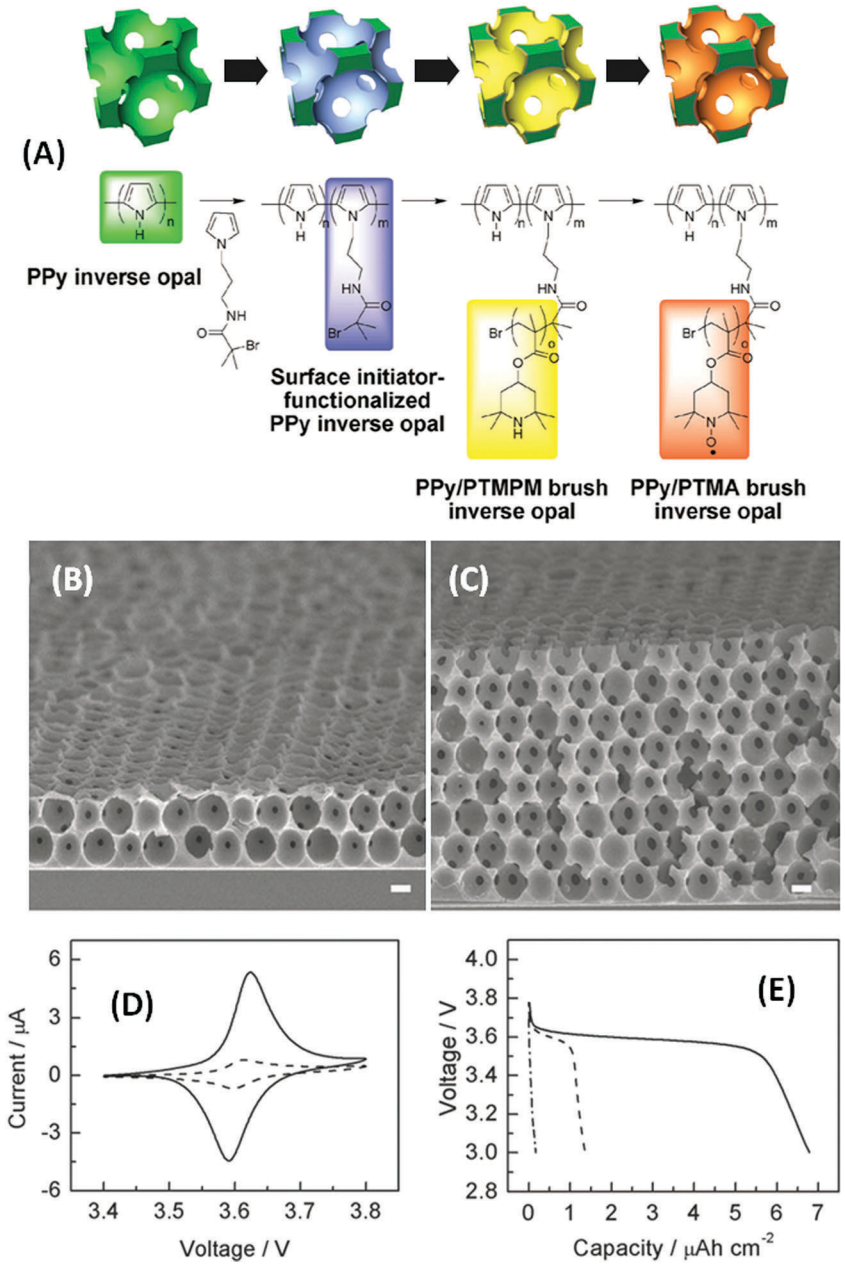


Fig. 12 (A) Schematic illustration describing the construction of the PPy/PTMA brush inverse opal electrode. Scanning electron microscope images displaying the cross section view of PPy/PTMA brush inverse opal electrodes with thicknesses of (B) 3.5 μm and (C) 13.8 μm. Scale bar: 1 μm. (D) Cyclic voltammograms corresponding to a planar PPy/PTMA brush thin-film electrode (dashed line) and a nanoarchitectured PPy/PTMA brush electrode (solid line). Scan rate: 0.1 mV $s^{-1}$. (E) Discharge curves corresponding to a planar PPy/PTMA brush thin-film electrode (dash-dotted line) and PPy/PTMA brush inverse opal electrodes with thicknesses of 3.5 μm (dashed line) and 13.8 μm (solid line). Adapted and reproduced with permission from Lin *et al.*, *Macromol. Rapid Commun.*, 2012, **33**, 107–113. Copyright 2012 Wiley-VCH Verlag GmbH & Co. KGaA.

 

by polystyrene colloidal crystal templating followed by sequential electropolymerization of polypyrrole (PPy) and an initiator-functionalized PPy layer for further SI-ATRP. Subsequent polymerization in the presence of (2,2,6,6-tetramethylpiperidin-4-yl methacrylate) resulted in the formation of nanoarchitectured PPy inverse opals bearing PTMPM brushes (Fig. 12B). Electrochemical tests demonstrated that the performance of the architectured macroporous electrodes bearing polymer brushes was superior to the performance of planar PTMA brush electrodes. The voltammetric current is higher in the case of the macroporous electrode due to the greater effective area exposing PTMA brushes (Fig. 12C). The discharge capacity of the planar PTMA brush electrode at a discharge rate of 5C was 0.17 μA h $cm^{-2}$ whereas for macroporous PTMA brush electrodes with thicknesses of 3.5 and 13.8 μm was 1.37 and 6.79 μA h $cm^{-2}$, respectively (Fig. 12D). The boost in discharge capacity upon increasing the thickness of the opal structure can be interpreted in terms of the significant increment in effective surface area. As a whole, this strategy based on the integration PTMPM/PTMA brushes on conductive micro/nanoarchitectured scaffolds seems to offer an interesting alternative to conventional planar brushes in order to improve the energy density and power density of organic radical batteries.

TEMPO-bearing polymer brushes can be also assembled on electrode surfaces *via* a "grafting-to" approach using block copolymers of 2,2,6,6-tetramethyl-4-piperidyl methacrylate (PMA) and reactive glycidyl methacrylate (GMA) (Fig. 13A).[92] The block copolymer, PGMA-*b*-PPMA, can be immobilized on ITO substrates by simply dip-coating in a copolymer solution and subsequent annealing resulting in smooth polymer films (Fig. 13B). These brush layers are then efficiently converted to TEMPO-bearing polymer brushes showing excellent reversible redox cycling at 0.81 V *vs.* Ag/AgCl. Interestingly, TEMPO-bearing polymer brushes "grafted-to" the ITO surface exhibited sufficient charge diffusivity ($10^{-10}$ $cm^2$ $s^{-1}$), very large storage capacity (120 mC $cm^{-2}$) and a linear dependence between the capacity and the thickness of the copolymer layer (Fig. 13C).

Another strategy to optimize the construction of ORBs relies on the grafting of nitroxide-bearing polymer brushes on multi-walled carbon nanotubes (MWCNTs). Gohy and co-workers[93] demonstrated that well-defined electroactive brush–CNT composites can be prepared through SI-ATRP of 2,2,6,6-tetramethylpiperidin-4-yl methacrylate (TMPM) brushes from initiator-modified MWCNTs and their subsequent oxidation into poly(2,2,6,6-tetramethylpiperidin-1-oxyl-4-yl methacrylate) (PTMA). This synthetic procedure led to MWCNT-*g*-PTMA composites displaying core–shell morphology. Electrochemical characterization of these composite electrodes revealed good cycling stability, involving 87% of capacity retention after 200 cycles, and remarkable specific capacity (85% of the theoretical capacity).

This composite material was then employed by the same research group in lithium battery applications.[94] One of the advantages of MWCNT-*g*-PTMA hybrids (Fig. 14A) is the controlled integration of the PTMA polymer chains onto the MWCNTs that ultimately leads to an intimate contact between the redox building blocks and the conductive network. The performance of the MWCNT-*g*-PTMA-based electrodes was evaluated through electrochemical characterizations in a half-cell configuration *vs.* $Li/Li^+$ (Fig. 14B). Galvanostatic measurements indicated excellent capacity (85% of the theoretical capacity) as well as good cycling stability (>80% retention of the initial capacity after 150 cycles) (Fig. 14C). Interestingly, additional measurements also demonstrated that MWCNT-*g*-PTMA hybrids can sustain high charge/discharge rate capabilities

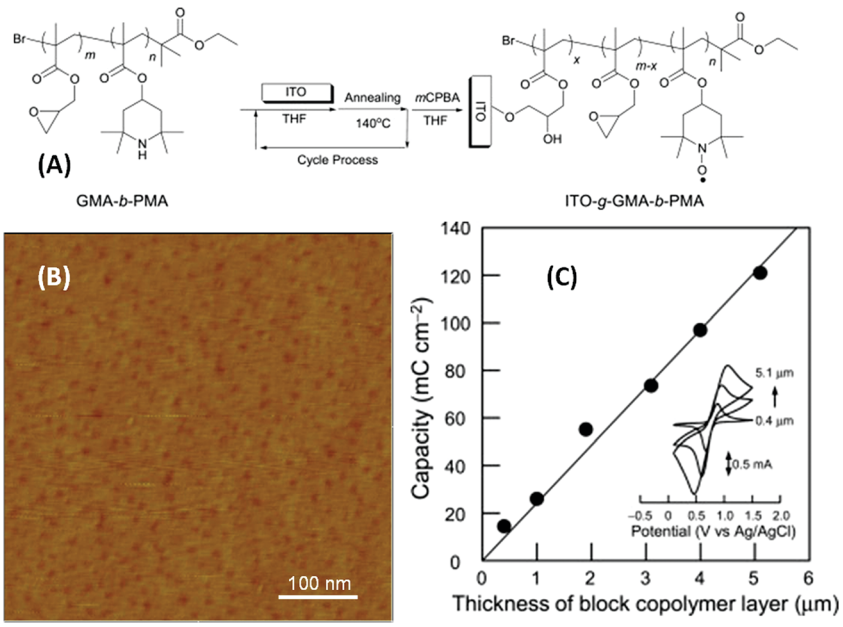


Fig. 13 (A) "Grafting-to" strategy leading to the formation of surface-grafted PGMA-*b*-PPMA films on ITO substrates. (B) Atomic force microscopy image of a PGMA-*b*-PPMA film grafted onto an ITO substrate. (C) Electrochemical capacity as a function of the thickness of the grafted PGMA-*b*-PTMA layer. Reproduced with permission from Takahashi *et al.*, *Polymer*, 2015, **68**, 310–314. Copyright 2015 Elsevier B.V.

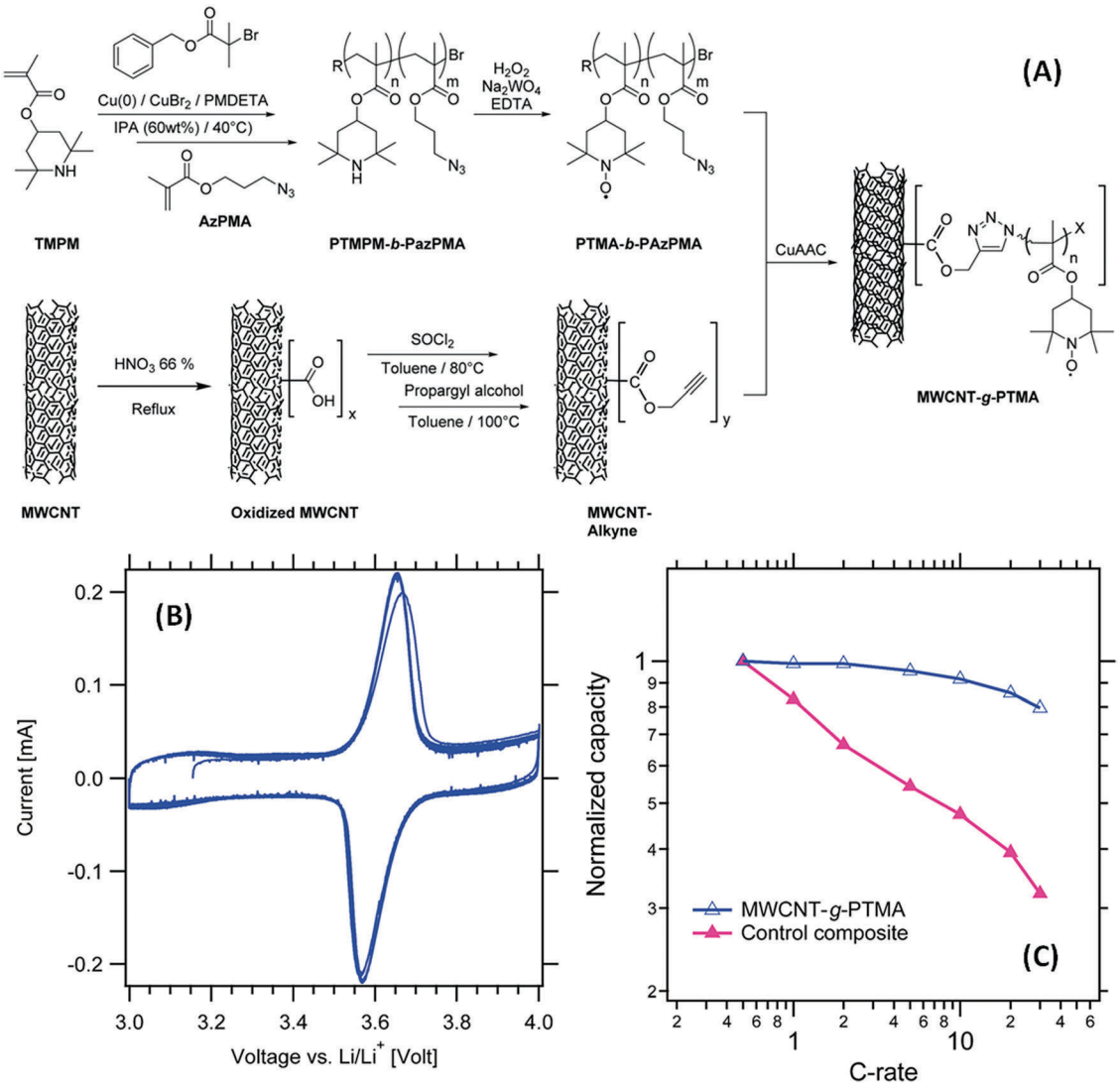


Fig. 14 (A) Synthesis of PTMA brushes on multi-walled carbon nanotubes (MWCNT-*g*-PTMA). (B) Cyclic voltammograms of MWCNT-*g*-$PTMA_{60}$ electrodes. Electrolyte: 1 M $LiPF_6$ in EC/DEC 1 : 1 v/v. Scan rate: 0.2 mV $s^{-1}$. (C) Capacity retention at various C rates for MWCNT-*g*-$PTMA_{60}$ and control composite electrodes. Electrolyte: 1 M $LiPF_6$ in EC/DEC 1 : 1 v/v. Scan rate: 0.2 mV $s^{-1}$. Reproduced with permission from Ernould *et al.*, *RSC Adv.*, 2017, **7**, 17301. Copyright 2017 Royal Society of Chemistry.

as compared to classical transition metal oxides for Li-ion batteries.[95]

A similar concept was further extended to the functionalization of graphene sheets with PTMA brushes (G-*g*-PTMA) *via* SI-ATRP and its subsequent use in electrochemical energy-storage devices.[96] Composite cathodes constituted of G-*g*-PTMA and reduced graphene oxide (RGO) as active material and conductive additive, respectively, exhibited high specific capacity up to 466 mA h $g^{-1}$. It is worth noting that this value based on the nominal mass of PTMA in the composite is higher than the theoretical capacity of PTMA. This remarkable electrochemical performance has been ascribed to the fast redox reaction of G-*g*-PTMA and surface faradaic reaction of RGO promoted by G-*g*-PTMA. In this scenario G-*g*-PTMA hybrids would play a dual role, as functional units providing redox reaction of PTMA and as structural units facilitating the surface faradaic reaction-based lithium storage of RGO. Regarding this latter, we should bear in mind that access to active groups on the graphene surface by ions is crucial to maximize the lithium storage capabilities. In this context, the grafted polymer chains play a key structural role by hindering the restacking of the graphene sheets and allowing the exposure of graphene surface groups to the surrounding electrolyte. Cyclic voltammograms of G-*g*-PTMA/RGO composite electrodes display reversible redox peaks at ~3.6 V (*vs.* $Li/Li^+$) corresponding to the redox switching between PTMA nitroxyl radicals and oxoammonium cations. The overlap between subsequent voltammetric scans indicates no appreciable loss of PTMA during the charging/discharging cycles (Fig. 15a). In addition to the voltammetric peaks, a nearly rectangular voltammetric shape was observed in the electrochemical response of G-*g*-PTMA/RGO electrode compared to those of G-*g*-PTMA and RGO electrodes (Fig. 15b). This pseudocapacitive behavior

 

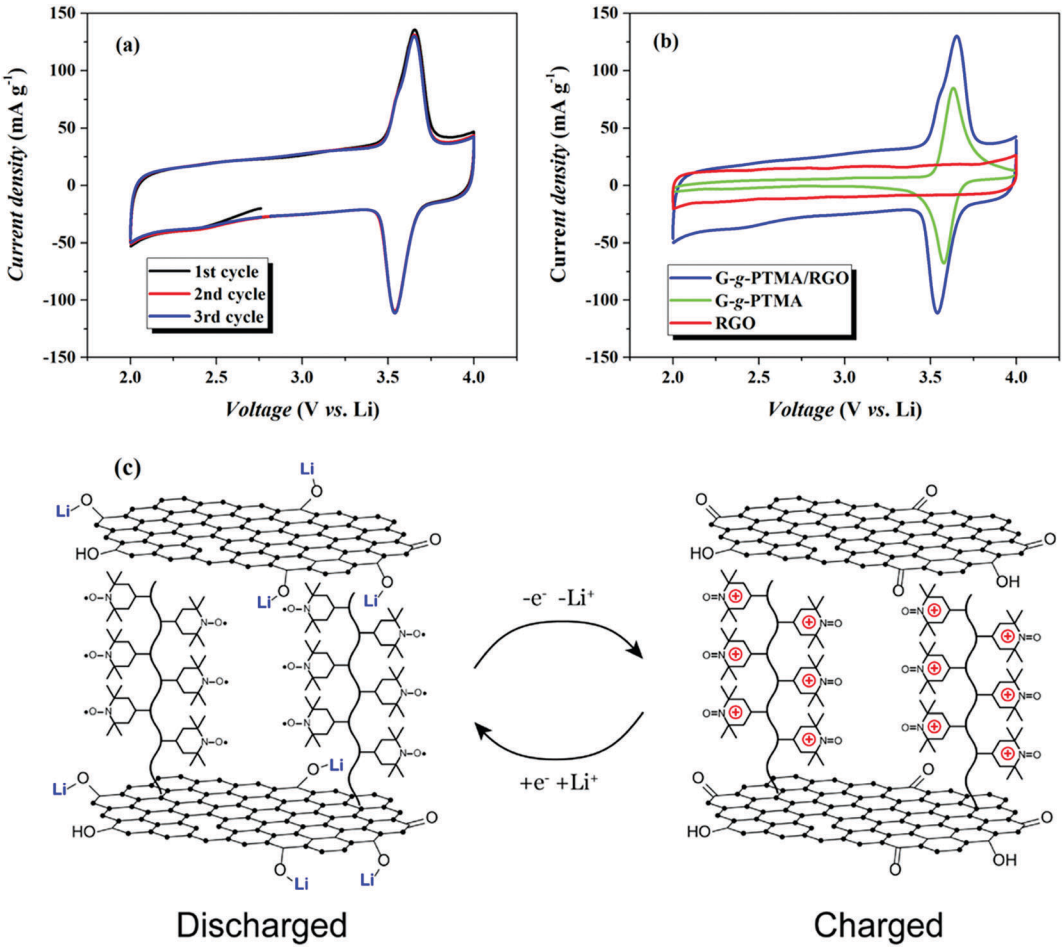


Fig. 15 (a) Cyclic voltammograms (three initial scans) of G-*g*-PTMA/RGO electrode. Scan rate: 0.5 mV $s^{-1}$ and (b) comparison of electrochemical response of G-*g*-PTMA/RGO, G-*g*-PTMA, and RGO electrodes. Scan rate: 0.5 mV $s^{-1}$. (c) Energy storage mechanism of G-*g*-PTMA/RGO cathode. Reproduced with permission from Li *et al.*, *ACS Appl. Mater. Interfaces* 2016, **8**, 17352. Copyright 2016 American Chemical Society.

stems from the Faradaic reactions of surface oxygen-rich functional groups of RGO and lithium ions. According to these authors, the energy storage mechanism might be associated to a charge process consisting of the oxidation of nitroxide radicals to oxoammonium cations with a concomitant release of lithium ions from RGO, and a discharge process involving the reduction of oxoammonium cations to nitroxide radicals and the uptake of lithium ions by RGO (Fig. 15c).

## Oxygen reduction and evolution reactions

Rechargeable metal–air batteries (MAB) have gained increasing visibility in the past years due to their high energy densities with their concomitant application in electric vehicles.[97] Electrochemical systems based on MABs possess theoretical energy densities higher than those of lithium-ion batteries; however, in most of cases MABs exhibit relatively low performances and poor long-term stability due to the lack of efficient air electrocatalysts. One of the key aspects to improve the performance and capabilities of rechargeable metal–air batteries is to find "bifunctional" electrocatalysts exhibiting high activity for the oxygen reduction reaction (ORR) (during battery discharge) and the oxygen evolution reaction (OER) (during battery recharge). As is well known, the sluggish kinetics of ORR and OER, control the overall performance of MABs.

In this regard, Ghilane and co-workers[98] proposed an approach for developing efficient electrocatalysts for the ORR based on polymer brushes bearing ionic liquid-like moieties (Fig. 16A). These authors demonstrated that poly(vinyl-imidazolium-methyl), poly(VImM), brushes exhibit electrocatalytic activity toward ORR and they can be used as macromolecular platforms to synergistically host Pt electrocatalysts.

Glassy carbon (GC) electrodes modified with poly(VImM) brushes *via* SI-ATRP displayed a pronounced electrocatalytic ORR activity when compared to bare GC electrodes (Fig. 16B and C). Indeed, a direct comparison between both systems reveals that the presence of poly(VImM) brushes prompts a ~80 mV positive onset potential shift as well as a peak current density increase from 0.18 to 0.45 mA $cm^{-2}$ The enhanced ORR activity of poly(VImM) brushes has been ascribed to the presence of nitrogen atoms in the imidazolium ring that induces a high electron density. Consequently, this would also generate a

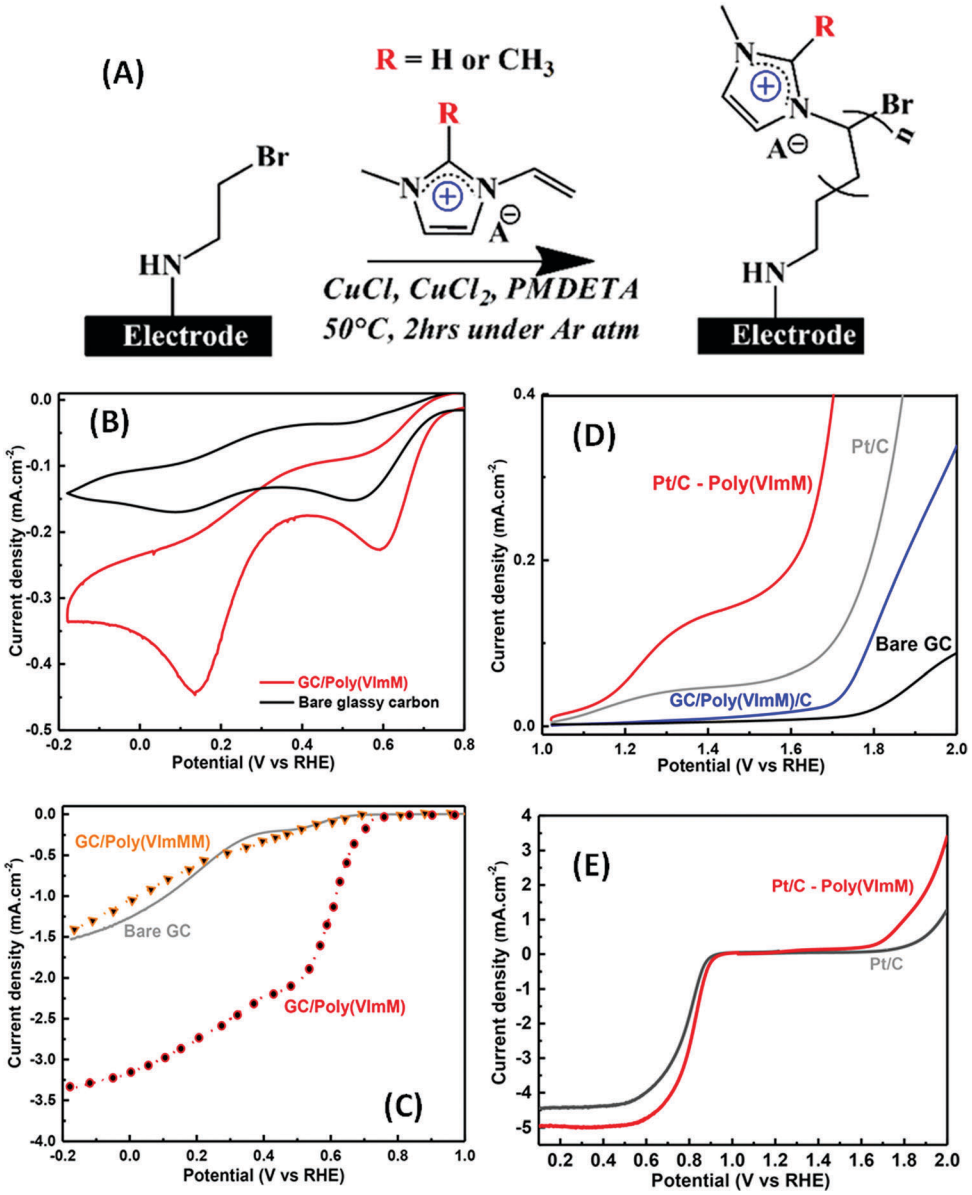


Fig. 16 (A) Synthesis of polymer brushes bearing ionic liquid-like moieties *via* surface-initiated atom transfer radical polymerization (SI-ATRP). R = H corresponds to poly(VImM); R = $CH_3$ corresponds to poly(VImMM) (B) CV of bare GC and GC/poly(VImM) in $O_2$-saturated 0.1 M KOH solution. (C) Oxygen reduction reaction (ORR) polarization curves using rotating disk electrode (RDE) at rotation 900 rpm for bare GC, GC/poly(VImM), and GC/poly(VImMM). Scan rate: 10 mV $s^{-1}$. (D) Oxygen evolution reaction (OER) polarization curves at 1600 rpm in $O_2$-saturated 0.1 M KOH solution recorded on bare GC, poly-(VImM), Pt/C, and Pt/C/poly(VImM). Scan rate: 10 mV $s^{-1}$. (E) Voltammetric plots comparing the ORR and OER response of Pt/C and Pt/C/poly(VImM) electrodes. Reproduced with permission from Truong *et al.*, *ACS Catal.*, 2018, **8**, 869. Copyright 2018 American Chemical Society.

positive charge density in the carbon atom located between the nitrogen atoms.

Concomitantly, the hierarchical 3D organization of polymer brush layer favors not only the electron transfer but also the transport of water and oxygen in the vicinity of the electrochemical interface. These interesting properties of poly(VImM) brushes were successfully extended to the synergistic integration of conventional Pt/C electrocatalysts, thus generating hybrid platform with higher electrocatalytic activity and tolerance to methanol injection. Poly(VImM) brushes have a small electrocatalytic activity when compared with Pt/C; however, Pt/C/poly(VImM) exhibits an electrocatalytic activity that surpasses that of Pt/C (Fig. 16D). The strong influence of the polymer brush is evidenced by comparing the functional properties of Pt/C and Pt/C/poly(VImM) hybrids. Fig. 16E shows that the Pt/C/poly(VImM) interfacial nanoarchitecture leads to higher current densities and lower overpotentials for both ORR and OER reactions.

It is hypothesized that the enhancement of the OER activity originates from the chemical composition and the 3D organization of the poly(VImM) macromolecular assembly. In the present case, it is believed that the carbon atoms adjacent to

 

nitrogen atoms in the monomer units bear positive charges that, in turn, facilitate the adsorption of $OH^-$ ions and boost the electrocatalytic activity of the macromolecular interface.

These experimental results not only demonstrate that surface-grafted polymeric ionic liquids offer new avenues for ORR electrocatalysis but also show the potential of poly(VImM)/Pt hybrids as efficient bifunctional electrocatalysts for ORR and OER reactions.

On the other hand, surface modification of carbon nanotubes with polymer brushes has also been demonstrated to be a successful strategy to improve the electrocatalytic properties of the carbonaceous nanocomposites. To confer hydrophilic characteristics to multiwalled carbon nanotubes (MWCNTs), dendritic sulfonated hyperbranched poly(ether-ketone) (SHPEK) assemblies were covalently grafted to the nanotube surface (Fig. 17A).[99] This modification was carried out through a Friedel–Crafts acylation reaction followed by a sulfonation reaction in the presence of chlorosulfonic acid. The grafting process introduced oxygenated groups that improved the processability of the composites resulting in an enhanced electrocatalytic activity toward the ORR. Fig. 17 displays the voltammetric response of pristine MWCNT, HPEK-*g*-MWCNT and SHPEK-*g*-MWCNT electrodes in $O_2$ saturated solution. Results shows that the electrocatalytic properties of SHPEK-*g*-MWCNT composite electrodes are better – in terms of low overpotential and high current density – that those of pristine MWCNT, HPEK-*g*-MWCNT and commercial Pt/C.

The modification of glassy carbon with PANI-grafted multiwall carbon nanotubes (GC/PANI-*g*-MWNT) represents another interesting strategy to create electrocatalytic platforms (Fig. 18A).[100] GC/PANI-*g*-MWNT hybrid architectures have shown remarkable electrocatalytic activity toward the ORR that has been attributed to the synergistic combinations of MWNTs and PANI. While MWNTs enable the formation of interfacial architectures with high surface area, the conducting polymer facilitates the rapid electron transfer through the hybrid matrix. In fact, a comparison with a PANI-modified electrodes (GC/PANI) reveals that a GC/PANI-*g*-MWNT hybrid electrode exhibits a higher amperometric current at a more anodic onset potential (Fig. 18B), thus evidencing the excellent electrocatalytic activity for ORR.

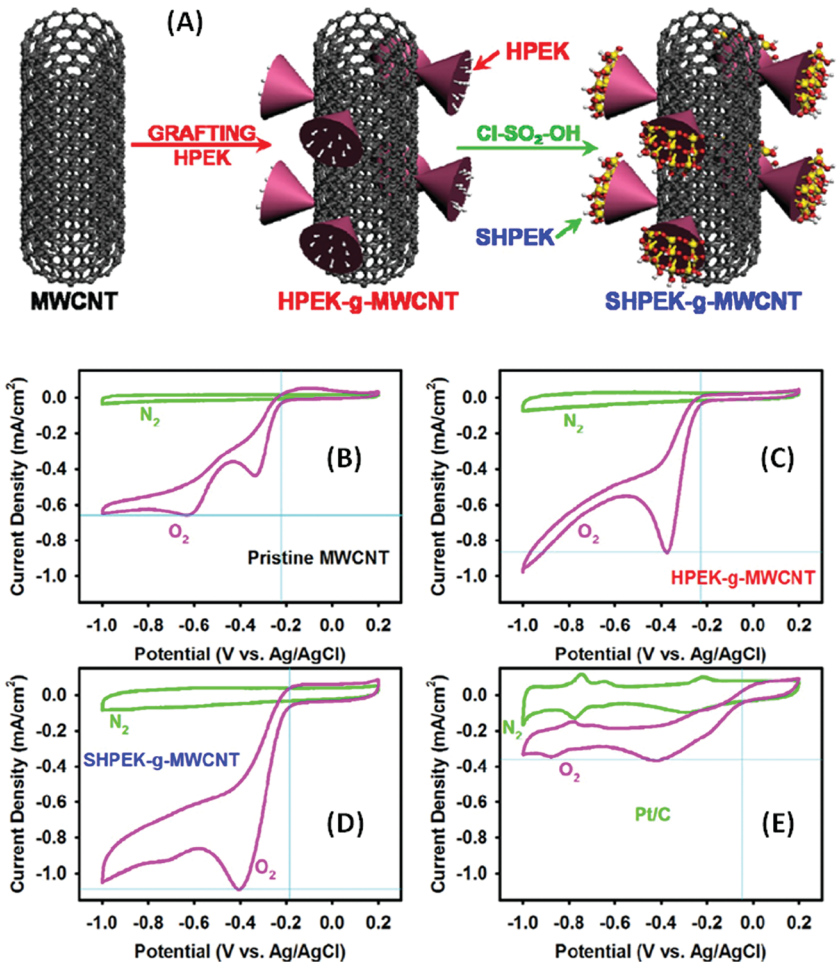


Fig. 17 (A) Schematic depiction of grafting procedure of the dendritic hyperbranched HPEK on the MWCNT surface and the subsequent sulfonation to yield SHPEK-*g*-MWCNT. (B) Cyclic voltammograms of films supported on glassy carbon (GC) electrodes in nitrogen- and oxygen-saturated aqueous electrolyte: (B) pristine MWCNT; (C) HPEK-*g*-MWCNT; (D) SHPEK-*g*-MWCNT; (E) Pt/C. Electrolyte: 0.1 M KOH. Scan rate: 10 mV $s^{-1}$. Reproduced with permission from Sohn *et al.*, *ACS Nano*, 2012, **6**, 6345–6355. Copyright 2012 American Chemical Society.

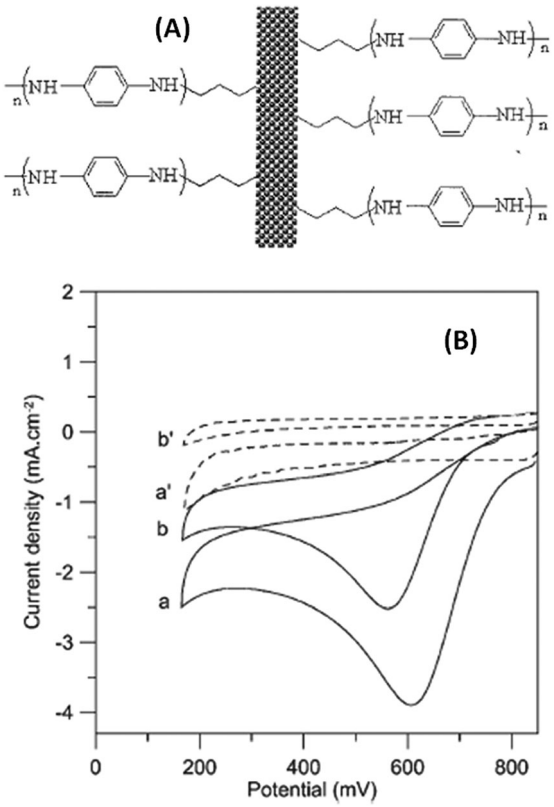


Fig. 18 (A) Schematic illustration of the PANI-*g*-MWNT nanohybrid. (B) Cyclic voltammograms of films supported on glassy carbon (GC). Plots (a) and (b) correspond to the electrochemical response of PANI-*g*-MWNT/GC and PANI/GC, respectively, in $O_2$ saturated electrolyte. Plots (a′) and (b′) correspond to the electrochemical response of PANI-*g*-MWNT/GC and PANI/GC, respectively, in deoxygenated electrolyte (blank experiment). Electrolyte: 0.5 M $H_2SO_4$. Reproduced with permission from Manesh *et al.*, *Electroanalysis* 2006, 18, 1564–1571. Copyright 2006 Wiley-VCH Verlag GmbH & Co. KGaA.

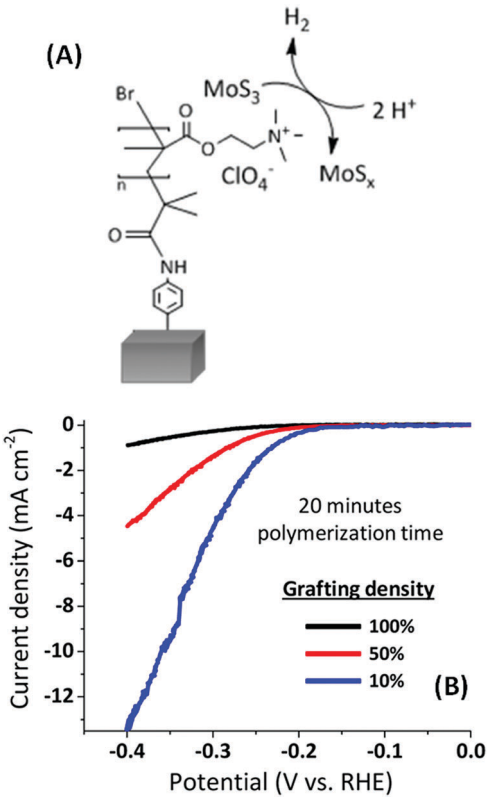


Fig. 19 (A) Schematic representation of the poly(2-(methacryloyloxy)-ethyl ammonium) brushes including the precatalyst formation and hydrogen evolution reaction (HER) catalysis. (B) Voltammetric scans of $MoS_x$-loaded polymer brushes with different grafting densities. The catalyst loadings for the different grafting densities are 0.17, 0.12, and 0.35 μg $cm^{-2}$ for 100, 50, and 10% grafting densities, respectively. Electrolyte: 1 M $H_2SO_4$. Scan rate: 1 mV $s^{-1}$. Electrode pretreatment: ten consecutive scans from 0.1 to −0.4 V (*vs.* reversible hydrogen electrode, RHE) to convert the precatalyst into the catalytic active species $MoS_x$. Reproduced with permission from Stern *et al.*, *ACS Appl. Mater. Interfaces* 2018, **10**, 6253. Copyright 2018 American Chemical Society.

## Hydrogen evolution reaction

Electrocatalytic water splitting represents an environmentally friendly technology for hydrogen production.[101] The nature of the hydrogen evolution reaction (HER) catalyst at the cathode of the electrolytic device defines to a large extent the efficiency of the whole electrochemical system.[102] Historically, Pt-based electrode materials have exhibited the highest catalytic activities for the HER; however, the high cost of these materials precludes their widespread use in large-scale industrial applications.

In recent years, dichalcogenides such as molybdenum sulfide gained increasing attention as promising electrocatalysts for the HER due to their high activity and excellent chemical and electrochemical stability.[103]

One of the strategies to integrate the electrocatalytic material onto the electrode surface is through the formation of $MoS_x$–polymer hybrids.[104] The embedding of the $MoS_2$ nanostructures into a polymer matrix facilitates the anchoring the electrocatalytic material on the electrode, but it might affect the electrocatalytic properties of the dichalcogenide.

Within this framework, Klok and co-workers[105] reported an approach to control the integration of amorphous molybdenum sulfide on graphite electrodes by using poly(dimethylaminoethyl methacrylate) brushes as templates (Fig. 19A). The strategy relied on the *in situ* formation of the nanostructures after binding the anionic $MoS_4^{2-}$ precursors into the cationic polymer brushes. Then the oxidation of the $MoS_4^{2-}$ and subsequent electrochemical treatment lead to the formation of the amorphous $MoS_x$ electrocatalyst (Fig. 19B). If we consider that surface-initiated polymerization of polymer brushes offers ample control over film thickness and grafting density of a wide variety of chemical functional groups, it is plausible to think that these 3D polymer layers can act as templates for the formation of hybrid interfacial architectures. In fact, one of the advantages of using polymer brushes at electrochemical interfaces is the flexibility for the three dimensional integrating of the electrocatalytic material on the electrode surface. According to these authors, the *in situ* formation of amorphous $MoS_x$ electrocatalyst on poly(dimethylaminoethyl methacrylate)-modified graphite electrodes resulted in turnover frequencies up to

 

1.3 and 4.9 $s^{-1}$ at overpotentials of 200 and 250 mV, respectively, in 1 M $H_2SO_4$. It is worth noting that these values are among the highest reported values for nanostructured molybdenum sulfide catalysts.

These results illustrate the potential of polymer brushes as templates to control the 3D assembly of HER catalysts on electrode surfaces.

## High performance supercapacitors

Electrochemical capacitors, also known as supercapacitors, are considered one of the most prominent energy storage devices due to their long cycle life, fast charge–discharge capabilities and low maintenance cost.[106] In this respect, in recent years increasing attention has been given to different pseudocapacitive electrode materials,[107] such as $RuO_2$ or $MnO_2$, owing to their high volumetric capacitance.[108] However, one limitation of these materials is their low power density and slow frequency response. To circumvent these limitations, carbon-based supercapacitors integrating graphene and pseudocapacitive materials were developed.[109] In particular, $MnO_2$ results in a very attractive choice for pseudocapacitive materials provided that it has a high theoretical specific capacitance (1400 F $g^{-1}$).

The emerging challenge associated with the construction of supercapacitors is to devise strategies to bridge the performance gap between these materials and construct hybrid nanoarchitectures in which graphene and metal oxide nanoparticles can interact together without disrupting their own function.

To this end, Feng and co-workers[110] proposed the use of poly(sodium methacrylic acid) brushes grafted onto graphene oxide and reduced graphene oxide in order to grow $MnO_2$ particles on the carbonaceous surface in a controlled manner. The strategy to create the hybrid architecture was based on exploiting the capability of poly(sodium methacrylic acid) brushes grafted on the graphene surface to coordinate and uptake Mn(II) ions with high efficiency. Then, these brush-confined $Mn^{2+}$ ions were converted into amorphous $MnO_2$ nanoparticles by oxidation in the presence of $KMnO_4$. The presence of the polymer brushes hinders the formation of crystalline phases and favors the formation of an amorphous nanomaterial, which is highly desirable for achieving a better insertion–deinsertion behavior of $Li^+$ ions. These $MnO_2$–polymer brush–graphene nanocomposites displayed an excellent performance as electrode materials for pseudocapacitors. Electrochemical characterization indicated that the specific capacitance reaches up to 372 F $g^{-1}$ at a current density of 0.5 A $g^{-1}$, and only 8% drop after 4000 charge–discharge cycles at the same current density. This remarkable capacitance performance has been ascribed to the 3D nature of the polymer brush that confers large specific areas to the interfacial architecture together with the presence of $MnO_2$ nanoparticles that provide more surface sites and facilitate charge transfer.

Covalent grafting of polyaniline (PANI) layers on different electrode materials has shown great potential for the molecular design of supercapacitors. Due to its low cost, ease of synthesis, fast redox rate and high reversible pseudocapacitance PANI has frequently been integrated in nanocomposites with carbonaceous nanomaterials for the preparation of supercapacitors.[111–113] Kotal *et al.* described a strategy to develop supercapacitors based on carbon nanofiber–polyaniline (CNF–PANI) composites synthesized by densely grafting brush-type PANI chains onto isocyanate functionalized CNFs. Electrochemical characterization of these CNF–PANI nanocomposites revealed a capacitance ~557 F $g^{-1}$ and a capacity retention of 86% after 2000 charge/discharge cycles at a current density of 0.3 A $g^{-1}$.[114]

Graphene holds great potential as an electrode material for electrochemical energy storage; however, in some cases its surface functionalization is mandatory in order to improve its capacitive properties.[115] Within this framework, one of the most frequently explored strategies for enhancing the electrochemical capacitive energy storage capabilities is the creation of graphene-conducting polymer nanocomposites.[116,117] Along these lines, Baek and co-workers[118] reported a method to prepare highly conducting polyaniline-grafted reduced graphene oxide (PANi-*g*-rGO) nanocomposites based on the covalent functionalization of amine-protected 4-aminophenol to acylated GO, followed by the polymerization in the presence of aniline (Fig. 20). This chemical strategy resulted in highly conducting hybrids displaying a remarkable electrochemical performance as supercapacitor electrodes.

Graphene covalently functionalized with poly(*p*-phenylenediamine) (RGO-PPD) has also been devised as a high performance electrode material for constructing supercapacitors. This nanocomposite material was prepared by grafting poly(*p*-phenylenediamine) on chlorinated graphene oxide (GO-COCl) sheets through amidation and polymerization processes. Assessment of the capacitive properties of RGO–PPD nanocomposites indicated that these materials exhibit a high specific capacitance of 347 F $g^{-1}$ at a discharge rate of 1 A $g^{-1}$ while maintaining 90.1% of its initial capacitance at 10 A $g^{-1}$ after 1000 charge/discharge cycles.[119]

Another approach to fabricate supercapacitors by tethering poly(*o*-phenylenediamine) chains on graphene surfaces involves the modification of graphene oxide (GO) with aniline groups *via* diazotization reaction followed by polymerization of *o*-phenylenediamine (oPD) monomers onto the GO surface (Fig. 21A).[120] Then, the GO–PoPD composite is washed repeatedly and only the PoPD linked to the surface aniline groups on the GO sheets remain in the form of single-chain structure. Subsequently, the composite is reduced by hydrazine hydrate at 95 °C for 3 h to obtain the reduced graphene oxide/poly *o*-phenylenediamine hybrid nanomaterial. Electrochemical tests confirmed that rGO–PoPD nanocomposites exhibit a high specific capacitance of 381 F $g^{-1}$ in 1 M $H_2SO_4$ at 1 A $g^{-1}$, and 230 F $g^{-1}$ in 6 M KOH at 1 A $g^{-1}$ as well as excellent stability and capacity retention (~90%) after 5000 cycles (Fig. 21B).

Covalently grafted PANI layers were successfully grown on reduced graphene oxide nanosheets using aminophenyl groups as anchors, thus leading to stable three-dimensional polyaniline-grafted graphene hybrid materials for supercapacitor electrodes.

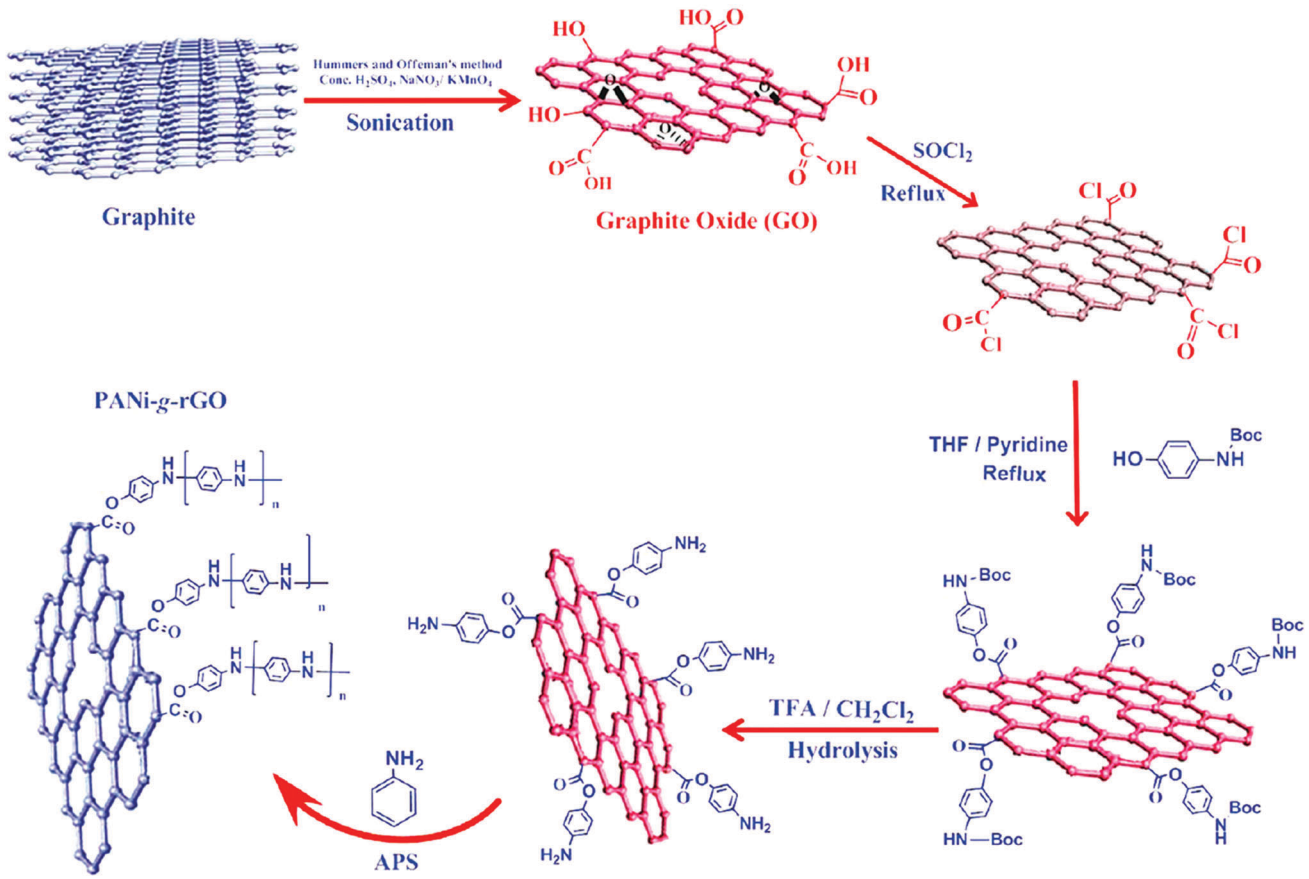


Fig. 20 Schematic presentation for the preparation of PANi-*g*-rGO nanohybrids. Reproduced with permission from Kumer *et al.*, *ACS Nano*, 2012, **6**, 1715–1723. Copyright American Chemical Society.

The specific capacitance of this composite reached up to 1045.51 F $g^{-1}$ at 0.2 A $g^{-1}$ and the electrochemical tests indicated that 95% of the initial specific capacitance can be retained after 1000 cycles.[121] This value is much higher than that of the pure PANI and other PANI–rGO composites prepared by noncovalent interactions.[122] Hence, one can infer that one of the key elements for the remarkable electrochemical performance is the covalent grafting of the conducting polymer layer on the graphene nanosheets. Chemically grafted graphene–polyaniline composites were prepared by polymerization of aniline onto *p*-aniline functionalized graphene substrates. This strategy involved a diazotization reaction of *p*-phenylenediamine to anchor *p*-aniline groups on the graphene surface (the diazonium addition method[123]) that ultimately act as reactive sites for the chemical grafting and subsequent polymerization of aniline.[124] Electrochemical characterization of these nanocomposites demonstrated high electrochemical capacitance (422 F $g^{-1}$) at discharge rate of 1 A $g^{-1}$. Later on, the diazonium addition method was employed to create 3D hierarchically nanostructured graphene sheets covalently modified with PANI assemblies yielding supercapacitors with high electrochemical capacitance (1295 F $g^{-1}$ at 1 A $g^{-1}$) and long cycling life.[125] A similar approach based on the synthesis of polyaniline-grafted reduced graphene oxide *via* azobenzene pendants resulted in supercapacitors with 80% capacity retention after 1500 cycles.[126]

More recently, Hoa and coworkers[127] proposed an interesting twist to the creation of supercapacitors by using three-dimensional reduced graphene oxide-grafted polyaniline aerogels as active materials. Graphene oxide sheets were grafted with PANI chains and subsequently RGO-*g*-PANI aerogels were obtained by hydrothermal and drying processes. Aerogel composites were integrated as active materials in supercapacitors resulting in electrochemical storage devices with a specific capacitance of 1600 F $g^{-1}$ at very high current densities (12 A $g^{-1}$) and excellent capacity retention after 3000 cycles ($\sim$91%). Chemical grafting of polyaniline chains onto aniline-functionalized graphene has been employed as a route to create PANI–graphene oxide–$TiO_2$ nanotube composite for high electrochemical capacitance applications. These systems exhibited good long-term electrochemical stability provided that the specific capacitance decreased gradually from 816 F $g^{-1}$ to 720 F $g^{-1}$ after 2000 cycles, thus retaining 88% of the initial capacity.[128]

Covalent grafting of polythiophene chains on graphene oxide sheets also yielded supercapacitors with excellent capacitance retention.[129] The grafting process involved the simultaneous reduction and covalent anchoring of thiophene derivatives on graphene oxide sheets to generate polythiophene chains homogeneously distributed on rGO sheets (PT-*g*-rGO hybrids). The maximum specific capacitance of these hybrids was 230 F $g^{-1}$ and the capacitance retention was $\sim$100% after 5000 cycles.

 

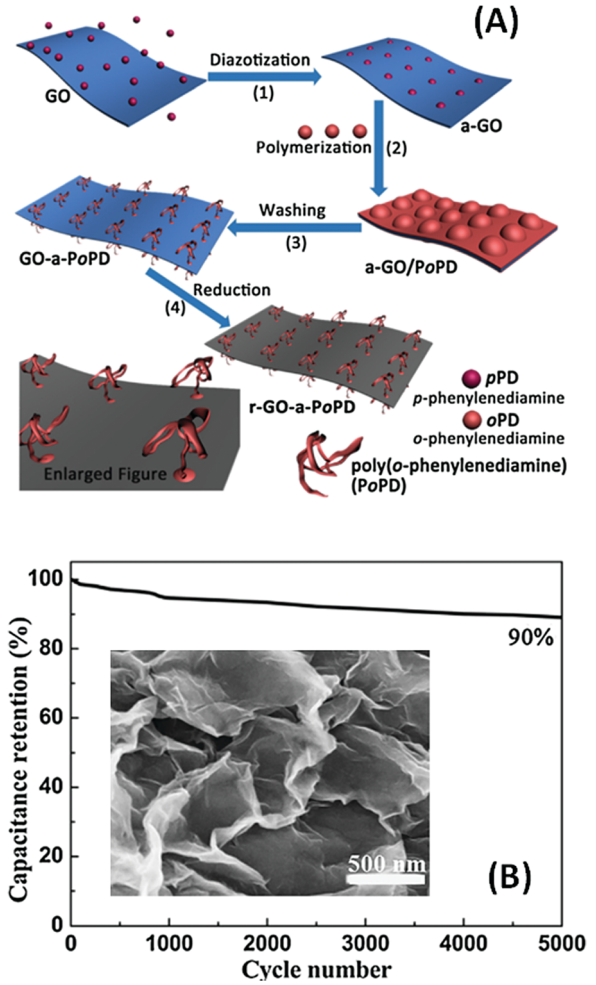


Fig. 21 (A) Schematic presentation for the preparation of poly(*o*-phenylenediamine) (PoPD)-reduced graphene oxide nanohybrids. (B) Cycling capability of poly(*o*-phenylenediamine) (PoPD)-reduced graphene oxide nanocomposite (scan rate: 50 mV $s^{-1}$). The plot includes a SEM image of poly(*o*-phenylenediamine) (PoPD)-reduced graphene oxide nanohybrids. Reproduced with permission from Yang *et al.*, *Electrochim. Acta* 2017, **245**, 41–50. Copyright 2017 Elsevier B.V.

It has been hypothesized that the interfacial configuration of the polythiophene chains on the graphene oxide sheets facilitates the ionic and electronic transport thus improving the electrochemical performance of the PT-*g*-rGO hybrids.

If we bear in mind that the properties of nanocomposites depend not only on the individual components used but also on the morphology and the interfacial characteristics, then we can conclude from these experiments that polymer brushes play a valuable role as structural building blocks integrating dissimilar nanomaterials in order to develop supercapacitors with improved properties.

## Solar hydrogen production

Conversion of solar energy into chemical energy by using photoelectrochemical cells constitutes a carbon-free, environmentally friendly solution to the increasing demand for clean energy.[130,131] In this regard, optimizing the generation of hydrogen fuel *via* water splitting with semiconductor electrodes constitutes a core task of the electrochemistry community. At present, there is a consensus that no single material satisfies all of the efficiency, stability, and cost-effective conditions required for large-scale industrial application of these energy conversion systems. In recent years, polymer brushes emerged as suitable building blocks for designing heterostructural photoelectrodes for hydrogen generation.

One of the first attempts to integrate polymer brushes into photoelectrochemical interfaces for solar-to-fuels technologies has been reported by Cedeno *et al.*[132] These authors described the attachment of difluoroborylcobaloxime catalysts to polyvinylpyridine (PVP)-modified p-type gallium phosphide electrodes resulting in improved hydrogen production levels and photoelectrochemical performance as compared with PVP-modified electrodes without catalyst functionalization.

Beiler *et al.*[133] also proposed the use of polymer brushes containing pendant ligands for organizing and controlling molecular catalysts on the photoelectrode surface. Gallium phosphide (100) electrodes were derivatized with polymer brushes bearing pyridyl or imidazole ligands with attached cobaloximes catalysts. Photoelectrochemical testing of the electrodes modified with cobaloxime-appended polymer brushes revealed a 3-fold increase in hydrogen production as compared to electrodes without cobaloxime functionalization.

Later on, the same research group performed the successful assembly of hydrogen-producing cobaloxime catalysts on GaP(111) surface through the coordination to polyvinylimidazole (PVI) brushes (Fig. 22A). Photoelectrochemical measurements in neutral aqueous conditions indicated that cobaloxime coordination to the PVI brushes exhibit a 4-fold increase in current density as compared to results obtained using cobaloxime-free PVI electrodes. Indeed, simulated solar illumination (100 mW $cm^{-2}$), of the cobaloxime–PVI-modified photocathodes resulted in a current density $\approx$1 mA $cm^{-2}$ when polarized at 0 V (*vs.* the reversible hydrogen electrode) (Fig. 22B). Noteworthy, this hybrid interface integrating a catalytic macromolecular nanoarchitecture onto a semiconducting electrode displayed near-unity faradaic efficiency for hydrogen production.[134]

Then, these notions were further extended to the modification of p-type GaP semiconductor electrodes with polyvinyl pyridine brushes bearing cobalt porphyrin catalysts. In these macromolecular platforms the Co centers of the porphyrins are attached to the substrate through the coordination to pyridyl groups of the polymer brush. Photoelectrochemical characterization confirmed that the catalyst–polymer–semiconductor hybrid cathodes are highly active and efficient for hydrogen production.[135]

These results illustrate the versatility of polymer brushes to create functional interfaces capable of integrating light capture nanoarchitectures on photoelectrochemical platforms for generating fuels using sunlight as an energy input.

## Photovoltaic devices

Generating electricity from sunlight in large scale, at low cost and in an efficient manner is one of the grand challenges of our

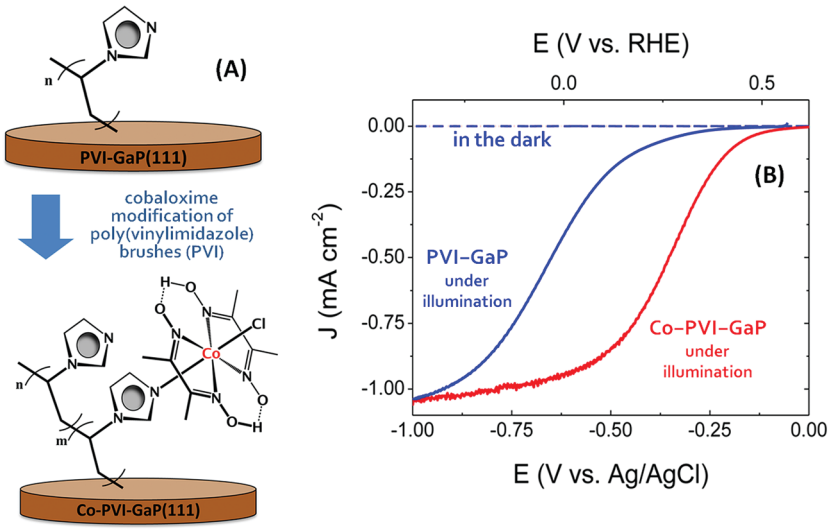


Fig. 22 (A) Schematic representation of the immobilization of hydrogen-producing cobaloxime catalysts onto p-type gallium phosphide substrates *via* coordination to poly(vinylimidazole) brushes. (B) Linear sweep voltammograms corresponding to PVI–GaP (blue trace) and Co–PVI–GaP (red trace) electrodes under 100 mW $cm^{-2}$ illumination. The plot also includes the electrochemical response in the dark (dashed-dotted blue lines). All measurements were performed at pH 7. Reproduced with permission from Beiler *et al.*, *ACS Appl. Mater. Interfaces*, 2016, **8**, 10038. Copyright 2016 American Chemical Society.

century. Our planet receives an incredible supply of energy from the Sun, but it is vitally necessary to improve the efficiency and performance of our photovoltaic devices in order to better harness the power of that formidable and inexhaustible resource. Over the past decades polymer solar cells (PSC) have attracted considerable attention and interest due to their advantages of mechanical flexibility, solution-processability and cost-effective fabrication.[136,137] PSC are based on bulk heterojunctions (BHJ) where the active layer is constituted of a composite of a p-type (donor) and an n-type (acceptor) material. This configuration maximizes the internal donor–acceptor interfacial area, thus allowing for efficient charge separation. Within this framework different research groups have resorted to interface engineering to optimize interfacial properties with the aim of controlling the active layer morphology and improving material compatibilities.[138] Among the different strategies of interfacial engineering, the use of polymer brushes provides a number of advantages over traditional physical deposition techniques: (i) they prevent film delamination; (i) they facilitate the integration of multiple polymer layers exhibiting similar solubility; (ii) their polymer backbone is oriented perpendicular to the substrate, this being a structural feature that could be necessary to facilitate charge injection. Regarding this latter, we should note that traditional solution processing methods such as spin-coating or drop-casting are not able to confer specific orientations to the polymer chains deposited on the substrates.

The first example of the valuable contribution of polymer brushes to the design of photovoltaic devices was contributed by Huck and co-workers.[139] These authors achieved molecular organization in polymeric semiconductors *via* alignment of polymer chains using surface-initiated polymerization. Polyacrylate brushes bearing triarylamine side groups exhibited high mobilities for hole transport and were then employed in composite diodes integrating CdSe nanocrystals. Physical characterization also revealed that the transport in the nanocrystal phase was dramatically improved as compared to that of a spin-coated polymer/nanocrystal blend film. The controlled polymer architecture and morphology results in better charge carrier transport properties in organic devices provided that charge-transporting polymer brushes exhibit up to 3 orders of magnitude increase in current density normal to the substrate as compared with a spin-coated film.[140]

Electrochemically crosslinked surface-grafted poly(*N*-vinylcarbazole) (PVK) brushes as hole transport layers on a photovoltaic devices have been demonstrated by Advincula and coworkers[141] using surface initiated-reversible addition–fragmentation chain transfer (SI-RAFT) polymerization. This strategy relied on the use of electrodeposited chain transfer agents to grow polymer brushes from ITO electrode surfaces. Contrary to general approaches based on self-assembled silane initiators, the electrodeposition of macroprecursors provides well-defined and selective anchoring points from where the polymer brush can grow provided that the electropolymerization only occurs in the conducting regions of the electrode support and ensures an efficient way to yield a good control over the film thickness and a good surface coverage due to the high grafting densities.

Greenham and co-workers[142] also reported the formation carbazole-containing brushes for photovoltaic devices. They described the development of a new polymer brush architecture based on carbazole-functionalized polyisocyanopeptide brushes. Polyisocyanides are unique polymers that exhibit a well-defined structure due to their helical backbone and can form surface-confined macromolecular scaffolds for the arrangement of electronically active moieties. This is a particularly interesting aspect if we consider that there is a correlation between the device

 

performance and the capacity to infiltrate the polymer brush film with a second component. The experimental evidence showed that after spin-coating a solution of the acceptor on top of the carbazole-bearing brushes, the photovoltaic devices exhibited better photovoltaic characteristics as compared to blended donor–acceptor architectures created on amorphous spin-coated PVK film. This improvement in device performance has been ascribed to the large interfacial area between components stemming from the controllable interfacial architecture as well as the good charge generation.

Densely packed conjugated polymer brushes can tune the interfacial energy at the electrode with potential improvement on the active layer morphology.[143,144] However, depending on the nature of the monomer units, the formation of well-defined conjugated polymers brushes can be quite challenging. Chen *et al.*[145] reported the synthesis of poly(*para*-phenylene) (PPP) brushes of various grafting density by aromatizing well-defined, end-tethered poly(1,3-cyclohexadiene) (PCHD) "precursor brushes". This interesting approach provides a very stringent control over the grafting density of high molecular weight conjugated polymer brushes that would otherwise be insoluble.

In the same spirit, Kiriy *et al.* reported the first preparation of poly(3-hexylthiophene) (P3HT) brushes from different surfaces *via* surface-initiated Kumada catalyst-transfer polycondensation (SI-KCTP).[146,147] From that moment on, several groups explored the use of SI-KCTP to grow conjugated polymer brushes, such as polyfluorenes and poly(dialkoxy-*p*-phenylenes), from different surfaces.[148,149]

In particular, Yang *et al.*[150] reported the formation of uniform poly(3-methylthiophene) (P3MT) brushes on ITO surfaces using SI-KCTP from surface-bound arylnickel(II) bromide initiators (Fig. 23A). These researchers successfully demonstrated the use P3MT brushes as a viable hole-transporting layers (HTL) for solution-processed polymer solar cells through the fabrication of devices with efficiencies comparable to those obtained from poly(3,4-ethylenedioxythiophene)–poly(styrenesulfonate) (PEDOT:PSS)-based devices (Fig. 23B). In a similar vein, Kilbey and co-workers[151] proposed the use poly(3-hexylthiophene) (P3HT) brushes as anode buffer layers in P3HT–PCBM (phenyl-C61-butyric acid methyl ester) bulk heterojunction devices. Current–voltage characterization confirmed a significant enhancement in short circuit current, thus illustrating the capabilities of these nanostructured buffer layers to replace the PEDOT:PSS buffer layer in solar cells applications.

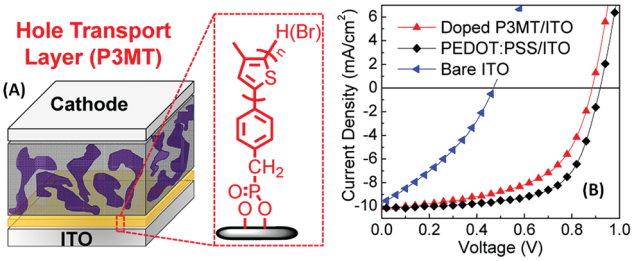


Fig. 23 (A) Illustration of the photovoltaic device based on a bulk heterojunction (BHJ) polymer solar cell using P3MT brushes as interfacial layer. P3MT brushes are covalently bound to ITO electrodes *via* surface-initiated Kumada catalyst-transfer poly-condensation (SI-KCTP). (B) Current–voltage (*J*–*V*) curves of the BHJ solar cell devices based on P3HT brushes under illumination (100 mW $cm^{-2}$). Reproduced with permission from Yang *et al.*, *ACS Appl. Mater. Interfaces* 2012, **4**, 5069. Copyright 2012 American Chemical Society.

Modification of electrode surfaces with thiophene-based brushes was also accomplished through the combination of surface-initiated polymerization and electrochemical techniques. Poly(terthiophene methyl methacrylate) (PTTMM) were grown from Au and ITO surface *via* SI-ATRP. Then, these brushes were electrochemically crosslinked to form a conjugated polymer network on the electrode surface.[152] More recently, Youm *et al.* reported the formation of polythiophene brushes through highly controlled surface-initiated Kumada catalyst transfer polymerization. Detailed structural studies revealed that these polythiophene brushes display a complex molecular organization. In particular, they have observed that polythiophene chains assemble into lateral crystalline domains with individual polymer chains folded to form in-plane aligned and densely packed oligomeric segments within each domain.[153] It is evident that the strong confinement effects resulting from the tethering of the polymer chains have strong implications for the mesoscale organization of the grafted polymer layer. And more importantly, this level of supramolecular organization is almost impossible to attain *via* traditional solution processing methods such as spin-coating or drop-casting.

The development of hybrid bulk heterojunctions (BHJ) integrating conjugated polymers brushes with n-type inorganic semiconductors stems from the need to combine the characteristics of both constituents to achieve more efficient and reliable devices. Polymer brushes offer structural stability and tailorable design of conjugated polymers whereas inorganic semiconductors contribute thermal and ambient stabilities as well as high electron mobility. However, the contrast between the hydrophilic surface of the oxide nanoparticle and the hydrophobic characteristics of the conjugated polymers may pose challenging issues to the successful integration of the hybrid BHJ. In most cases, the incompatibility between both constituents promotes the phase segregation between electron donor and acceptor counterparts, with a concomitant decrease in carrier-dissociation efficiency.

In this context, polymer brushes came to light as a plausible strategy to improve the compatibility, miscibility and dispersion stability of conjugated polymer-oxide nanoparticle and conjugated polymer–semiconductor nanocrystal hybrid materials[154,155] without affecting the intrinsic electron transfer properties of the nanocomposite system. One of the first attempts to construct nanoparticle–polymer brush hybrids *via* surface-initiated Kumada catalyst-transfer polycondensation was reported by Senkosvskyy *et al.*[156] and involved the modification of submicrometer $SiO_2$ particles with densely grafted P3HT brushes. These hybrid systems were then successfully applied in bulk heterojunction solar cells. Along the same line, SI-KCTP was also employed by Boon *et al.* to grow dense P3HT brushes from $TiO_2$ particles.[157] These authors observed improved photo-induced electron-transfer efficiency in the hybrid P3HT–$TiO_2$

material compared with a simple mixture of P3HT and $TiO_2$ particles. This improvement in the photoinduced electron-transfer process has been ascribed to the intimate contact between P3HT and $TiO_2$ counterparts. It is important to note that the influence of the grafted chains is observed even in the case of P3HT–$TiO_2$ hybrids prepared *via* a "grafting-onto" approach. For example, the grafting of carboxylic end-functionalized P3HT chains onto $TiO_2$ nanoparticles produced an improvement in the photoinduced electron-transfer efficiency even when the polymer mass fraction was very low, 3%.[158] In a similar way, it has been shown that by grafting P3HT brushes onto ZnO nanoparticles the dispersion of the nanomaterials within a P3HT matrix can be greatly promoted with a concomitant improvement of the photoinduced charge transfer process. As a result, the performance and efficiency of hybrid photovoltaic devices based on P3HT/P3HT-modified ZnO nanocomposites is higher than those devices fabricated by physical mixture of P3HT and ZnO.[159]

The use of polymer brush–carbonaceous nanomaterial hybrids has also proved useful in optimizing the photovoltaic properties of solar cell devices. In this regard, Lee *et al.*[160] demonstrated that maleimide–thiophene copolymer-functionalized graphite oxide sheets and carbon nanotubes act as efficient charge-transport promoters when integrated in the photoactive layers of polymer solar cells. The use of ethoxylated polyethylenimine grafted on GO (GO:PEIE) enabled the construction of transparent conducting electrodes for high performance photovoltaic devices.[161] It has been demonstrated that the application of GO:PEIE films as electron transport layers (ETL) improves the performance of organic solar cells with active layers consisting of poly({4,8-bis[(2-ethylhexyl)oxy]benzo[1,2-*b*:4,5-*b*′]dithiophene-2,6-diyl}{3-fluoro-2-[(2 ethylhexyl)carbonyl]thieno[3,4-*b*]thiophenediyl}) (PTB7) mixed with [6,6]-phenyl C71 butyric acid methyl ester (PC71BM). Photovoltaic characterization of PTB7:PC71BM bulk heterojunctions with different electron transport layers showed that the average power conversion efficiency (PCE) of devices integrating GO:PEIE (8.15%) is higher than those involving the use of GO (7.28%) or PEIE (6.89%). The functional performance improvement has been attributed to a slower electron extraction rate of PEIE, and GO, that ultimately leads to an enhanced possibility of charge recombination due to electron accumulation at the interface of the PTB7:PC71BM and the ETL.

Furthermore, it has been shown that chemical grafting of poly(3-hexylthiophene) (P3HT) chains on graphene oxide (GO) sheets facilitates the device fabrication by solution processing. The chemical grafting of P3HT chains onto the graphene surface induces a strong electronic interaction that promotes an enhanced electron delocalization and a narrower band gap than that of pure P3HT. By way of example, Dai and co-workers[162] demonstrated that a bilayer photovoltaic device based on the solution-cast of GO–P3HT/C60 heterostructures exhibit a 200% increase in the power conversion efficiency with respect to an analogue P3HT/C60 device. The same group explored a similar strategy using carbon nanotubes covalently modified with grafted P3HT chains (P3HT-CNT) and observed that the power conversion efficiency of bilayer photovoltaic devices employing a thin film of P3HT-CNT as the electron donor and C60 as the electron-acceptor layer was 40% higher than their counterpart based on pure P3HT.[163]

On a different note, dye-sensitized solar cells (DSSCs) have evolved as an alternative to conventional silicon-based inorganic solar cells due to the affordable production costs and (relatively) high light-to-electric energy conversion efficiencies. In addition, the use of carbonaceous nanomaterials as materials for counter electrodes (CE) in DSSCs began to attract the interest of chemists and materials scientists due to their low cost and good electrocatalytic activity. In this regard, poly(styrene-4-sodiumsulfonate) (PSSNa) brushes were grafted on MWCNTs (MWCNT-*g*-PSSNa) using a "grafting to" route and, subsequently, the aqueous dispersion was employed to fabricate MWCNT-*g*-PSSNa thin films through an electrostatic spray technique (Fig. 24).[164] This strategy led to the formation of uniform thin films constituted of highly interconnected MWCNT-*g*-PSSNa network structures that were used as the counter electrode in DSSCs. The MWCNT-*g*-PSSNa thin film showed high efficiency as a counter electrode in DSSCs whereas – even in the case of very thin films, $\sim$300 nm – the power conversion efficiency (PCE) of fabricated photovoltaic devices using MWCNT-*g*-PSSNa hybrid counter electrodes was $>$6%. Fig. 23B shows the *J*–*V* characteristics of the six DSSCs constructed with MWCNT-*g*-PSSNa thin film counter electrodes of different thickness under illumination (100 mW $cm^{-2}$, AM 1.5G). For the sake of comparison, the plot also includes the *J*–*V* characteristics of a DSSC fabricated with a Pt counter electrode (DSSC-Pt). Physical characterization of these systems showed that PCE was comparable to that of the DSSC-Pt when the CE thickness was optimized to $\sim$1 μm, thus highlighting the potential of polymer brush–MWCNT hybrids as low-cost materials for the alternative fabrication of Pt-free counter electrodes for DSSC through simple wet chemical routes.

The possibility of substituting Pt by a nanostructured polymer conductor as electrocatalyst on the counter electrode of a DSSC has been also extended to the application of graphene oxide nanosheets modified with covalently grafted poly(*o*-methoxyaniline) chains (POMA–FGO) doped with camphorsulfonic acid (CSA) (Fig. 25A).[165] Physical characterization has shown that POMAFGO–CSA counter electrodes exhibit reduced interfacial impedance due to the combination of the effective dispersion of FGO promoted by the soluble conducting polymer grafted on the FGO surface and the doping effect of CSA. Noteworthy, the efficiency of a DSSC based on the POMA–FGO–CSA counter electrodes is 8.81%, which is higher than that of DSSCs fabricated with a conventional platinum counter electrode. Fig. 25B illustrates the *J*–*V* plots of DSSCs fabricated with hybrids of different composition. The addition of FGO, enhances the crystallinity, electrochemical properties, and surface area of the counter electrode, with a concomitant improvement of the DSSCs efficiency. However, an excess amount of FGO might reduce the efficiency of the photovoltaic device. Results also indicate that the presence CSA improves the efficiency of the DSSCs. The electron transfer mechanism behind the operation (Fig. 25C) of this hybrid counter electrode strongly relies on the formation of a FGO–POMA–CSA conductive network in which

 

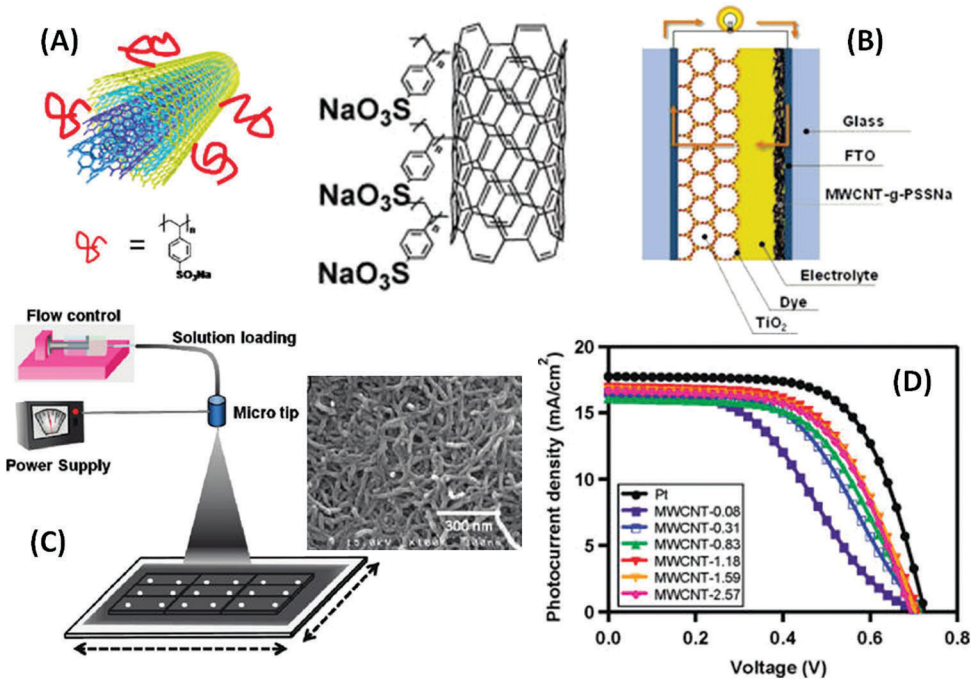


Fig. 24 (A) Structure of MWCNT-*g*-PSSNa, (B) schematic representation of dye-sensitized solar cell (DSSC) employing MWCNT-*g*-PSSNa network structures as counter electrode. (C) Illustration of spray technique used for MWCNT-*g*-PSSNa thin film fabrication. (D) *J*–*V* characteristics of DSSC-Pt and DSSC-MWCNT-*X* at various CE thickness under illumination. *X* refers to the CE thickness in microns. Reproduced with permission from Han *et al.*, *ACS Nano*, 2010, **4**, 3503–3509. Copyright 2010 American Chemical Society.

direct electron transfer to POMA–CSA polymer chains plays a major role.[166] It has been suggested that FGO might be involved in the electrocatalytic reaction with triiodide electrolyte; however, the main contribution of this nanomaterial seems to be related to an increase in active surface area due to the particulate morphology that enhances the contact area with the electrolyte.

Polyaniline-grafted silica nanocomposites have been also employed as gel electrolytes for quasi-solid-state dye-sensitized solar cells.[167] PANI–$SiO_2$ hybrids were synthesized by the chemical oxidative grafting polymerization of aniline on $NH_2$-modified $SiO_2$ nanoparticles. The incorporation of the PANI–$SiO_2$ hybrids into the ionic-liquid electrolyte resulted in the formation of a gel electrolyte displaying higher conductivity and diffusion coefficient of $I_3^-$ ions as compared to nanocomposite-free ionic-liquid electrolyte. Photovoltaic characterization of the DSSCs indicated promising results for quasi-solid-state DSSC applications provided that the use of 15 wt% PANI–$SiO_2$ in the gel electrolyte yielded an efficiency of 7.15%. The high performance of the composite gel electrolyte stems from its nanoarchitecture as the interconnected conducting network generates channels and pathways that facilitate the transport of ions and charge.

On the other hand, covalent grafting of polythiophene brushes on $TiO_2$ surfaces has gained increasing acceptance as a plausible strategy to integrate sensitizers in DSSCs. Contrary to the physisorption approach in which polythiophene chains weakly interact with the substrate, the covalent "grafting-to" assembly of oligothiophene brushes facilitates the injection of electrons into the $TiO_2$.[168] Carboxylated polythiophenes were found to be efficient light harvesting polymers for nanostructured $TiO_2$ photovoltaic cells.[169] The overall solar-to-electric energy conversion efficiency found in these hybrid nanoarchitectured systems is typically 0.9–1.5%. However, the presence of deconjugated moieties between the thiophene monomer units and the carboxylic anchoring group might limit the electron injection rate. Within this framework, Warman *et al.*[170] explored the use of poly(3-hexylthiophene) functionalized either with a cyanoacetic acid (CA) or a rhodanine-3-acetic acid (RA) anchoring group. In this strategy, the anchoring group has been designed to enable the chemical binding of the dye to the semiconductor surface, enhance the electron injection efficiency and promote the photoinduced electron transfer process. According to these authors, a direct comparison between both anchoring groups revealed that poly(3-hexylthiophene) functionalized with CA anchors have much broader photoresponse range and enhanced light harvesting efficiency. For instance, photovoltaic measurements performed on DSSCs using cyanoacetic acid-functionalized poly(3-hexylthiophene) bearing 13 monomers units showed energy conversion efficiencies of 3% under light irradiation of 100 mW $cm^{-2}$.

From another point of view, Feng and co-workers[171] reported the formation CdS/CdSe quantum dots (QDs) co-sensitized graphene nanocomposites for potential photovoltaic applications using polymer brushes as templates or structural units. Their approach relied on the modification of graphene sheets with (polymethacrylate cadmium) brushes. The cadmium ions hosted in the polyelectrolyte chains acted as precursors for

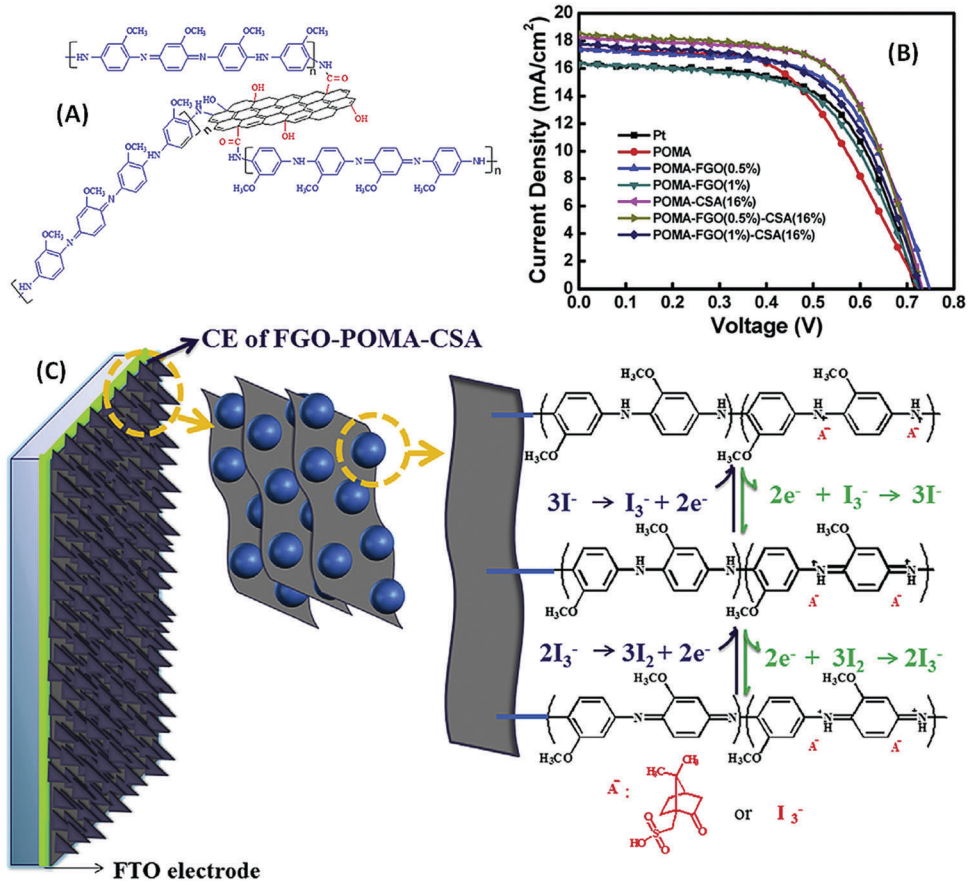


Fig. 25 (A) Graphene oxide nanosheets modified with covalently grafted poly(*o*-methoxyaniline) chains (POMA–FGO). (B) *J*–*V* curves of the DSSCs using various CEs. POMA-FGO (*X*), *X* refers to the percentage of FGO in the preparation of the hybrid. POMA-FGO-CSA (*Y*), *Y* refers to the percentage (by weight) of CSA added to the prepared POMA–FGO hybrid to create the POMA–FGO(*X*)–CSA(*Y*) hybrid. (C) Scheme of the proposed electron transfer mechanism taking place at the hybrid interfacial architecture. Reproduced with permission from Yu *et al.*, *Org. Electron.* 2017, **42**, 209–220. Copyright 2017 Elsevier B.V.

the formation of QDs. The semiconducting CdS and CdSe QDs were prepared through the reaction with $H_2S$ gas and $Na_2SeSO_3$ solution, respectively. After the reaction, subsequent uptake of cadmium ions by remaining carboxylate moieties enables the further formation of QDs. In this way, the loading of QDs hosted in the brush layer can be substantially increased by repeated steps. Physicochemical characterization of CdS/CdSe QD–polymer brush–graphene nanocomposites showed that the hybrid nanoarchitecture exhibit a significant enhancement of visible light response as compared to plain graphene. The same group employed a similar approach to create high density CdS/CdSe quantum dots onto $TiO_2$ nanotubes by using polymer brushes as nanoreactors.[172] In this case, $TiO_2$ nanotubes were modified through surface initiated polymerization of cadmium dimethacrylate brushes. Subsequently, CdS and CdSe QDs with high loading and narrow size distribution were synthesized *via* simple gas–solid and liquid–solid reactions. In this configuration, polymer brushes not only act as templates but also stabilizing agents preventing further nucleation and uncontrolled aggregation of the QDs. Photoelectrochemical measurements indicated that the light absorption of CdS/CdSe DQ–polymer brush–$TiO_2$ nanocomposites was extended to the visible light region, displaying good photocurrent and photovoltage response characteristics.

The use of graphene derivatized with polymer brushes for photovoltaic applications has been also proposed by Taylor and co-workers.[173] These authors resorted to the use of graphene nanosheets modified with polystyrene-based polymer brushes bearing Ru(II) polypyridine chromophores (PSRu). In recent years, there has been an increasing interest in combining this type of complexes with polymeric scaffolds and nanomaterials to create metallopolymer hybrids for potential applications in photoenergy conversion. In this regard, photophysical evaluation of photovoltaic cells based on graphene–polymer brush assembly in the configuration, ITO/PEDOT:PSS/RGO-PSRu/PC60BM/Al, revealed a 5-fold enhancement of photocurrent and power conversion efficiencies relative to devices with the configuration, ITO/PEDOT:PSS/PSRu/PC60BM/Al. These results eloquently illustrate the advantages of working with polymer brushes to optimize the properties graphene/metallopolymer hybrids.

More recently, Caterino *et al.*[174] demonstrated the use of polymer brushes as key elements in biosolar cell applications. Carboxylate-bearing polymer brushes decorated with ferrocene

 

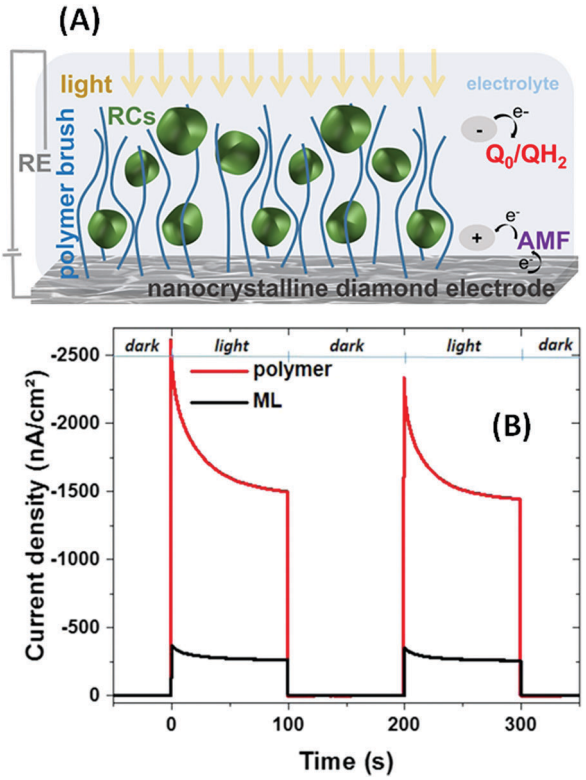


Fig. 26 (A) Schematic illustration of the bio-hybrid system consisting of bacterial photoactive reaction centers (RCs) immobilized on a diamond electrodes modified with polymer brushes. The figure describes the different electron transfer processes involved in the photocurrent generation. AMF: aminomethylferrocene (redox mediator). $Q_0/QH_2$: quinone/dihydroquinone redox pair. (B) Photocurrents measured under periodical light exposure for a diamond electrode modified with interfacial architecture involving the use of self-assembled monolayers (ML) (black curve) and polymer brushes (red curve). Reproduced with permission from Caterino *et al.*, *ACS Appl. Mater. Interfaces*, 2015, **7**, 8099. Copyright 2015 American Chemical Society.

units or cytochrome *c* were employed as 3D scaffolds capable of hosting bacterial photoactive reaction centers (RCs) on conductive nanocrystalline diamond surfaces (Fig. 26A). In this particular setting, the cytochrome *c* and ferrocene groups act as redox mediators promoting the generation of photocurrents. Their work shows the critical role of polymer brushes as structural and functional units in the construction of bio-photovoltaic hybrid systems. Fig. 26B displays the photoresponse of a diamond electrode in which RCs were immobilized on 6-phosphonohexanoic acid self-assembled monolayers (ML) (black trace) and that of an electrode constituted of RCs integrated into carboxylate-bearing polymer brushes (red trace). The plot shows that photocurrents measured in the "polymer brush configuration" ($\sim$1.5 μA $cm^{-2}$) are three times higher than the photocurrents measured with monolayer-modified electrodes. Due to their 3D characteristics and high surface density of functional groups, polymer brushes are critical to attain an efficient entrapment of photoreactive proteins and increase the loading of photoreactive units on the electrode surface. If we consider that these protein complexes are able to transform sunlight into electricity with high efficiency, then this strategy using polymer brushes as functional scaffolds would open new avenues to design biophotovoltaic devices.

## Conclusions and outlook

"For our sustainable energy future, there is a common global objective that needs to be met and that is "getting more from less for more"".[175]

R. A. Mashelkar

As we move further into the 21st century, we must recognize that the development of clean and high-efficient energy storage and conversion technologies is becoming more and more important for the sustainable development of our societies. This is particularly relevant if we consider that it is forecasted that by 2050 the demand for energy could double or even triple as the global population grows and developing countries expand their economies.[176] We can say from a historical point of view that our civilization evolved hand in hand with our ability to harness energy from different sources. Nowadays, we need to be prepared for a world of complex social and economic challenges that will require – more than ever – our ability to find, use and improve clean energy sources with ever increasing dexterity and ingenuity.

In this respect, we must say that the creativity of chemistry and materials science can be of great help in assisting us to face the energy challenge. Research in these two disciplines is increasingly contributing to a sustainable future based on clean and efficient energy generation and storage. In that spirit, this review presented the concepts, ideas and strategies that are being developed based on the practical use of polymer brushes for improving the performance and efficiency of energy conversion and storage devices.

There is a broad consensus that interfaces have a strong influence on the synergistic effects resulting from the combination of different materials and, consequently, hold the key to the comprehensive properties of hybrid materials that are ultimately integrated as active components in energy conversion and storage devices. The magnitude and performance of the processes taking place in these devices rely almost exclusively on nanoscale interfacial phenomena in which the integration of thin polymer layers may play a major role. Here is when polymer brushes come into the picture as valuable tools to engineer interfacial properties with exquisite control. In contrast to other functionalization techniques, polymer brushes offer a broad variety of resources to gain nanoscale control over the size, sequence, conformation, and spatial distribution of functional building blocks (Fig. 26). This is why, over the past several years, we have witnessed the appearance of different approaches exploring the practical use of polymer brushes in energy-related applications.

Advances in materials science have demonstrated that the incorporation of organic–inorganic hybrids in proton exchange membranes can improve the proton conducting properties of the composite material. It is now widely accepted that the proton conductivity is strongly correlated with the interfacial

structures present in the inner environment of these membranes. As shown, the surface modification of inorganic fillers with polymer brushes has a pronounced influence not only on the interface morphology of the hybrid membrane but also on the generation of sites and pathways for proton transport. The same concept has been also easily extended to the transport of $Li^+$ ions. It has been demonstrated that the use of polyelectrolyte brushes instead of monolayer assemblies to modify nanoparticles incorporated in hybrid membranes leads to a significant increase in carrier concentration. In fact, additional molecular modification of the polymer brush with PEGylated units facilitated the dispersion of the particles into the polymeric PEO matrix improving the mobility of lithium ions.

On the other hand, redox functionalization with polymer brushes[177] gained increasing attention within the electrochemistry community as an alternative route to increase the performance of batteries and electrochemical capacitors. In this case, the interest is two-fold: (i) depending on the polymerization time or layer thickness, polymer brushes can greatly increase the number of electrons exchanged per grafted molecule, and (ii) the use of a redox polymer covalently anchored to the active material would replace both the use of binders and the conductive carbon additives. Several experimental observations have demonstrated that electrochemical storage devices incorporating polymer brush–inorganic nanoparticle hybrids show increased specific capacities and rate capabilities as well as better cycling stability when compared with unmodified inorganic nanoparticles. One of the advantages of polymer brushes is their mechanical stability, *i.e.*: increased elastic moduli and plasticity, stemming entropic effect lowering the stress contribution.[178] These superior mechanical properties facilitate the processing of the polymer brushes in different configurations, *e.g.*: nanoparticles, nanosheets, nanotubes or planar surfaces, and their incorporation into different nanocomposites (Fig. 26).

For instance, grafted redox polymer brushes have been successfully used as cathode active materials in organic radical batteries without evident dissolution of the organic electrode material. Note that in many cases, redox polymers tend to dissolve into certain organic solvents, thereby affecting the energy density, self-discharge, and cycle-life performance of batteries. In general, this technical problem is overcome by means of crosslinking methods, even though this strategy can alter the electroactivity of the redox polymer. On the contrary, the implementation of covalently anchored redox polymer brushes not only prevents the polymer from dissolving into the electrolyte but also improves the electrochemical properties of the system.

Polyelectrolyte brushes are particularly useful matrices for the preparation of supercapacitors if we consider that the charge storage mechanism of these devices depends primarily on the electrosorption of ions on the electrode surface to form an electrical double layer.[179] The presence of flexible polyelectrolyte chains on the electrode surface promotes remarkable alterations in the charge screening, ionic rearrangement and confinement, with the significant concomitant effects on the capacitance and charging dynamics.

Conjugated polymers play a central role in the development of polymer solar cells. Devising strategies to manipulate the nanostructure, composition and energetics of the polymer–inorganic interface is of paramount importance to exert control over charge injection and charge transport processes. Much effort has been devoted to engineering the polymer–inorganic interface in polymer solar cells to improve the power conversion efficiency. The formation of conjugated polymer brushes on electrode surfaces has shown interesting improvements in transport properties due to the generation of clear pathways for charge transport in the direction normal to the substrate.[180] Experimental evidence suggests that rates of charge injection and charge harvesting could be also ascribed to the covalent attachment of conducting polymer to the conducting oxide.[181] In this regard, we should also note that the use of polymer brushes has proven to be a successful and essential tool for the construction of optimized bulk heterojunctions relying on the formation of conducting polymer–nanomaterial heterostructures.[182]

On the other hand, photoelectrochemical production of fuels using sunlight has greatly depended on the ingenuity of chemists and materials scientists in devising appropriate strategies to assemble molecular catalysts for hydrogen evolution onto semiconducting surfaces. Design and synthesis of molecular components for enhancing photoelectrochemical fuel production has been a primary, perennial goal of many researchers. However, the performance of these molecular components is sometimes limited when photocorrosion in aqueous conditions takes place. This is an undesired phenomenon as it affects the efficient transfer of photogenerated carriers at the semiconductor–electrolyte interface. Molecular modification of semiconductors with polymer brushes has proven to be a successful strategy not only to confer chemical stability to the photoelectrode surface but also to optimize interfacial properties and improve the efficiency of photoelectrochemical fuel production. This has been accomplished on the basis of a combination of attributes of polymer brushes that include precise surface attachment chemistries, control over orientation and organization of molecular components, control of grafting density and surface loading of molecular catalysts, and modulation of interfacial energetics. In this sense, we should understand the role of polymer brushes as structural and functional building blocks efficiently interfacing the molecular components to the semiconductor surface.

Macromolecular assemblies integrating electrocatalytic materials on electrode surfaces represent an attractive way to create interfacial architectures with deliberate configurations suitable for the development of novel electrocatalytic systems for energy conversion schemes. Electrocatalytic surfaces have customarily been prepared by solution-casting from their colloidal suspensions onto supporting electrodes. Unfortunately, this simple process is typically accompanied by aggregation of the nanomaterials that ultimately leads to inhibition of electrocatalytic active sites as well as hindered mass transport. The use of polymer brushes as molecular building blocks for such composite interfacial assemblies is of particular interest because their structure, thickness, and chemical functionality can be

 

exquisitely controlled. We should bear in mind that one of the most desired features of electrocatalytic platforms is their ability to attain high current densities in order to produce large amounts of hydrogen in HER. By and large, this is obtained by controlling two parameters: the loading of electrocatalytic nanomaterials into the interfacial architecture, and the effective electrocatalytic area of the electrode surface. Hence, control over film thickness (dimensional control), modulation of polymer matrix hydrophilicity (optimization of solvent transport) and good nanomaterial dispersion in the nanocomposite layer (optimization of active sites) are key aspects to consider if we are to successfully design a hybrid electrocatalytic composite. Because of their intrinsic capabilities, polymer brushes are able to fulfill these requirements and offer a unique opportunity for the optimization of electrocatalytic surfaces through the fabrication of structurally controlled and well-defined nano-architected 3D films.

Our ability to manipulate active materials at the nanoscale or even molecular level is raising expectations for the performance of energy storage and conversion devices. The new horizons provided by polymer brushes appear very wide and the future offers the prospect of many developments. In this sense, it is clear that continual effort is essential to convert the concepts discussed in this review into real-world technologies.

In summary, this work has provided a broad description of relevant examples of practical uses of polymer brushes in sustainable energy-related applications. We hope that every reader can find stimulation for further exploration of this most inspiring research topic with certain wonder, surprise and curiosity, just after reading these pages.

## Conflicts of interest

There are no conflicts to declare.

## Acknowledgements

The authors acknowledge financial support from ANPCyT (PICT-2013-0905, PICT-2016-1680), Fundación Petruzza, Universidad Nacional de La Plata (PPID-X016), CONICET (PIP 0370), the Marie Curie project ''*Hierarchical Functionalization and Assembly of Graphene for Multiple Device Fabrication*'' (HiGRAPHEN) (Grant ref: 612704), and the Austrian Institute of Technology GmbH (AIT-CONICET Partner Lab: ''*Exploratory Research for Advanced Technologies in Supramolecular Materials Science*'' – Exp. 4947/11, Res. no. 3911, 28-12-2011). J. M. G., M. L. C., W. A. M. and O. A. are CONICET fellows.

## References

1 D. Elliot, *Energy, Society and Environment*, Routledge, London, 2nd edn, 2003.
2 H. H. Schobert, *Energy and Society: An Introduction*, CRC Press, Boca Raton, 2nd edn, 2014.
3 D. P. Tabor, L. M. Roch, S. K. Saikin, C. Kreisbeck, D. Sheberla, J. H. Montoya, S. Dwaraknath, M. Aykol, C. Ortiz, H. Tribukait, C. Amador-Bedolla, C. J. Brabec, B. Maruyama, K. A. Persson and A. Aspuru-Guzik, *Nat. Rev. Mater.*, 2018, **3**, 5–20.
4 S. Chu, Y. Cui and N. Liu, *Nat. Mater.*, 2017, **16**, 16–22.
5 R. Raccichini, A. Varzi, S. Passerini and B. Scrosati, *Nat. Mater.*, 2015, **14**, 271–279.
6 A. S. Aricó, P. Bruce, B. Scrosati, J.-M. Tarascon and W. van Schalkwijk, *Nat. Mater.*, 2005, **4**, 366–377.
7 *Electrochemically Enabled Sustainability: Devices, Materials and Mechanisms for Energy Conversion*, ed. K.-Y. Chan, C.-H. V. Li(s), CRC Press, Boca Raton, 2014.
8 (*a*) M. Aono, Y. Bando and K. Ariga, *Adv. Mater.*, 2012, **24**, 150–151; (*b*) K. Ariga, M. V. Lee, T. Mori, X.-Y. Yu and J. P. Hill, *Adv. Colloid Interface Sci.*, 2010, **154**, 20–29; (*c*) M. Ramanathan, L. K. Shrestha, T. Mori, Q. Ji, J. P. Hill and K. Ariga, *Phys. Chem. Chem. Phys.*, 2013, **15**, 10580–10611; (*d*) A. H. Khan, S. Ghosh, B. Pradhan, A. Dalui, L. K. Shrestha, S. Acharya and K. Ariga, *Bull. Chem. Soc. Jpn.*, 2017, **90**, 627–648; (*e*) K. Ariga, V. Malgras, Q. Ji, M. B. Zakaria and Y. Yamauchi, *Coord. Chem. Rev.*, 2016, **320–321**, 139–152.
9 K. Ariga, S. Watanabe, T. Mori and J. Takeya, *NPG Asia Mater.*, 2018, **10**, 90–106.
10 J. O. Zoppe, N. C. Ataman, P. Mocny, J. Wang, J. Moraes and H.-A. Klok, *Chem. Rev.*, 2017, **117**, 1105–1318.
11 J. M. Giussi, M. L. Cortez, W. A. Marmisollé and O. Azzaroni, in *Polymer and Biopolymer Brushes: for Materials Science and Biotechnology*, ed. O. Azzaroni, I. Szleifer, JohnWiley & Sons, Hoboken, 1st edn, 2018, ch. 1, pp. 1–27.
12 B. Zdyrko and I. Luzinov, *Macromol. Rapid Commun.*, 2011, **32**, 859–869.
13 K. Matyjaszewski, D. Hongchen, W. Jakubowski, J. Pietrasik and A. Kusumo, *Langmuir*, 2007, **23**, 4528–4531.
14 S. Edmondson, V. L. Osborne and W. T. S. Huck, *Chem. Soc. Rev.*, 2004, **33**, 14–22.
15 W. J. Brittain and S. Minko, *J. Polym. Sci., Part A: Polym. Chem.*, 2007, **45**, 3505–3512.
16 (*a*) H. Yamaguchi, M. Kikuchi, M. Kobayashi, H. Ogawa, H. Masunaga, O. Sakata and A. Takahara, *Macromolecules*, 2012, **45**, 1509–1516; (*b*) O. Azzaroni, A. A. Brown and W. T. S. Huck, *Angew. Chem., Int. Ed.*, 2006, **45**, 1770–1774.
17 (*a*) O. Roling, L. Stricker, J. Voskuhl, S. Lamping and B. J. Ravoo, *Chem. Commun.*, 2016, **52**, 1964–1966; (*b*) A. Synytska, E. Svetushkina, D. Martina, C. Bellmann, F. Simon, L. Ionov, M. Stamm and C. Creton, *Langmuir*, 2012, **28**, 16444–16454; (*c*) A. Synytska, E. Svetushkina, N. Puretskiy, G. Stoychev, S. Berger, L. Ionov, C. Bellmann, K.-J. Eichhorn and M. Stamm, *Soft Matter*, 2010, **6**, 5907–5914; (*d*) A. Drechsler, A. Synytska, P. Uhlmann, M. Stamm and F. Kremer, *Langmuir*, 2012, **28**, 15555–15565.
18 (*a*) R. A. E. Wright, K. Wang, J. Qu and B. Zhao, *Angew. Chem., Int. Ed.*, 2016, **55**, 8656–8660; (*b*) R. M. Bielecki, E. M. Benetti, D. Kumar and N. D. Spencer, *Tribol. Lett.*, 2012, **45**, 477–487.

19 (*a*) B. T. Seymour, R. A. E. Wright, A. C. Parrott, H. Gao, A. Martini, J. Qu, S. Dai and B. Zhao, *ACS Appl. Mater. Interfaces*, 2017, **9**, 25038–25048; (*b*) B. T. Seymour, W. Fu, R. A. E. Wright, H. Luo, J. Qu, S. Dai and B. Zhao, *ACS Appl. Mater. Interfaces*, 2018, **10**, 15129–15139.
20 M. Krishnamoorthy, S. Hakobyan, M. Ramstedt and J. E. Gautrot, *Chem. Rev.*, 2014, **114**, 10976–11026.
21 (*a*) F. Polzer, D. A. Kunz, J. Breu and M. Ballauff, *Chem. Mater.*, 2010, **22**, 2916–2922; (*b*) B. E. Humphreys, E. J. Wanless and G. B. Webber, *J. Colloid Interface Sci.*, 2018, **516**, 153–161.
22 (*a*) L. T. Strover, J. Malmström, L. A. Stubbing, M. A. Brimble and J. Travas-Sejdic, *Electrochim. Acta*, 2016, **188**, 57–70; (*b*) C. D. Grande, M. C. Tria, G. Jiang, R. Ponnapati and R. Advincula, *Macromolecules*, 2011, **44**, 966–975; (*c*) E.-Y. Choi, O. Azzaroni, N. Cheng, F. Zhou, T. Kelby and W. T. S. Huck, *Langmuir*, 2007, **23**, 10389–10394; (*d*) G. E. Fenoy, J. M. Giussi, C. von Bilderling, E. M. Maza, L. I. Pietrasanta, W. Knoll, W. A. Marmisollé and O. Azzaroni, *J. Colloid Interface Sci.*, 2018, **518**, 92–101; (*e*) Y. Pei, J. Travas-Sejdic and D. E. Williams, *Langmuir*, 2012, **28**, 8072–8083; (*f*) L. Strover, C. Roux, J. Malmström, Y. Pei, D. E. Williams and J. Travas-Sejdic, *Synth. Met.*, 2012, **162**, 381–390.
23 (*a*) M. Lemieux, D. Usov, S. Minko, M. Stamm, H. Shulha and V. V. Tsukruk, *Macromolecules*, 2003, **36**, 7244–7255; (*b*) M. C. LeMieux, S. Peleshanko, K. D. Anderson and V. V. Tsukruk, *Langmuir*, 2007, **23**, 265–273; (*c*) M. C. LeMieux, Y. H. Lin, P. D. Cuong, H. S. Ahn, E. R. Zubarev and V. V. Tsukruk, *Adv. Funct. Mater.*, 2005, **15**, 1529–1540.
24 A. Kopyshev, N. Lomadze, D. Feldmann, J. Genzer and S. Santer, *Polymer*, 2015, **79**, 65–72.
25 (*a*) A. Dirani, X. Laloyaux, A. E. Fernandes, B. Mathy, O. Schicke, O. Riant, B. Nysten and A. M. Jonas, *Macromolecules*, 2012, **45**, 9400–9408; (*b*) X. Laloyaux, B. Mathy, B. Nysten and A. M. Jonas, *Macromolecules*, 2010, **43**, 7744–7751; (*c*) S. Burkert, E. Bittrich, M. Kuntzsch, M. Müller, K. J. Eichhorn, C. Bellmann, P. Uhlmann and M. Stamm, *Langmuir*, 2010, **26**, 1786–1795.
26 T. Sakakiyama, H. Ohkita, M. Ohoka, S. Ito, Y. Tsujii and T. Fukuda, *Chem. Lett.*, 2005, **34**, 1366–1367.
27 B. Mu, M. F. Zhao and P. J. Liu, *J. Nanopart. Res.*, 2008, **10**, 831–838.
28 R. E. Behling, B. A. Williams, B. L. Staade, L. M. Wolf and E. W. Cochran, *Macromolecules*, 2009, **42**, 1867–1872.
29 K. Sill and T. Emrick, *Chem. Mater.*, 2004, **16**, 1240–1243.
30 A. C. C. Esteves, L. Bombalski, T. Trindade, K. Matyjaszewski and A. Barros-Timmons, *Small*, 2007, **3**, 1230–1236.
31 Q. J. Cai, G. D. Fu, F. R. Zhu, E.-T. Kang and K.-G. Neoh, *Angew. Chem.*, 2005, **117**, 1128–1131.
32 (*a*) S. Christau, T. Möller, Z. Yenice, J. Genzer and R. von Klitzing, *Langmuir*, 2014, **30**, 13033–13041; (*b*) O. Azzaroni, A. A. Brown, N. Cheng, A. Wei, A. M. Jonas and W. T. S. Huck, *J. Mater. Chem.*, 2007, **17**, 3433–3439; (*c*) S. Gupta, M. Agrawal, P. Uhlmann, F. Simon, U. Oertel and M. Stamm, *Macromolecules*, 2008, **41**, 8152–8158; (*d*) S. Gupta, M. Agrawal, P. Uhlmann, F. Simon and M. Stamm, *Chem. Mater.*, 2010, **22**, 504–509.
33 W. Wu, N. V. Tsarevsky, J. L. Hudson, J. M. Tour, K. Matyjaszewski and T. Kowalewski, *Small*, 2007, **3**, 1803–1810.
34 H. Kong, W. W. Li, C. Gao, D. Y. Yan, Y. Z. Jin, D. R. M. Walton and H. W. Kroto, *Macromolecules*, 2004, **37**, 6683–6686.
35 Y. Yang, X. Song, L. Yuan, M. Li, J. Liu, R. Ji and H. J. Zhao, *J. Polym. Sci., Part A: Polym. Chem.*, 2012, **50**, 329–337.
36 N. Borodinov, D. Gil, M. Savchak, C. E. Gross, N. S. Yadavalli, R. Ma, V. V. Tsukruk, S. Minko, A. Vertegel and I. Luzinov, *ACS Appl. Mater. Interfaces*, 2018, **10**, 13941–13952.
37 C. M. Hui, J. Pietrasik, M. Schmitt, C. Mahoney, J. Choi, M. R. Bockstaller and K. Matyjaszewski, *Chem. Mater.*, 2014, **26**, 745–762.
38 Q. Yu, L. K. Ista, R. Gu, S. Zauscher and G. P. López, *Nanoscale*, 2016, **8**, 680–700.
39 T. Chen, R. Ferris, J. Zhang, R. Ducker and S. Zauscher, *Prog. Polym. Sci.*, 2010, **35**, 94–112.
40 C. J. Galvin and J. Genzer, *Prog. Polym. Sci.*, 2012, **37**, 871–906.
41 I. Luzinov, S. Minko and V. V. Tsukruk, *Soft Matter*, 2008, **4**, 714–725.
42 O. Azzaroni, *J. Polym. Sci., Part A: Polym. Chem.*, 2012, **50**, 3225–3258.
43 S. Peng and B. Bhushan, *RSC Adv.*, 2012, **2**, 8557–8578.
44 F. Barbir, *PEM Fuel Cells: Theory and Practice*, Academic Press, San Diego, 2nd edn, 2013.
45 S. Srinivasan, *Fuel Cells: From Fundamentals to Applications*, Springer, New York, 2006.
46 K. A. Mauritz and R. B. Moore, *Chem. Rev.*, 2004, **104**, 4535–4586.
47 M. Bass, A. Berman, A. Singh, O. Konovalov and V. Freger, *Macromolecules*, 2011, **44**, 2893–2899.
48 B. Yameen, A. Kaltbeitzel, A. Langner, H. Duran, M. F. Müller, U. Gösele, O. Azzaroni and W. Knoll, *J. Am. Chem. Soc.*, 2008, **130**, 13140–13144.
49 B. Yameen, A. Kaltbeitzel, G. Glasser, A. Langner, F. Müller, U. Gösele, W. Knoll and O. Azzaroni, *ACS Appl. Mater. Interfaces*, 2010, **2**, 279–287.
50 B. Yameen, A. Kaltbeitzel, A. Langner, F. Müller, U. Gösele, W. Knoll and O. Azzaroni, *Angew. Chem., Int. Ed.*, 2009, **48**, 3124–3128.
51 Y. Dong, J. Feng, D. Lu, H. Zhang, M. Pan and P. Fang, *Eur. Polym. J.*, 2017, **88**, 183–190.
52 A. Khabibullin, S. D. Minteer and I. Zharov, *J. Mater. Chem. A*, 2014, **2**, 12761–12769.
53 E. Green, E. Fullwood, J. Selden and I. Zharov, *Chem. Commun.*, 2015, **51**, 7770–7780.
54 I. Zharov and A. Khabibullin, *Acc. Chem. Res.*, 2014, **47**, 440–449.
55 H. Bai, H. Zhang, Y. He, J. Liu, B. Zhang and J. Wang, *J. Membr. Sci.*, 2014, **454**, 220–232.
56 J. Feng, Y. Huang, Z. Tu, H. Zhang, M. Pan and H. Tang, *Sci. Rep.*, 2014, **4**, 6225.

 

57 X. Zheng, K. Liu, Y. Huang, H. Tang, W. Tu, M. Pan and H. Zhang, *Eur. Polym. J.*, 2015, **64**, 93–100.
58 A. Farrukh, F. Ashraf, A. Kaltbeitzel, X. Ling, M. Wagner, H. Duran, A. Ghaffar, H. ur Rehman, S. H. Parekh, K. F. Domke and B. Yameen, *Polym. Chem.*, 2015, **6**, 5782–5789.
59 W. Zhang, B. Zhang, G. He, B. Liu, Z. Jiang, X. Yang and C. Li, *RSC Adv.*, 2015, **5**, 5343–5356.
60 G. He, C. Chang, M. Xu, S. Hu, L. Li, J. Zhao, Z. Li, Z. Li, Y. Yin, M. Gang, H. Wu, X. Yang, M. D. Guiver and Z. Jiang, *Adv. Funct. Mater.*, 2015, **25**, 7502–7511.
61 L. Ahmadian-Alam, M. Teymoori and H. Mahdavi, *J. Polym. Res.*, 2018, **25**, 13.
62 L. Zhao, Y. Li, H. Zhang, W. Wu, J. Liu and J. Wang, *J. Power Sources*, 2015, **286**, 445–457.
63 M.-Y. Lim and K. Kim, *Polymers*, 2018, **10**, 569.
64 J. Wang, H. Bai, J. Zhang, L. Zhao, P. Chen, Y. Li and J. Liu, *J. Membr. Sci.*, 2017, **531**, 47–58.
65 X. He, G. He, A. Zhao, F. Wang, X. Mao, Y. Yin, L. Cao, B. Zhang, H. Wu and Z. Jiang, *ACS Appl. Mater. Interfaces*, 2017, **9**, 27676–27687.
66 T. Yang, Z. Li, H. Lyu, J. Zheng, J. Liu, F. Liu, Z. Zhang and H. Rao, *RSC Adv.*, 2018, **8**, 15740–15753.
67 G. He, J. Zhao, S. Hu, L. Li, Z. Li, Y. Li, Z. Li, H. Wu, X. Yang and Z. Jiang, *ACS Appl. Mater. Interfaces*, 2014, **6**(17), 15291–15301.
68 L. Long, S. Wang, M. Xiao and Y. Meng, *J. Mater. Chem. A*, 2016, **4**, 10038–10069.
69 *Polymer Electrolyte Fuel Cell Durability*, ed. F. N. Büchi, M. Inaba, T. J. Schmidt, Springer, New York, 2009.
70 M. J. Park, I. Choi, J. Hong and O. Kim, *J. Appl. Polym. Sci.*, 2013, 2363–2376.
71 T. Sato, T. Morinaga, S. Marukane, T. Narutomi, T. Igarashi, Y. Kawano, K. Ohno, T. Fukuda and Y. Tsujii, *Adv. Mater.*, 2011, **23**, 4868–4872.
72 T. Morinaga, S. Honma, T. Ishizuka, T. Kamijo, T. Sato and Y. Tsujii, *Polymers*, 2016, **8**, 146.
73 P. Wang, Y.-N. Zhou, J.-S. Luo and Z.-H. Luo, *Polym. Chem.*, 2014, **5**, 882–891.
74 H. Zhao, Z. Jia, W. Yuan, H. Hu, Y. Fu, G. L. Baker and G. Liu, *ACS Appl. Mater. Interfaces*, 2015, **7**, 19335–19341.
75 J. L. Schaefer, D. A. Yanga and L. A. Archer, *Chem. Mater.*, 2013, **25**, 834–839.
76 Y. Kim, S. J. Kwon, H. Jang, B. M. Jung, S. B. Lee and U. H. Choi, *Chem. Mater.*, 2017, **29**, 4401–4410.
77 J. Shim, D.-G. Kim, H. J. Kim, J. H. Lee, J.-H. Baik and J.-C. Lee, *J. Mater. Chem. A*, 2014, **2**, 13873–13883.
78 Y.-S. Ye, H. Wang, S.-G. Bi, Y. Xue, Z.-G. Xue, X.-P. Zhou, X.-L. Xie and Y.-W. Mai, *J. Mater. Chem. A*, 2015, **3**, 18064–18073.
79 (*a*) B. Scrosati and J. Garche, *J. Power Sources*, 2010, **195**, 2419–2430; (*b*) M. G. Kim and J. Cho, *Adv. Funct. Mater.*, 2009, **19**, 1497–1514.
80 Y. Tang, Y. Zhang, W. Li, B. Ma and X. Chen, *Chem. Soc. Rev.*, 2015, **44**, 5926–5940.
81 K. Chen, S. Song, F. Liu and D. Xue, *Chem. Soc. Rev.*, 2015, **44**, 6230–6257.
82 S. Guo and S. Dong, *Chem. Soc. Rev.*, 2011, **40**, 2644–2672.
83 D. A. Dikin, S. Stankovich, E. J. Zimney, R. D. Piner, G. H. B. Dommett, G. Evmenenko, S. T. Nguyen and R. S. Ruoff, *Nature*, 2007, **448**, 457–460.
84 T. D. Dao, J.-E. Hong, K.-S. Ryu and H. M. Jeong, *Chem. Eng. J.*, 2014, **250**, 257–266.
85 (*a*) S. Muench, A. Wild, C. Friebe, B. Häupler, T. Janoschka and U. S. Schubert, *Chem. Rev.*, 2016, **116**, 9438–9484; (*b*) Y. Liang, Z. Tao and J. Chen, *Adv. Energy Mater.*, 2012, **2**, 742–769.
86 C. Friebe and U. S. Schubert, *Top. Curr. Chem.*, 2017, **375**, 19.
87 T. Jähnert, B. Häupler, T. Janoschka, M. D. Hager and U. S. Schubert, *Macromol. Rapid Commun.*, 2014, **35**, 882–887.
88 H.-C. Lin, C.-C. Li and J.-T. Lee, *J. Power Sources*, 2011, **196**, 8098–8103.
89 (*a*) H. Nishide, S. Iwasa, Y.-J. Pu, T. Suga, K. Nakahara and M. Satoh, *Electrochim. Acta*, 2004, **50**, 827; (*b*) K. Oyaizu and H. Nishide, *Adv. Mater.*, 2009, **21**, 2339.
90 M.-K. Hung, Y.-H. Wang, C.-H. Lin, H.-C. Lin and J.-T. Lee, *J. Mater. Chem.*, 2012, **22**, 1570–1577.
91 C.-H. Lin, W.-J. Chou and J.-T. Lee, *Macromol. Rapid Commun.*, 2012, **33**, 107–113.
92 K. Takahashi, K. Korolev, K. Tsuji, K. Oyaizu, H. Nishide, E. Bryuzgin, A. Navrotskiy and I. Novakov, *Polymer*, 2015, **68**, 310–314.
93 B. Ernould, M. Devos, J.-P. Bourgeois, J. Rolland, A. Vlad and J.-F. Gohy, *J. Mater. Chem. A*, 2015, **3**, 8832–8839.
94 B. Ernould, O. Bertrand, A. Minoia, R. Lazzaroni, A. Vlad and J.-F. Gohy, *RSC Adv.*, 2017, **7**, 17301–17310.
95 A. Vlad, N. Singh, J. Rolland, S. Melinte, P. Ajayan and J.-F. Gohy, *Sci. Rep.*, 2014, **4**, 4315.
96 Y. Li, Z. Jian, M. Lang, C. Zhang and X. Huang, *ACS Appl. Mater. Interfaces*, 2016, **8**, 17352–17359.
97 (*a*) D. U. Lee, P. Xu, Z. P. Cano, A. G. Kashkooli, M. G. Park and Z. Chen, *J. Mater. Chem. A*, 2016, **4**, 7107–7134; (*b*) M. Nagao, K. Kobayashi, Y. Yamamoto, T. Yamaguchi, A. Oogushi and T. Hibino, *ChemElectroChem*, 2016, **3**, 247–255.
98 T. N. Pham Truong, H. Randriamahazaka and J. Ghilane, *ACS Catal.*, 2018, **8**, 869–875.
99 G.-J. Sohn, H.-J. Choi, I.-Y. Jeon, D. W. Chang, L. Dai and J.-B. Baek, *ACS Nano*, 2012, **6**, 6345.
100 K. M. Manesh, P. Santhosh, A. I. Gopalan and K.-P. Lee, *Electroanalysis*, 2006, **18**, 1564–1571.
101 *PEM Electrolysis for Hydrogen Production: Principles and Applications*, ed. D. Bessarabov, H. Wang, H. Li, N. Zhao, CRC Press, Boca Raton, 2016.
102 *Fuel Cells and Hydrogen: From Fundamentals to Applied Research*, ed. V. Hacker, S. Mitsushima, Elsevier, New York, 2018.
103 (*a*) J. D. Benck, T. R. Hellstern, J. Kibsgaard, P. Chakthranont and T. F. Jaramillo, *ACS Catal.*, 2014, **4**, 3957–3971; (*b*) D. Merki and X. Hu, *Energy Environ. Sci.*, 2011, **4**, 3878–3888.

104 (*a*) X. Zeng, L. Niu, L. Song, X. Wang, X. Shi and J. Yan, *Metals*, 2015, **5**, 1829–1844; (*b*) X. Dai, K. Du, Z. Li, H. Sun, Y. Yang, X. Zhang, X. Li and H. Wang, *Chem. Eng. Sci.*, 2015, **134**, 572–580; (*c*) Y. Lattach, A. Deronzier and J.-C. Moutet, *ACS Appl. Mater. Interfaces*, 2015, **7**, 15866–15875.
105 L.-A. Stern, P. Mocny, H. Vrubel, T. Bilgic, H.-A. Klok and X. Hu, *ACS Appl. Mater. Interfaces*, 2018, **10**, 6253–6261.
106 *Supercapacitors: Materials, Systems, and Applications*, ed. F. Beguin, E. Frackowiak, Wiley-VCH, Weinheim, 2013.
107 G. Wang, L. Zhang and J. Zhang, *Chem. Soc. Rev.*, 2012, **41**, 797–828.
108 F. Wang, X. Wu, X. Yuan, Z. Liu, Y. Zhang, L. Fu, Y. Zhu, Q. Zhou, Y. Wu and W. Huang, *Chem. Soc. Rev.*, 2017, **46**, 6816–6854.
109 X. Peng, L. Peng, C. Wu and Y. Xie, *Chem. Soc. Rev.*, 2014, **43**, 3303–3323.
110 B. Zhang, B. Yu, F. Zhou and W. Liu, *J. Mater. Chem. A*, 2013, **1**, 8587–8592.
111 N. A. Kumar and J.-B. Baek, *Chem. Commun.*, 2014, **50**, 6298–6308.
112 Y. Liang, W. Zhang, D. Wu, Q.-Q. Ni and M. Q. Zhang, *Adv. Mater. Interfaces*, 2018, **5**, 1800430.
113 W. A. Marmisollé and O. Azzaroni, *Nanoscale*, 2016, **8**, 9890–9918.
114 M. Kotal, A. K. Thakur and A. K. Bhowmick, *ACS Appl. Mater. Interfaces*, 2013, **5**, 8374–8386.
115 Z. Lei, J. Zhang, L. L. Zhang, N. A. Kumar and X. S. Zhao, *Energy Environ. Sci.*, 2016, **9**, 1891–1930.
116 F. Shen, D. Pankratov and Q. Chi, *Curr. Opin. Electrochem.*, 2017, **4**, 133–144.
117 R. R. Salunkhe, Y.-H. Lee, K.-H. Chang, J.-M. Li, P. Simon, J. Tang, N. L. Torad, C.-C. Hu and Y. Yamauchi, *Chem. – Eur. J.*, 2014, **20**, 13838–13852.
118 N. A. Kumar, H.-J. Choi, Y. R. Shin, D. W. Chang, L. Dai and J.-B. Baek, *ACS Nano*, 2012, **6**, 1715–1723.
119 Z. Liu, H. Zhou, Z. Huang, W. Wang, F. Zeng and Y. Kuang, *J. Mater. Chem. A*, 2013, **1**, 3454–3462.
120 W. Yang, H. Zhou, Z. Huang, H. Li, C. Fu, L. Chen, M. Li, S. Liu and Y. Kuang, *Electrochim. Acta*, 2017, **245**, 41–50.
121 X. Liu, P. Shang, Y. Zhang, X. Wang, Z. Fan, B. Wang and Y. Zheng, *J. Mater. Chem. A*, 2014, **2**, 15273–15278.
122 K. Zhang, L. L. Zhang, X. Zhao and J. Wu, *Chem. Mater.*, 2010, **22**, 1392–1401.
123 J. R. Lomeda, C. D. Doyle, D. V. Kosynkin, W.-F. Hwang and J. M. Tour, *J. Am. Chem. Soc.*, 2008, **130**, 16201–16206.
124 Z. Gao, F. Wang, J. Chang, D. Wu, X. Wang, X. Wang, F. Xu, S. Gao and K. Jiang, *Electrochim. Acta*, 2014, **133**, 325–334.
125 Y. Liu, Y. Ma, S. Guang, F. Ke and H. Xu, *Carbon*, 2015, **83**, 79–89.
126 U. Male, J. K. R. Modigunta and D. S. Huh, *Polymer*, 2017, **110**, 242–249.
127 N. V. Hoa, T. T. H. Quyen, N. V. Hieu, T. Q. Ngoc, P. V. Thinh, P. A. Dat and H. T. T. Nguyen, *Synth. Met.*, 2017, **223**, 192–198.
128 M. Faraji and R. Hasanzadeh, *Energy Technol.*, 2017, **5**, 1998–2004.
129 S. K. Yadav, R. Kumar, A. K. Sundramoorthy, R. K. Singh and C. M. Koo, *RSC Adv.*, 2016, **6**, 52945–52949.
130 G. Zini and P. Tartarini, *Solar Hydrogen Energy Systems: Science and Technology for the Hydrogen Economy*, Springer, Milano, 2012.
131 *Solar Hydrogen Generation: Toward a Renewable Energy Future*, ed. K. Rajeshwar, R. McConnell, S. Licht, Springer, New York, 2008.
132 D. Cedeno, A. Krawicz, P. Doak, M. Yu, J. B. Neaton and G. F. Moore, *J. Phys. Chem. Lett.*, 2014, **5**, 3222–3226.
133 A. M. Beiler, D. Khusnutdinova, S. I. Jacob and G. F. Moore, *Ind. Eng. Chem. Res.*, 2016, **55**, 5306–5314.
134 A. M. Beiler, D. Khusnutdinova, S. I. Jacob and G. F. Moore, *ACS Appl. Mater. Interfaces*, 2016, **8**, 10038–10047.
135 A. M. Beiler, D. Khusnutdinova, B. L. Wadsworth and G. F. Moore, *Inorg. Chem.*, 2017, **56**(20), 12178–12185.
136 *Stability and Degradation of Organic and Polymer Solar Cells*, ed. F. C. Krebs, John Wiley & Sons, Chichester, 2012.
137 *Organic Solar Cells: Fundamentals, Devices, and Upscaling*, ed. B. P. Rand and H. Richter, CRC Press, Boca Raton, 2014.
138 A. Bousquet, H. Awada, R. C. Hiorns, C. Dagron-Lartigau and L. Billon, *Prog. Polym. Sci.*, 2014, **39**, 1847–1877.
139 H. J. Snaith, G. L. Whiting, B. Sun, N. C. Greenham, W. T. S. Huck and R. H. Friend, *Nano Lett.*, 2005, **5**, 1653–1657.
140 G. L. Whiting, H. J. Snaith, S. Khodabakhsh, J. W. Andreasen, D. W. Breiby, M. M. Nielsen, N. C. Greenham, R. H. Friend and W. T. S. Huck, *Nano Lett.*, 2006, **6**, 573–578.
141 M. C. Tria, K.-S. Liao, N. Alley, S. Curran and R. Advincula, *J. Mater. Chem.*, 2011, **21**, 10261–10264.
142 E. Lim, F. Gao, E. Schwartz, J. J. L. M. Cornelissen, R. J. M. Nolte, A. E. Rowan, N. C. Greenham and L.-M. Do, *J. Nanosci. Nanotechnol.*, 2012, **12**, 503–507.
143 S. K. Sontag, G. R. Sheppard, N. M. Usselman, N. Marshall and J. Locklin, *Langmuir*, 2011, **27**, 12033.
144 N. Doubina, J. L. Jenkins, S. A. Paniagua, K. A. Mazzio, G. A. MacDonald, A. K. Y. Jen, N. R. Armstrong, S. R. Marder and C. K. Luscombe, *Langmuir*, 2012, **28**, 1900–1908.
145 J. Chen, J. Alonzo, X. Yu, K. Hong, J. M. Messman, I. Ivanov, N. V. Lavrik, M. Banerjee, R. Rathore, Z. Sun, D. Li, J. W. Mays, B. G. Sumpter and S. M. Kilbey II, *J. Mater. Chem. A*, 2013, **1**, 13426–13432.
146 V. Senkovskyy, N. Khanduyeva, H. Komber, U. Oertel, M. Stamm, D. Kuckling and A. Kiriy, *J. Am. Chem. Soc.*, 2007, **129**(20), 6626–6632.
147 N. Khanduyeya, V. Senkovskyy, T. Beryozkina, M. Horecha, M. Stamm, C. Uhrich, M. Riede, K. Leo and A. Kiriy, *J. Am. Chem. Soc.*, 2009, **131**(1), 153–161.
148 N. Marshall, S. K. Sontag and J. Locklin, *Chem. Commun.*, 2011, **47**(20), 5681–5689.
149 M. Alonzi, D. Lanari, A. Marrochi, C. Petrucci and L. Vaccaro, *RSC Adv.*, 2013, **3**(46), 23909–23923.
150 L. Yang, S. K. Sontag, T. W. LaJoie, W. Li, N. E. Huddleston, J. Locklin and W. You, *ACS Appl. Mater. Interfaces*, 2012, **4**, 5069–5073.

 

151 J. Chen, J. Alonzo, X. Yu, K. Hong, J. M. Messman, I. Ivanov, N. V. Lavrik, M. Banerjee, R. Rathore, Z. Sun, D. Li, J. W. Mays, B. G. Sumpter and S. M. Kilbey II, *Nanoscale*, 2013, **5**, 9357–9364.

152 S. Saha and G. L. Baker, *J. Appl. Polym. Sci.*, 2015, **132**, 41363.

153 S. G. Youm, E. Hwang, C. A. Chavez, X. Li, S. Chatterjee, K. L. Lusker, L. Lu, J. Strzalka, J. F. Ankner, Y. Losovyj, J. C. Garno and E. E. Nesterov, *Chem. Mater.*, 2016, **28**, 4787–4804.

154 P. Reiss, E. Couderc, J. De Girolamo and A. Pron, *Nanoscale*, 2011, **3**, 446–489.

155 Q. Zhang, T. P. Russell and T. Emrick, *Chem. Mater.*, 2007, **19**, 3712–3716.

156 V. Senkosvskyy, R. Tkachov, T. Beryozkian, H. Komber, U. Oertel, M. Horecha, V. Bocharova, M. Stamm, S. A. Gervogyan, F. Krebs and A. Kiriy, *J. Am. Chem. Soc.*, 2009, **131**(45), 16445–16453.

157 F. Boon, D. Moerman, D. Laurencin, S. Richeter, Y. Guari, A. Mehdi, P. Dubois, R. Lazzaroni and S. Clément, *Langmuir*, 2014, **30**, 11340–11347.

158 F. Boon, A. Thomas, G. Clavel, D. Moerman, J. De Winter, D. Laurencin, O. Coulembier, P. Dubois, P. Gerbaux, R. Lazzaroni, S. Richeter, A. Mehdi and S. Clément, *Synth. Met.*, 2012, **162**, 1615–1622.

159 F. Li, Y. Du and Y. Chen, *Thin Solid Films*, 2012, **526**, 120–126.

160 R.-H. Lee, J.-L. Huang and C.-H. Chi, *J. Polym. Sci., Part B: Polym. Phys.*, 2013, **51**, 137–148.

161 J. Kim, H. Lee, S. J. Lee, W. J. da Silva, A.R. b. M. Yusoff and J. Jang, *J. Mater. Chem. A*, 2015, **3**, 22035–22042.

162 D. Yu, Y. Yang, M. Durstock, J.-B. Baek and L. Dai, *ACS Nano*, 2010, **4**, 5633–5640.

163 B. K. Kuila, K. Park and L. Dai, *Macromolecules*, 2010, **43**, 6699–6705.

164 J. Han, H. Kim, D. Y. Kim, S. M. Jo and S.-Y. Jang, *ACS Nano*, 2010, **4**, 3503–3509.

165 Y.-H. Yu, I.-J. Teng, Y.-C. Hsu, W.-C. Huang, C.-J. Shih and C.-H. Tsai, *Org. Electron.*, 2017, **42**, 209–220.

166 C.-H. Tsai, W.-C. Huang, Y.-C. Hsu, C.-J. Shih, I.-J. Teng and Y.-H. Yu, *Electrochim. Acta*, 2016, **213**, 791–801.

167 P. Ma, J. Tan, H. Cheng, Y. Fang, Y. Wang, Y. Daic, S. Fang, X. Zhou and Y. Lin, *Appl. Surf. Sci.*, 2018, **427**, 458–464.

168 (*a*) S. Tan, J. Zhai, H. Fang, T. Jiu, J. Ge, Y. Li, L. Jiang and D. Zhu, *Chem. – Eur. J.*, 2005, **11**, 6272; (*b*) W. J. E. Beek and R. A. J. Janssen, *J. Mater. Chem.*, 2004, **14**, 2795; (*c*) W. J. E. Beek and R. A. J. Janssen, *Adv. Funct. Mater.*, 2002, **12**, 519; (*d*) N. Koumura, Z.-S. Wang, S. Mori, M. Miyashita, E. Suzuki and K. Hara, *J. Am. Chem. Soc.*, 2006, **128**, 14256.

169 (*a*) Y. G. Kim, J. Walker, L. A. Samuelson and J. Kumar, *Nano Lett.*, 2003, **3**, 523; (*b*) K. Shankar, G. K. Mor, H. E. Prakasam, O. K. Varghese and C. A. Grimes, *Langmuir*, 2007, **23**, 12445; (*c*) R. Senadeera, T. Kitamura, Y. Wada and S. Yanagida, *Sol. Energy Mater. Sol. Cells*, 2005, **88**, 315; (*d*) R. H. Lohwasser, J. Bandara and M. Thelakkat, *J. Mater. Chem.*, 2009, **19**, 4126–4130.

170 J. Warnan, Y. Pellegrin, E. Blart, F. Odobel, W. Zhang, B. Liu, V. J. Babu and S. Ramakrishna, *Macromol. Rapid Commun.*, 2011, **32**, 1190–1194.

171 J. Yan, Q. Ye, X. Wang, B. Yua and F. Zhou, *Nanoscale*, 2012, **4**, 2109–2116.

172 J. Yan, Q. Ye and F. Zhou, *RSC Adv.*, 2012, **2**, 3978–3985.

173 Z. Fang, A. Ito, A. C. Stuart, H. Luo, Z. Chen, K. Vinodgopal, W. You, T. J. Meyer and D. K. Taylor, *ACS Nano*, 2013, **7**, 7992–8002.

174 R. Caterino, R. Csiki, A. Lyuleeva, J. Pfisterer, M. Wiesinger, S. D. Janssens, K. Haenen, A. Cattani-Scholz, M. Stutzmann and J. A. Garrido, *ACS Appl. Mater. Interfaces*, 2015, **7**, 8099–8107.

175 ''This has to be interpreted in different ways. Whereas enterprises aim at getting more (performance) at less (cost) for more (profit), they must also aim at getting more (performance) at less (cost) for more and more (people)'' – Raghunath Anant Mashelkar. Quotation from Green Energy: Technology, Economics and Policy edited by U. Aswathanarayana, T. Harikrishnan and K. M. Thayyib Sahini (CRC Press, Boca Raton, 2010).

176 R. Foster, M. Ghassemi and A. Cota, *Solar Energy: Renewable Energy and the Environment*, CRC Press, Boca Raton, 2010.

177 A. A. Golriz, T. Kaule, M. B. Untch, K. Kolman, R. Berger and J. S. Gutmann, *ACS Appl. Mater. Interfaces*, 2013, **5**, 2485–2494.

178 D. Tranchida, E. Sperotto, A. Chateauminois and H. Schönherr, *Macromolecules*, 2011, **44**, 368–374.

179 J. M. Griffin, A. C. Forse, W.-Y. Tsai, P.-L. Taberna, P. Simon and C. P. Grey, *Nat. Mater.*, 2015, **14**, 812–819.

180 G. L. Whiting, H. J. Snaith, S. Khodabakhsh, J. W. Andreasen, D. W. Breiby, M. M. Nielsen, N. C. Greenham, R. H. Friend and W. T. S. Huck, *Nano Lett.*, 2006, **6**, 573–578.

181 (*a*) A. W. Hains, C. Ramanan, M. D. Irwin, J. Liu, M. R. Wasielewski and T. J. Marks, *ACS Appl. Mater. Interfaces*, 2010, **2**, 175–185; (*b*) H. Ma, H.-L. Yip, F. Huang and A. K.-Y. Jen, *Adv. Funct. Mater.*, 2010, **20**, 1371–1388.

182 (*a*) S. Inaoka and D. M. Collard, *Langmuir*, 1999, **15**, 3752–3758; (*b*) H. Nakashima, K. Furukawa, K. Ajito, Y. Kashimura and K. Torimitsu, *Langmuir*, 2005, **21**, 511–515.